DESIGN, FABRICATION AND CHARACTERIZATION OF THIN-FILM POLYMERIC OPTICAL SPLITTERS

THESIS

Submitted in partial fulfillment

of the requirements for the degree of

DOCTOR OF PHILOSOPHY

by

RAHUL SINGHAL

Under the Supervision of

DR. M. N. SATYANARAYAN

BIRLA INSTITUTE OF TECHNOLOGY AND SCIENCE

PILANI (RAJASTHAN) INDIA

2013

Dedicated to My Mother…

BIRLA INSTITUTE OF TECHNOLOGY AND SCIENCE

PILANI (RAJASTHAN)

CERTIFICATE

This is to certify that the thesis entitled **DESIGN, FABRICATION AND CHARACTERIZATION OF THIN-FILM POLYMERIC OPTICAL SPLITTERS** which is submitted for award for Ph.D. Degree of the institute, embodies original work done by him under my supervision.

Signature in full of the Supervisor:_____

Name in capital block letters:_____

Designation:_____

Date:

ACKNOWLEDGEMENTS

This thesis marks my journey of research during last few years. Along this journey, people those have contributed to this research objective deserve a special mention. I am glad to take this opportunity to express my gratitude to them through my humble acknowledgement.

First of all, I would like to thank Prof. B. N. Jain, Vice-Chancellor, BITS, Pilani and Prof. G. Raghurama, Director, BITS, Pilani Campus for constant support, concern and motivation. I am grateful to Prof. S. K. Verma, Dean, ARD for his support.

I would like to express the deepest gratitude to my supervisor, Dr. M. N. Satyanarayan, for his invaluable supervision, suggestions, for answers to all my queries, as well as providing me with literature from early stages to throughout the project. He has been a great inspiration. His experiences encouraged me to experiment with my creativity and nourish my knowledge in the area of photonics. His excellence, creativity, perfection, patience, encouragement and support have transformed my thinking and attitude towards work as well as life.

Thanks to Dr. Suchandan Pal, Scientist EII (Principal Scientist) at ODG, CSIR-CEERI, Pilani for being a great support to this research work. I truly admire his insights. His philosophy toward work has taught me how to innovate. He has encouraged me to think novel and ingrained the creativity in me. I thank project assistants, Mr. Nirmal and Mr. Mukesh for their help and availabiltiy, and also would like to thank Mr. Ravi Bhatia, Sr. Tech. Assistant, SNG, CEERI, Pilani for his technical help with Mask Aligner during the step of UV exposure and development of waveguides. Working along with Members at CSIR-CEERI, Pilani was a pleasant experience.

I would like to take this opportunity to express my gratitude to the faculty members - Mr. Pawan Sharma and Dr. Abhijeet Asati for helping me in learning L-Edit Tanner Tools for development of mask to fabricate waveguides and splitters. I am grateful to the members of SAMEER, Mumbai, especially Dr. Anuj Bhatnagar and Mr. Indrajit Boiragi for their help and support throughout the characterization of the waveguides.

I am grateful to Dr. Chandrasekhar, Director, CSIR-CEERI, Pilani for providing us the research opportunity in CSIR-CEERI laboratories. I am also indebted to DeitY, MCIT, Govt. of India to fund this research. A special thank goes to Dr. (Mrs.) Niloufer Shroff, Scientist G & Head (Electronics Materials and Components Division), DeitY, MCIT, Govt. of India.

I appreciate the help and support from my Doctoral Advisory Committee (DAC) members – Prof. R. P. Khare and Prof. V. K. Chaubey. I have greatly benefitted from their inputs. I learned from Prof. Khare how to become a humble yet efficient person. Prof. Chaubey's theoretical and analytical prowess motivated me for finer research. I also thank Prof. Chaubey for allowing me to utilize all the equipment in optical communication laboratory to facilitate this research work.

I also appreciate the support from Prof. Sudeept Mohan, Dean Admissions and Prof. Anu Gupta, Head, Department of Electrical and Electronics Engineering, for keeping me away from long hours of divisional and departmental administrative duties.

Finally, no words can express the support I have got from my parents. Whenever everything seemed gloomy in moments of life, I have derived all my inner strength from them. Thank you, Mom and Dad, for all I have inherited from you.

Thanks to my beautiful wife, Geetika, my lovely daughter, Pehal, and my adorable son, Shrestha to understand and to permit me to spend time, actually meant to spend with them, on this work.

Thanks to all my friends and my family members who whenever needed were in constant touch with me.

I would also like to take this opportunity to express my gratitude to my colleagues who were important to the successful realization of this thesis, as well as express my apology that I could not mention personally one by one.

Finally, I would like to thank GOD for always guiding me.

RAHUL SINGHAL

ABSTRACT

Polymers have been accepted as a new-generation material for an optical integrated circuit due to its various advantages as compared to other optical materials. Some features of polymers worth highlighting are ease of handling, tailoring the properties by doping, direct deposition on any substrate and complete compatibility with semiconductor processing techniques. Polymeric materials became popular in integrated optics because they permitted rapid fabrication of complex and innovative optical elements with very simple technologies like spin-coating and replication methods. However, those facts depend heavily on the fabrication method and particular polymer. Photonic polymer-based devices are particularly attractive because of their ability to be processed rapidly with high yields, they are cost effective, and at the same time perform comparatively well. Optical waveguides are structures that confine and direct optical signals in a region of higher effective index than its surrounding media. An optical waveguide forms the basis for all integrated photonic devices. Thus, it becomes significantly necessary to develop a cost-effective technology for fabrication of low-loss polymeric optical waveguides before initiation of development of polymeric photonic devices. This thesis presents the fabrication of polymeric optical channel and branching waveguides in photosensitive polymer buried in optical adhesive on a planar silicon substrate.

Epoxy-polymer SU-8 2002, a photosensitive polymer from MicroChem Corporation, USA was used to form the core of optical planar and channel waveguides. SU-8 2000 series resists have high functionality and high optical transparency and are sensitive to near-UV radiation. Pre- and post-exposure bake times are comparatively smaller for SU-8 2000 than the traditional SU-8. Lithographically defined SU-8 can provide simpler fabrication processes. Images having exceptionally high aspect ratios and straight sidewalls are readily formed in thick and thin films by contact proximity or projection printing. Another epoxy polymer, Norland Optical Adhesive 61 (NOA 61) from Norland Products, USA, popularly utilized as an optical adhesive, was applied here as under- and over- clad material to develop the symmetrical wave-guiding structure. The refractive index of NOA 61 was found to be near to and lower than that of SU-8 2002, making it suitable for cladding material of optical planar and channel waveguides. When fully cured, NOA 61 has very good adhesion and solvent

resistance. Curing time is remarkably fast and is dependent upon the thickness applied and the amount of ultraviolet light energy available.

The geometrical features of the waveguide were designed and simulated for performance analysis by Beam-Propagation Method in BeamProp^{TM} (RSoft Design Group, USA) environment to obtain the optimum structure for waveguide fabrication. For our design inputs, we used the refractive index of cured NOA 61 as 1.54 while that of SU-8 2002 as 1.57 at 1550 nm, verified over a Metricon 2010 Prism coupler. The waveguide cross-section was chosen to be 2.5 × 2.5 μm to ensure single mode propagation at 1550 nm. Single mode buried channel waveguides were fabricated using low cost photolithographic techniques and wet chemical etching processes. Channel waveguides were obtained on development after a cross-linkable negative tone epoxy SU-8 2002 polymer is exposed to UV through a photomask. SU-8 optical waveguides with an over and under cladding of optical adhesive NOA 61, on silicon substrate, were realized. Conventional Y-branches and cascaded Y-branches were realized based on polymeric channel waveguides.

The experimental results have demonstrated light-wave guiding and power splitting in the polymer material. The average insertion loss estimated was 11 dB (TE_{00}) for a 2-cm waveguide at 1550 nm. The average insertion loss of 1 × 2 splitter was estimated to be 13 dB for a 7.2 mm device at 1550 nm. The Y-branches of the 1 × 2 device were separated by 254 μm at the output ends. The average insertion loss of 1.70 cm long conventionally designed 1 × 4 power splitter with output ends separated by 127 μm was estimated to be around 17 dB assuming excess losses. Besides propagation loss, the coupling losses estimated were 7.4 dB including field mismatch losses of 3.5 dB/port and fresnel reflection losses of 0.2 dB per port. The estimation of insertion loss was based on previous work reported in literature. Characterization of a conventional 1 × 4 splitter with cleaved input and output ends resulted in an average insertion loss of 19.32 dB at 1550 nm. The optical power distribution among the outputs was highly non-uniform.

Polymer residues are generally left in the Y-junctions of the conventional splitters. Besides increased insertion loss, the Y-junction residue results in asymmetric distribution of power at device outputs. An analysis of the device performance in the presence of junction residue is presented in this work. The process to fabricate single-mode polymeric channel waveguide-

based optical splitters using simple direct ultraviolet (UV) photolithography was optimized to reduce the residual resist at the Y-junction and presented. A design to overcome the non-uniformities in output power distribution brought about by the presence of the residue was proposed. The proposed design incorporates a tapered waveguide beam expander and cosine S-bends. The Y-branches are kept separated by a distance at splitting junction considering fabrication limitations, which results in some extra propagation loss in the simulated results. This additional loss is compensated by reduction in overall device length and in the residue length after fabrication. A 1 × 4 device based on the proposed design was developed using the optimized fabrication process to achieve minimum residual polymer at Y-junction of branching waveguides. The average insertion loss obtained for a 1.43 cm 1 × 4 device was 18.14 dB at 1550 nm. After characterization, performance comparison of both devices is done and the results obtained concluded that proposed design offered better uniformity in power distribution among the output branches of the branching waveguides. The characterization of the proposed 1 × 4 optical power splitter shows improvements of ~1.2 dB in insertion loss and better uniformity in comparison to the conventional one at 1550 nm.

TABLE OF CONTENTS

LIST OF TABLES

LIST OF FIGURES

LIST OF ACRONYMS

2D	Two Dimensional
3D	Three Dimensional
AWG	Array Waveguide Grating(s)
BPM	Beam Propagation Method
CAD	Computer-Aided Design
CATV	Community Access Television
CCD	Charge-Coupled Device
CEERI	Central Electronics Engineering Research Institute
CP	Cyclopentanone
CSIR	Council of Scientific and Industrial Research
CVD	Chemical Vapor Deposition
CW	Continuous Wave
DUV	Deep Ultraviolet
DWDM	Dense-Wavelength Division Multiplexing
EBL	Electron-Beam Lithography
EIM	Effective-Index Method
FBT	Fiber Biconic Taper
FD-BPM	Finite Difference-Beam Propagation Method
FDM	Fourier Decomposition Method
FEM	Finite Element Method

FTTH	Fiber to the Homes
FTTP	Fiber to the Premises
GBL	Gamma-butyrolactone
GDS-II	Graphic Database System - II
GI	Graded-index
ICP	Inductively Coupled Plasma
IL	Insertion Loss
LED	Light emitting diode
$LiNbO_3$	Lithium Niobate
LWD	Long Working Distance
MeV	Million Electron Volts
MFD	Mode-Field Diameter
MMI	Multimode Interferometers
NA	Numerical Aperture
NOA	Norland Optical Adhesive
PCB	Printed Circuit Board
PGMEA	Propylene Glycol Methyl Ether Acetate
PIC	Photonic Integrated Circuit
PLC	Planar Lightwave Circuit
PMMA	Polymethyl-methacrylate
PON	Passive Optical Network

RF	Radio Frequency
RIE	Reactive-Ion Etching
SAMEER	Society for Applied Microwave Electronics Engineering & Research
SDF	Semiconductor Devices Fabrication
SEM	Scanning Electron Microscopy
SI	Step-Index
TE	Transverse Electric
TM	Transverse Magnetic
UV	Ultra-violet
VCSEL	Vertical Cavity Surface Emitting Laser Sources
VLSI	Very Large Scale Integration
VOA	Variable Optical Attenuator
WDM	Wavelength Division Multiplexing

CHAPTER 1

INTRODUCTION

Semiconductor materials, integrated electronic circuit design, and automated micro-fabrication of integrated circuits revolutionized the computing and communicating speeds. The current generation of processing units is limited by the rate of information transfer between processors and its peripheral devices. Increasing processing speed and power is overloading the traffic a bus can handle. The limited bandwidth of bus constitutes a major bottleneck to efficient communications at the board to board data interface. However, currently bandwidth demand is outgrowing the performance of electronics in telecom and data communication networks. To overcome these barriers, we must enter a new computing and communications revolution based on photonics. The development of optical interconnects is desirable in order to achieve higher data throughput. Optical signal transmission and processing require optical interconnection technology designed to overcome bottlenecks resulting from high circuit densities for high data transmission and processing rates from increased data quantities. Photonics devices have already attracted a considerable attention as key elements in optical processing systems.

Photonic networks aim to organize and process signals in optical form as well as transmit them optically, expanding the realm of light. The ultimate goal is all-optical network, in which the transmission signal stays in optical form throughout the network. The huge success of optical dense wavelength division multiplexing (DWDM) has boosted network capacities. The continuing development of optical networks to accommodate future demands will eventually depend on availability of economic, reliable and rugged integrated optical waveguide devices for routing, switching and detection. The success of broadband communications in optical networking, metro/access communications will rely on the advancements in technology to develop economical optical interconnects, optical components or devices e.g. splitters, combiners, multiplexers, de-multiplexers, optical switches/ modulators, filters, variable attenuators, amplifiers etc. based on optical waveguides (Ma 2002) (Takahashi 2003). Broadband communications are penetrating from

metro area, to access, to intra-computer interconnects networks. Optical communication networks have been shown to extend to homes and premises (Green 2005).

Broadband communication can be realized through either guided-wave optics or free-space photonics. For device applications, waveguide structures can be effective in controlling low power optical signals. Optical waveguides may be thin-film deposits used in integrated optical circuits or a filament of dielectric material usually circular in the cross section used in fiber optics. Depending on the various possible patterns of propagating or standing electromagnetic fields, there are single-mode and multi-mode optical waveguides. Glass optical fibers are routinely used for high speed data transfer. Although glass fibers provide a convenient means for carrying optical information over long distances, they are inconvenient for complex high-density circuitry. Besides being fragile and vibration sensitive, optical fiber photonic devices are difficult to fabricate especially when they have a high port count and consequently are expensive.

Large scale deployment of optical communication networks currently is facing prohibitively high cost of components and subsystems. Cost of a component is dictated by the cost of raw materials, fabrication infrastructure and number of fabrication steps involved in producing a device. Polymer based technology has been known to provide low cost solution in production of components. Several devices produced using polymers have already successfully met Telcordia standards (Eldada 2005a). Polymer waveguides offer the potential to create highly complex integrated optical devices and optical interconnects on a planar substrate because their excellent properties can be tailored by using different polymers. Besides permitting mass production of low cost high port count photonic circuits in parallel on a planar substrate, polymer materials provide a much higher degree of ruggedness (Eldada 2000). Cost reduction of the optical modules such as optical splitter is required for the FTTH (Fiber to the homes) or FTTP (Fiber to the premises) market.

To enable widespread deployment of optical networks in a developing economy such as ours, the economical aspects mentioned above will be important and in this the photonic polymers will play a significant role. The demand in optical networking for photonic components that meet performance criteria as well as economic requirements has opened the door for technologies capable of high yield and low cost manufacturing while delivering high

performance and enabling unique functions. Polymeric materials are particularly attractive because of their ability to be processed rapidly, cost-effectively, and with high yields. Of that matter, photonic polymers have been accepted as new generation materials for optical integrated circuit due to their various advantages as compared to other optical materials. The polymer optical waveguide has been a candidate to reduce the cost due to its ease in processing. It is with this vision in mind that this research was undertaken. The outcome of research this research conveniently leads to a technology for mass production of passive polymeric photonic devices.

This chapter presents the background on optical materials used in integrated optics and discuss how gradually polymers became popular in the field. Here, polymeric materials that were reported in literature to develop distinct integrated photonic devices in past are also discussed. Polymer-based integrated photonic components those are necessary in realizing the next generation of integrated planar lightwave circuits are discussed in the chapter. Expensive materials and expensive silicon technology to develop photonic components motivated to take up this research objective. The motive to develop economical devices in the area of photonics is expressed in this chapter. Finally, the content of the chapters following this chapter in the thesis are outlined in the last section of the chapter.

1.1 Background

The phrase *integrated optics* was coined after Miller illuminated the idea of integrating optical circuits on a single substrate (Miller 1969). It was proposed to integrate optical components on a chip to form integrated optical circuits. This led to development of new technologies and materials for affordable devices. Historically, polymer components in optical communications have been pursued by many because of their perceived cost advantage over devices fabricated from high purity silica and glass (Shacklette 2004). Silica is also in common use in planar lightwave circuits (PLC) built with silica-on-silicon technology (Wosinski 2004) (Pal 2009) (Das 2009). PLCs have potential applications at the module and backplane level. Planar waveguides which can function as passive optical interconnects or as active or passive optical devices, are built on a substrate of silicon, glass or another polymer. Specifically, polymer waveguides can also be fabricated on flexible substrates, which is not possible with other competing inorganic materials. Generally, optical

polymer materials used may be either photopolymers or thermally curing polymers. Photopolymers have a distinct advantage over thermosetting polymers in that they can be directly fabricated into waveguides by means of selective photo-patterning using a mask compared to non-selective thermal treatment. Photosensitive materials are rapidly finding broader applications in micro-scale design. Such materials show viability as complete structural components, rather than simply as a means of patterning for subsequent etching and deposition.

Polymer integrated optics technology is particularly well suited for low-cost mass production and allows arrays of many low-power devices to be fabricated on a single substrate. Many research and commercial organizations plan to capitalize on processing flexibility for the fabrication of two-dimensional and three-dimensional integrated optics. With both performance and cost advantages, there are numerous communications and sensing applications for polymer opto-chips including: (i) high speed modulators with higher modulation speed (Leinse 2005), (ii) optical switching (Yuan 2005), (iii) rapidly tunable wavelength filters (Ahn 2005) for DWDM add/drop multiplexing, (iv) broadband electromagnetic field sensors (Gardelein 2006) and (v) higher-level integration of optical components on a single chip (Wang 2008).

The choice of an appropriate polymer materials technology rests on achieving a balance of desired and required properties (Eldada 2002). These desired and required attributes impact both device performance and manufacturing processes. The key performance characteristics which reflect choices for the optimal approach should be low absorption loss, low birefringence and polarization dependent loss, high thermo-optic coefficient, and high chemical and environmental stability (Eldada 2003). Some conventional (C-H containing) low-cost polymeric materials can meet these requirements because they can be deposited up to 100 µm film thickness by simple spin-coating techniques; they can be formulated for direct photo-patterning; their refractive indices can be tuned to yield waveguides with fiber-matched numerical apertures (NAs); and their transparency windows can coincide with the vertical cavity surface emitting laser source (VCSEL) wavelengths. The environmental stability of optical polymers is an important issue because most polymers do not have properties that are appropriate for operation in communication environments. For example,

polymers may be subject to yellowing upon thermal aging due to oxidation (Eldada 2003). The thermal decomposition results in increase in absorption loss but fortunately, this effect is more prominent at 400 – 500 nm, and the thermal stability can be high at the datacom wavelength of 850 nm and even greater at the telecom wavelengths of 1300 and 1550 nm. On humidity front, the resistance of polymers to water incursion is critical since optical absorption results from the overtone bands of the OH-stretch of water (Eldada 2003).

1.1.1 Polymer Optical Materials

The first demonstration of light guiding capabilities of a polymer material was reported in 1970s. In the past three decades, optical polymers were engineered in many laboratories worldwide in academia and industry. Four classes of polymers for use in integrated optics include : deuterated and halogenated polyacrylates (Kim 2007), fluorinated polyimides (Kan 2003), perfluorocyclobutyl aryl ether polymers (olefins) (Wong 2003) and nonlinear optical polymers (Khanarian 2001). Other significant and explored optical polymers include benzocyclobutene (Chen 2007), perfluorovinyl ether cyclopolymer (Chang-Yen 2007), tetrafluoroethylene (Manor 2003), silicone resin (Watanabe 1998), fluorinated poly(arylene ether sulfide) (Kang 2001), poly(pentafluorostyrene) (Asquini 2002), fluorinated dendrimers (Pitois 2002) and fluorinated hyperbranched polymers (Kang 2003). Currently the available optical polymers are highly transparent with absorption loss values below 0.1 dB/ cm at significant wavelength windows (850, 1310, and 1550 nm) (Ma 2002).

Polymethyl-methacrylate (PMMA) (Punke 2007) (Snakenborg 2006) is one of the typical polymers that offer low loss and processability. In visible spectrum, PMMA based polymers have the potential low loss of less than 1dB/m. They suffer from high optical loss in the near-IR region, 1.0 – 1.6 μm. The typical loss for PMMA based polymers in the near-IR region will be around 1 dB/cm. This loss can be reduced by fluorination and/or deuteration of hydrogen atoms in the polymer. Propagation losses as low as 0.1 dB/cm have been reported at a 1300 nm wavelength, however, the losses become relatively high (~1.5 dB/cm) at a 1550 nm wavelength. Single mode devices fabricated with fluorinated polymers show lossy performance comparable to that of silica based devices. The commercially available photodefinable polymers based on acrylate crosslinking form wet films after deposition. Photopatterning can only be done by using masks in the proximity mode, which degrades the

resolution and which is not suited for large uneven substrates like printed circuit boards (PCBs) where conformable (foil) masks have to be used. Moreover, the acrylate (free radical) crosslinking process requires inerting to avoid cure inhibition by ambient oxygen, which adds to the production costs. Photocurable epoxies do not possess these drawbacks. Their different (cationic) cure mechanism allows the processing of dry films with contact masks under normal ambient. In addition, epoxies are well known for their excellent adhesion, durability, dimensional stability, and chemical inertness. The negative photoresist SU-8 (MicroChem Corp.) is a well-known epoxy photopolymer which was also applied in planar optical waveguide applications (Borreman 2002).

SU-8 has received a lot of attentions in the field of microfabrication in last decade because of its mechanical stability, biocompatibility, and suitability for fabricating high aspect ratio features (Williams 2004). The photopatternable, negative tone epoxy resin SU-8 was introduced to the MEMS community in 1990s, originally developed and patented by IBM. SU-8 is a near-ultraviolet (UV) epoxy based negative photoresist formulated in EPON^{TM} SU-8 resin designed to produce uniform films in single spin-coating step. Up till now SU-8 has been extensively used for many applications particularly for structures varying between 1 μm and 1 mm in height and is the most well known because of its outstanding characteristics for high aspect ratio structures, its use as an etch mask, its excellent chemical resistance (cross-linked SU-8 is inert to most commonly used solvents), and it's interesting mechanical and optical properties.

The process capability of SU-8 may be improved by choosing cyclopentanone (CP) as solvent instead of gamma-butyrolactone (GBL) (Shaw 2003). SU-8 (formulated in GBL) and SU-8 2000 (formulated in CP) can cover a wide range of film thicknesses from <1μm to >200μm. SU-8 and SU-8 2000 resists have high functionality, high optical transparency and are sensitive to near UV radiation. Three dimensional complex structures were reported using multidirectional UV lithography (Yoon 2006). Cured SU-8 is highly resistant to solvents, acids and bases and has excellent thermal stability, making it well suited for applications in which cured structures are a permanent part of the device. The SU-8 resist is much harder than PMMA, the hardness of SU-8 being more than twice that of PMMA (Zhong 2005). Hardness is the property of being rigid and resistant to pressure. With higher hardness, SU-8

is also more resistant to scratch than PMMA. Thin-films (< 5 μm) based light guiding stable SU-8 structures still are a subject of interest for research.

When the PLC devices are used in practice, input and output fibers have to be connected to input and output ports of PLC's in order to utilize the integration capability of PLC devices. The fiber-connected devices are required to exhibit not only high optical performance such as low loss, wavelength flatness, low polarization dependence, but also long-term reliability. To attain low loss devices requires a precise connection method. Moreover, since a PLC consisting of a silicon substrate and silica glass is itself very stable, a fiber-to-PLC connection technique will lead directly to a highly reliable PLC device. Therefore, it is necessary to establish a precise connection technique and confirm its long-term stability in order to advance the practical use of PLC's. Up to now, many kinds of connection technique such as fiber fusion splice (Shimizu 1983), laser welding (Miya 1992), and adhesive connection (Wale 1990) have been undertaken. From a viewpoint of simplicity and cost, connection with UV-curable adhesives (Yamada 1992) (Hibino 1994) (Mitachi 2006) (Liu 2000) (Ho 2006) can be considered to be the most advantageous. Besides sufficient mechanical strength, high optical performance such as low loss, low reflection, thermal stability and long-term reliability (Hibino 1995) are obtained through the use of fiber connection technique using UV-curable adhesives.

One such popular UV-curable adhesive is Norland Optical Adhesive 61 (NOA 61). NOA 61 is a clear, colorless, liquid photopolymer that will cure when exposed to ultraviolet light. Curing time is remarkably fast, and is dependent upon the thickness applied and the amount of ultraviolet light energy available. NOA 61 is cured by ultraviolet light with maximum absorption within the range of 320-380 nm with peak sensitivity around 365nm. The recommended energy required for full cure is 3 Joules/sq. cm in these wavelengths. When fully cured, NOA 61 has very good adhesion and solvent resistance. Optimum adhesion can also be obtained by aging at 50° C for 12 hours. After aging, NOA 61 can withstand temperatures from -150° C to 125°C (Norland Products). In the last decade, a few researchers have reported utilizing NOA 61 as a waveguide material (Chang-Yen 2005) (Wong 2001). But the future prospects seem to be good for NOA 61 as refractive index of cured NOA 61

lies near to that of SU-8. Thus, guiding medium of low refractive index difference may be fabricated if SU-8 and NOA 61 are used as core and cladding materials respectively.

1.1.2 Photonic Polymer Devices

Polymer-based optical planar components provide an alternative approach for realizing the next generation of integrated planar lightwave circuits. These components can be integrated on any existing substrate popular in microelectronics industry. The simplest passive optical component is the splitter, a device that distributes optical power incident on the input port into specified power fractions at the output ports. A symmetrical 1 × N splitter divides the power into N ports with a fraction 1/N of the incident power at each output port. Thus, power is reduced by 3 dB at the outputs of 1 × 2 splitter. Optical splitters have been demonstrated using fiber biconic taper (FBT) fiber technology (Kieu 2006) and optical planar splitters have been realized using silica on silicon (Hibino 1994) (Hibino 1995) or polymer waveguides (Choi 2003). While FBT splitters suffered from narrowband performance, vibrational sensitivity, and difficulty in scaling for high port counts, planar splitters suffered from high insertion losses. Most of the splitters reported yet are multimode splitters, while single-mode splitters are still subject of interest for research.

A splitter can be used as one of the building blocks in constructing many components, such as power splitters, multiplexers, demultiplexers and optical switches. A power combiner combines power inputs of different wavelengths to a single output port. The variable optical attenuator (VOA) has attracted attention due its promising application to control the gain of optical amplifiers, thus equalizing the channel powers at add /drop nodes of DWDM systems (Llobera 2006). A VOA can also dynamically regulate the channel powers regardless of fluctuations in the input light power and polarization. A wavelength tunable filter (Kim 2008) is another important device for wavelength division multiplexing (WDM) systems because of its multichannel selectivity. The requirements for a practical tunable filter are high wavelength resolution, low polarization dependence, low levels of cross talk and low insertion loss. Other optical devices include optical amplifiers, arrayed waveguide grating multi-/demultiplexer, tunable optical add/drop multiplexers, thermo-optic switches, electro-optic modulators and optical waveguide sensors. To fully realize the function of polymer optical waveguide devices, the integration of optical source, transmission waveguides,

devices and detectors are necessary. Typical high-density PLC has a relative refractive index difference, $\Delta = 0.45\%$, whereas a typical optical fiber has $\Delta = 0.3\%$. This mismatch in relative refractive index difference increases splice loss between the optical fiber and the PLC chip (Momotsu 1999).

Polymer components needed for the telecom industry include single-mode splitters, couplers, routers, filters and switches. One of the earlier drivers for work with polymer waveguides was the concept of fiber-to-the-home, which raised the possible future need for low cost passive optical components (Ericson 2000). Another device application which takes advantage of special properties of polymer is gratings based tunable filters. Gratings can be printed across the arms of Mach-Zender interferometers to form optical add/drop multiplexers (Eldada 1998). Also, optical add/drop multiplexers may be designed based on Mach-Zender interferometers using 3-dB multimode interference couplers (Eldada 1998). Recent advances that propelled optical interconnects as the wideband technology of choice in datacom include VCSELs, polymer based optical waveguides, economical micro-optical components and low cost fabrication processes. The development of optical interconnects employing polymer waveguides demonstrated high-speed parallel optical data links between transmitting and receiving multichip modules on a board, and from board to board through a backplane (Eldada 2000).

1.2 Research Motivation

The potential of integrating optical circuits on a single substrate in optical communication networks led to development of new technologies and materials for the fabrication of better and economical optical chips. While the basic technologies for design and production of many integrated optical devices are now in place, there is no clear winner yet in the areas of materials. For example, Indium Phosphide based quaternary semiconductor materials are widely employed for waveguide devices (Pruessner 2005), but mainly due to their potential for integration with active devices such as lasers and photo-detectors operating at around 1550 nm. However, semiconductor processing remains complex and expensive, especially at the sales volume presently experienced for optical components. By using manufacturing techniques closely related to those employed for silicon integrated circuits, excellent optical components have already been demonstrated using silica-based planar lightwave circuits

(Miya 2000). The cost issue, high switching power needed in silica based devices, low wavelength tuning range, birefringence leading to polarization dependent loss and temperature dependence of central wavelength of silica based devices, are major problems with the technology (Ma 2002). In cost-sensitive areas of short distance optical communications, like datacom, CATV, optical interconnects in PCBs, and in optical sensing, a urgent need has emerged for low-cost planar waveguide structures to be applied in components like splitters and couplers or integrated in PCBs.

Among the candidate material systems high expectations have been placed on polymers as the materials choice for highly integrated optical components and circuits (Ma 2002). State of the art optical polymers are particularly attractive in integrated optical waveguide devices because they offer rapid processability, cost effectiveness, high yields, high performance, such as lower optical loss and smaller birefringence compared to silica, power efficient thermal actuation due to large thermo-optic coefficient than in silica, and compactness owing to a large refractive index contrast (Eldada 2002). Furthermore, polymers provide an ideal platform for the incorporation of more complex material functionalities through selective doping or reaction, thereby enabling refractive index tuning (Sanghadasa 2006), amplification (Balslev 2005) and electro-optic effects (Worboys 1990) (Wu 1991) (Fan 2012) (Willner 2012) to be achieved, once the passive optical polymer technology is established.

Each of the polymer systems available today has a unique set of properties that make it suitable for specific communication applications. Polymer waveguide technologies that meet optical interconnect requirements are available today. Their adoption has been slow in the computing platform, partly because of the cost of opto-devices and partly because conventional technology has managed to keep up the demand for higher speed. However, it is estimated that fundamental limits of conventional techniques will be reached soon, at which point that transition to optical processing domain is bound to start happening, at backplane, board level and eventually on chip level (Eldada 2005b). Needs of present state of research in polymer based integrated optics are development and characterization of suitable polymeric materials, development of high-yield manufacturing techniques for polymeric photonic devices, and full characterization of the resulting optical circuits. Transmission along single-

mode optical waveguides suffers higher attenuation compared to their optical fiber counterparts due to the waveguide cross-section geometry, surface roughness introduced during fabrication, material defects, etc. However, as the relative length of these devices is small (of the order of a few millimeters), the total propagation loss is not a major problem. Nonetheless, it is necessary to improve on the existing optical fabrication techniques to develop waveguides and devices with lower losses and lower production costs. Fabrication of high performance polymer waveguides and polymer based devices, and integration of board level system remains a challenge as a research topic.

1.3 Objectives and Scope of the Thesis

The major challenges addressed in this thesis work are summarized as follows:

1. Design of SU-8 based single-mode optical waveguides and 1 × N splitters.
2. Fabrication of thin-film SU-8 waveguides based on direct UV photolithography.
3. Characterization of fabricated waveguides and conventional splitter devices.
4. Analyses of defects/issues (if any) induced during process of fabrication and propose a solution for the defect/issue.
5. Fabrication and characterization of the device based on proposed design based on analytical results.
6. Comparison of proposed and conventional splitters characterization results.

Our target was to develop cost effective, stable, efficient polymer based integrated photonic 1 × N power splitters with performance comparable to or better than the devices currently being employed in WDM systems. These devices have to be compatible with the standard fibers combined with light-emitting diodes (LEDs) and VCSELs with their emission wavelength at 1550 nm.

The thesis work was broadly categorized into four components: design, fabrication, characterization and comparative analysis of the results obtained. The schematic designs were developed and optimized for suitable performance through BeamPROP^{TM}, a beam

propagation method (BPM) based simulation tool provided by RSoft design, USA. The fabrication of passive waveguides and splitters was carried out using direct UV lithography. Crucial fabrication parameters such as spin coating speeds, post- and pre-exposure baking temperatures, UV exposure and development times have been established. Characterization had been carried out using techniques like prism-coupling, end-fire coupling, etc. Characteristics like the refractive indices, propagation losses have been established. Characterization of physical aspects such as waveguide cross-section, surface roughness were performed using Scanning Electron Microscopy (SEM) and computer-controlled stylus profilometer. The performance of a passive splitter was analyzed to find a solution for better performance.

1.4 Outline of the Thesis

Chapter 1 outlines the background of polymeric materials and photonic devices developed in the last decade. The chapter discuss the evolution of optical materials used in integrated optics and how polymers became popular in the field. Here, polymeric materials reported in literature in the last few decades to develop integrated photonic devices are also discussed. Polymer-based integrated photonic components those are necessary in realizing integrated planar lightwave circuits due to increase in demand for broadband communication are discussed in the chapter. Expensive materials and expensive silicon technology to develop photonic components motivated to take up this research objective. To develop economical devices in the area of photonics is the foremost motive of this work. Chapter 1 defines the objective, scope of thesis work presented here and finally outlines the organization of this thesis.

Chapter 2 describes the fundamentals of theory of optical waveguides. An introduction to planar and rectangular channel waveguides is presented in the chapter. Guided transverse electric (TE) and transverse magnetic (TM) modes, cutoff conditions for planar and channel waveguides are described in the chapter. An overview of previous work to obtain approximate solutions for modal characteristics of non-planar dielectric waveguides is presented in the chapter. Principles of beam propagation method for mode-solving are discussed in the chapter. Modal cut-off and results of Mode-solving via BeamPROP^{TM} done

for rectangular waveguides for propagating single mode is presented in the last sections of the chapter.

Chapter 3 describes the design and fabrication of Y-branch waveguide which is the basis of the optical power splitter. The conventional Y-branch design for a 1 × 4 power splitter is presented in the chapter. The design of mask for fabrication of 1 × N splitters using L-Edit (Tanner Tools) is presented here. This chapter describes an overview of the micro-fabrication procedures and techniques for polymer waveguides. Finally the details of fabrication process used in this work is presented in the chapter.

Chapter 4 introduces the post-fabrication optical waveguide characterization of splitters. The facilities at Society for Applied Microwave Electronics Engineering & Research (SAMEER), Mumbai and Council of Scientific and Industrial Research - Central Electronics Engineering Research Institute (CSIR-CEERI), Pilani were utilized in waveguide characterization. Characterization aspects e.g. measurements of refractive indices, waveguide modes, waveguide surface analysis, waveguide losses, etc. are presented in the chapter. The experimental techniques for each characterization aspect are also discussed. Preparation of splitter chips using cleaving techniques is described in the chapter. In the last section, this chapter discuss the effect on the device performance in the presence of remnant resist at the splitting junction of the Y-branch.

Chapter 5 explains the proposed design to overcome the non-uniformities in output power distribution brought about by the presence of the remnant residue at Y-junction. The proposed Y-branch with tapered waveguide beam expander is discussed and presented in the chapter. The BPM simulation results of 1 × 4 splitters based on the proposed Y-branch design are presented in the chapter. The fabrication and characterization of the proposed 1 × 4 is presented and also compared with conventional 1 × 4 splitter in the chapter.

Chapter 6 is the final chapter which concludes the work and explores the possible future work that evolves from this present work.

CHAPTER 2

OPTICAL WAVEGUIDE THEORY

With the rapid advance of integrated optics, the significance of optical waveguides which are the fundamental elements of optical integrated circuits, has been widely recognized. Optical waveguides are structures that confine and transmit light over various distances, ranging from tens or hundreds of micrometers in integrated photonics to hundreds or thousands of kilometers in long-distance fiber-optic transmission. The theory of guided wave propagation, excitation, and the conjugation of optical films and strips not only got advanced to encompass all aspects in the analysis and design of these guiding structures, but also precise and reliable technologies had developed to fabricate planar optical waveguides and integrated optical circuits (Unger 1977)(Vassallo 1991). The capability of integrating active and passive components on the same chip allows the implementation of photonic integrated circuits (PIC) for numerous applications.

Optical waveguides confine the optical signals in a region of higher refractive index than its surrounding media. They form essential parts or key structures in many devices such as the waveguides providing optical confinement in semiconductor lasers, being one example. Furthermore, they form important passive photonic devices by themselves, such as corner bent waveguides, which change optical path direction; bent and S-shaped waveguides; tapered waveguides, for smooth expansion of the guide width without mode conversion; branching waveguides, used for both dividing and combining optical power; cross waveguides and directional waveguide couplers, for distributed mode coupling. Waveguide devices in photonic integrated circuits can also be classified as functional devices for optical wave control (Yamada 2006). In functional devices, guided waves are controlled either by electro-optic, magneto-optic, thermo-optic or non-linear optic effects. They are controlled by external input signals to achieve functional devices where the guided mode undergoes amplitude modulation, phase modulation, polarization-state rotation, frequency shift or optical path direction change. Two configurations of optical waveguides, planar slab waveguide and channel waveguide are mostly discussed.

Planar waveguide integrated optics involves the manipulation of sheet beams that are confined in one dimension. By loading a thin film with a higher refractive index than the substrate, the light can be trapped inside this film and waveguides are produced. The light can propagate in any direction parallel to the surface of a high-index guiding layer, which provides optical confinement in a single direction. If the cladding and the substrate materials have the same index of refraction, the waveguide is called symmetric; otherwise the waveguide is called asymmetric. A waveguide in which the index profile has abrupt changes between the core and the cladding is called a step-index (SI) optical waveguide, while the one in which the index profile varies gradually is called a graded-index (GI) optical waveguide.

The most fundamental building block of optical integrated circuits is a channel waveguide. A waveguide optically connect two points within a photonic integrated circuit. In a channel waveguide, the beams propagate along high index guiding channel. The beams are confined in two dimensions and so can only follow predefined pathways in the chip. The straight channel waveguides are the simplest structures for guiding light. These may be formed as ridges on the surface, or as buried channels. Although waveguides come in various forms and with a variety of functions, such as cross waveguides, which are used for combining, the fact remains that optical waveguides that are uniform in the direction of propagation are the most basic form (Mogul 1998). Therefore, the discussion in the following sections will be limited to optical waveguides in which materials constants, such as structure and refractive index, do not change in the direction of propagation.

The following sections of the chapter present an overview of guided-mode theory for planar waveguides which is then used to analyze the case of non-planar waveguides, here i.e., rectangular channel waveguides. The wave equations for solving planar waveguides are derived from Maxwell's equations and its solution can be made about the nature of the propagating field. The analysis of the planar and rectangular channel waveguides involves finding the propagation constants and field profiles of all the modes that the waveguide supports. Guided mode theory has been reported several times in published literature (Pal 2005) (Calvo 2007) (Okamoto 2005) (Snyder 2003) (Chang 2010) (Chen 2006) (Adams

1981) (Tien 1977) (Kapany 1972), to mention a few. For convenience of understanding the guided mode theory is expressed here, in its simplest form, as presented by (Liu 2005).

2.1 Modes in Planar Waveguides

The basic structure of a dielectric optical waveguide consists of a longitudinally extended high-index optical medium, commonly known as the core, which is transversely surrounded by low-index media, called the cladding. Figure 2.1(a) shows a typical three-layer SI planar waveguide, which can be formed by depositing a thin film of higher refractive index on a lower index substrate. The layer of higher refractive index is covered by a low-index layer, or can be left as it is, then air being the low-index cover. In a planar waveguide that has optical confinement in only one transverse direction, the core is sandwiched between upper and lower cladding layers in only one direction, say the x direction, with an index profile $n(x)$, as shown in Fig. 2.1(b). The core of a planar waveguide is sometimes called the film, while the upper and lower cladding layers are called the cover and the substrate, respectively. Optical confinement is provided only in the x direction by the planar waveguide. An optical waveguide that is uniform in the direction of propagation is the most basic type of waveguide. A guided optical wave propagates in the waveguide along its longitudinal direction which is usually taken as z-direction as shown in Fig. 2.1(a).

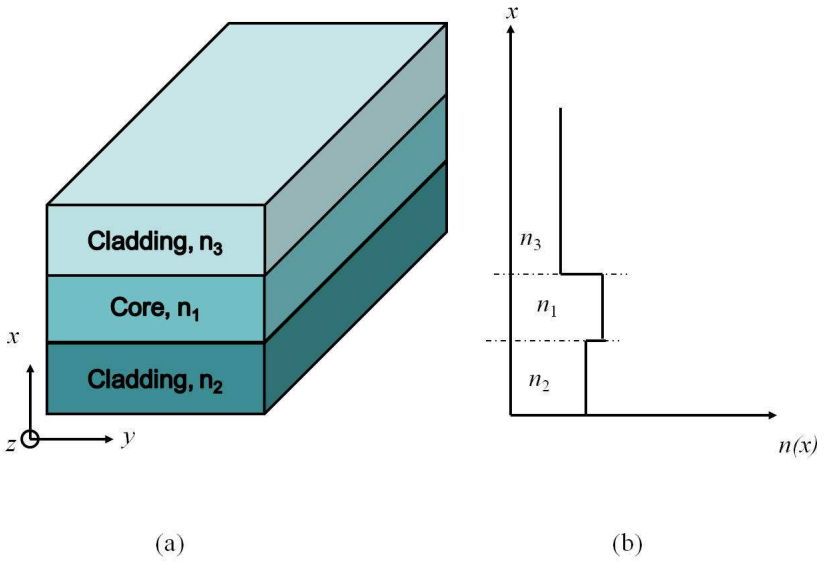

Figure 2.1. (a)Three layer SI planar slab waveguide (b) Refractive index profile.

A waveguide is characterized by the transverse profile of its dielectric permittivity $\varepsilon(x, y)$, which is independent of the z coordinate. For a waveguide made of optically isotropic media, the waveguide can be simply characterize with a single spatially dependent transverse profile of the index of refraction, $n(x)$. Waveguide modes exist that are characteristic of a particular waveguide geometry. A waveguide mode is a transverse field pattern whose amplitude and polarization profiles remain constant along the direction of propagation. Therefore, the electric and magnetic fields of a mode can be expressed in the form,

$$\vec{E}_\nu(r,t) = \vec{E}_\nu(x)e^{(i\beta_\nu z - i\omega t)} \tag{2.1a}$$

$$\vec{H}_\nu(r,t) = \vec{H}_\nu(x)e^{(i\beta_\nu z - i\omega t)} \tag{2.1b}$$

where, ν is the mode index, $\vec{E}_\nu(x)$ and $\vec{H}_\nu(x)$ are the mode field profiles, and β_ν is known as the propagation constant of the mode. For a planar waveguide, the mode fields are independent of the y coordinate. Here, the mode index, ν consists of a single parameter characterizing the field variation in the x dimension.

In a non-planar waveguide of two-dimensional transverse optical confinement, the core is surrounded by cladding in all transverse directions, and the refractive index, $n(x, y)$ is a function of both x and y coordinates. The rectangular channel waveguides, and the optical fibers are such waveguides. Therefore, the electric and magnetic fields of a mode as expressed in (2.1) may be rewritten in a two-dimensional form as follows:

$$\vec{E}_\nu(r,t) = \vec{E}_\nu(x,y)e^{(i\beta_\nu z - i\omega t)} \tag{2.2a}$$

$$\vec{H}_\nu(r,t) = \vec{H}_\nu(x,y)e^{(i\beta_\nu z - i\omega t)} \tag{2.2b}$$

For a waveguide of two-dimensional transverse optical confinement, there are two degrees of freedom in the transverse x-y plane, and consequently, the mode index ν consists of two parameters for characterizing the variations of the mode fields in these two transverse dimensions. For example, ν represents two mode numbers, $\nu = mn$ with integral m and n, for discrete guided modes. To get a general idea of the modes of a dielectric waveguide, the

qualitative behavior of an optical wave in the planar step-index waveguide as shown in Fig. 2.1 (a), where $n_1 > n_2 > n_3$, is considered for further discussion here.

For an optical wave of angular frequency ω and free-space wavelength λ, the propagation constants in the three different regions of the waveguide are defined and expressed as follows:

$$k_1 = n_1 \frac{\omega}{c},\ k_2 = n_2 \frac{\omega}{c}, \text{ and } k_3 = n_3 \frac{\omega}{c}, \text{ where } k_1 > k_2 > k_3 \qquad (2.3)$$

The paths of a plane optical wave, through a high index region in the waveguide, are shown in Fig. 2.2. The characteristics of the reflection and refraction of the wave at the interfaces depend on the angle of incidence θ and the polarization of the wave. There are two critical angles associated with the internal reflections at the lower and upper interfaces:

$$\theta_{c2} = \sin^{-1}\frac{n_2}{n_1}, \text{ and } \theta_{c3} = \sin^{-1}\frac{n_3}{n_1}, \qquad (2.4)$$

respectively. Since $n_2 > n_3$, $\theta_{c2} > \theta_{c3}$.

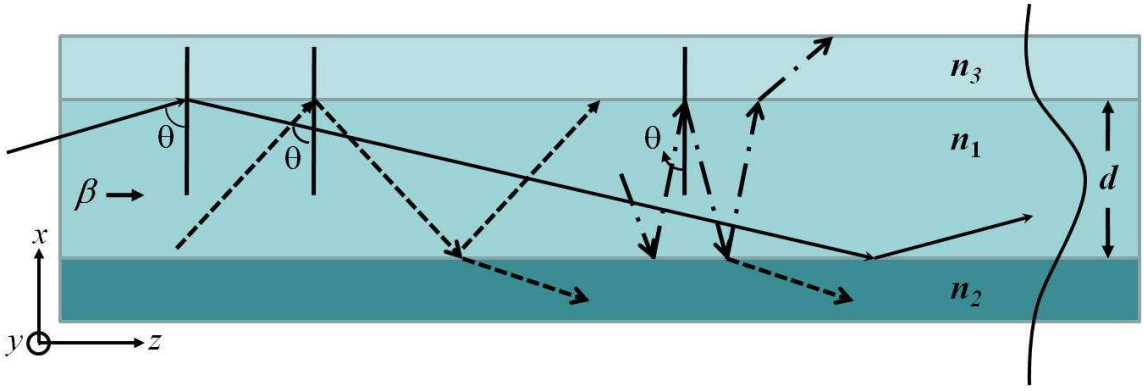

Figure 2.2. Modes in an asymmetric SI planar waveguide where $n_1 > n_2 > n_3$.

If $\theta > \theta_{c2} > \theta_{c3}$, the wave inside the core is totally reflected at both interfaces and is trapped by the core, resulting in guided modes. As the wave is reflected back and forth between the two interfaces, it interferes with itself. A guided mode (path traced by solid line in Fig. 2.2) can exist only when a transverse resonance condition is satisfied so that the repeatedly reflected wave has constructive interference with itself. In the core region, the x component

of the wave vector is $k_1\cos\theta$ for a ray with an angle of incidence θ, while the z component is $\beta = k_1\sin\theta$. The phase shift in the optical field caused by a round-trip transverse passage in the core of thickness d is $2dk_1\cos\theta$.

In addition, there are phase shifts φ_2 and φ_3 associated with the internal reflections at the lower and upper interfaces, respectively. Because φ_2 and φ_3 are functions of θ, the transverse resonance condition for constructive interference in a round-trip transverse passage is

$$2k_1 d\cos\theta + \varphi_2(\theta) + \varphi_3(\theta) = 2m\pi\,, \qquad (2.5)$$

where m is an integer. Because m is an integer, only certain discrete values of θ can satisfy (2.5). This results in discrete values of the propagation constant β_m for guided modes identified by the mode number m. The guided mode with $m = 0$ is called the fundamental mode and those with $m \neq 0$ are high-order modes.

Although the critical angles θ_{c2} and θ_{c3} are independent of the polarization of the wave, the phase shifts, $\varphi_2(\theta)$ and $\varphi_3(\theta)$, caused by internal reflection at a given angle θ depend on the polarization. As a result, TE and TM waves have different solutions for (2.5), resulting in different β_m and different mode characteristics for a given mode number m. For a given polarization, solution of (2.5) yields a smaller value of θ and a correspondingly smaller value of β for a larger value of m. Therefore, β_0 for the fundamental mode has the largest value among the allowed values for β.

When $\theta_{c2} > \theta > \theta_{c3}$, total reflection occurs only at one of the interfaces, here at the upper interface but not at the lower interface. As a result, an incident optical wave refracted at the lower interface is not confined to the core, but is transversely extended to infinity in the substrate. It is called a substrate radiation mode (path traced by dashed line in Fig. 2.2). In this case, the angle θ is not dictated by a resonance condition like (2.5) but can assume any value in the range of $\theta_{c2} > \theta > \theta_{c3}$. As a result, the allowed values of β form a continuum between k_2 and k_3, and the modes are not discrete.

When $\theta_{c2} > \theta_{c3} > \theta$, there is no total reflection at either interface. In this case, an optical wave incident from either side is refracted at both interfaces, and it can transversely extend to infinity on both sides of the waveguide, resulting in substrate–cover radiation modes (path

traced by dash-dot line in Fig. 2.2). These modes are not discrete, and the allowed values of β for them form a continuum between k_3 and 0.

In addition to the three types of modes discussed till now, there are also evanescent radiation modes, which have purely imaginary values of β that are not discrete. Their fields decay exponentially along the z direction. The approach of depicting an optical wave as an optical ray gives an intuitive picture of the waveguide modes and their characteristics. Nevertheless, this approach has many limitations (Marcuse 1991). For a complete description of the waveguide fields, electromagnetic wave equations based analyses are required.

For a linear, isotropic dielectric waveguide characterized by a spatial permittivity distribution of $\varepsilon(x,y)$, Maxwell's equations are expressed as:

$$\nabla \times \vec{E} = -\mu_0 \frac{\partial \vec{H}}{\partial t}, \tag{2.6a}$$

$$\nabla \times \vec{H} = \varepsilon \frac{\partial \vec{E}}{\partial t}, \tag{2.6b}$$

$$\vec{\nabla}.\vec{H} = 0, \tag{2.6c}$$

$$\vec{\nabla}.(\varepsilon\vec{E}) = 0, \Leftrightarrow \vec{\nabla}.\vec{E} = -\frac{\vec{\nabla}\varepsilon}{\varepsilon}.\vec{E}. \tag{2.6d}$$

Because the optical fields in the waveguide have the form of (2.2a) and (2.2b), Maxwell's equations in (2.6a) and (2.6b) may be expressed in the following form:

$$\frac{\partial E_z}{\partial y} - i\beta E_y = i\omega\mu_0 H_x, \tag{2.7a}$$

$$i\beta E_x - \frac{\partial E_z}{\partial x} = i\omega\mu_0 H_y, \tag{2.7b}$$

$$\frac{\partial E_y}{\partial x} - \frac{\partial E_x}{\partial y} = i\omega\mu_0 H_z, \tag{2.7c}$$

and,

$$\frac{\partial H_z}{\partial y} - i\beta H_y = -i\omega\varepsilon E_x , \tag{2.8a}$$

$$i\beta H_x - \frac{\partial H_z}{\partial x} = -i\omega\varepsilon E_y , \tag{2.8b}$$

$$\frac{\partial H_y}{\partial x} - \frac{\partial H_x}{\partial y} = -i\omega\varepsilon E_z , \tag{2.8c}$$

From (2.7) and (2.8), the transverse components of the electric and magnetic fields can be expressed in terms of the longitudinal components:

$$(k^2 - \beta^2)E_x = i\beta\frac{\partial E_z}{\partial x} + i\omega\mu_0\frac{\partial H_z}{\partial y} , \tag{2.9a}$$

$$(k^2 - \beta^2)E_y = i\beta\frac{\partial E_z}{\partial y} - i\omega\mu_0\frac{\partial H_z}{\partial x} , \tag{2.9b}$$

$$(k^2 - \beta^2)H_x = i\beta\frac{\partial H_z}{\partial x} - i\omega\varepsilon\frac{\partial E_z}{\partial y} , \tag{2.9c}$$

$$(k^2 - \beta^2)H_y = i\beta\frac{\partial H_z}{\partial y} + i\omega\varepsilon\frac{\partial E_z}{\partial x} , \tag{2.9d}$$

where,

$$k^2 = \omega^2\mu_0\varepsilon(x, y) , \tag{2.9e}$$

is a function of x and y that accounts for the transverse spatial homogeneity of the waveguide structure.

The relations in (2.9) are generally true for a longitudinally homogeneous waveguide of any transverse geometry and index profile where $\varepsilon(x, y)$ is not a function of z. They are equally true for step-index and graded-index waveguides. Therefore, once the longitudinal field components, E_z and H_z , are known, all field components in a waveguide can be obtained. All other components can be calculated by simply using (2.9a) - (2.9e). The fields in a waveguide can be classified based on the characteristics of the longitudinal field components

as a transverse electric and magnetic mode, or TEM mode ($E_z = 0$ and $H_z = 0$); a transverse electric mode, or TE mode ($E_z = 0$ and $H_z \neq 0$); a transverse magnetic mode, or TM mode ($H_z = 0$ and $E_z \neq 0$); or, a hybrid mode ($E_z \neq 0$ and $H_z \neq 0$). Dielectric waveguides do not support TEM modes and hybrid modes do not appear in planar waveguides but exist in non-planar waveguides of two-dimensional transverse optical confinement.

In general, it is only necessary to find E_z and H_z. The common approach to find E_z and H_z is to solve the wave equations together with boundary conditions. Using the Maxwell equations discussed till now with the vector identity: $\vec{\nabla} \times (\vec{\nabla} \times \vec{A}) = \vec{\nabla}(\vec{\nabla}.\vec{A}) - (\vec{\nabla}.\vec{\nabla})\vec{A}$, we have

$$\nabla^2 \vec{E} + k^2 \vec{E} = -\vec{\nabla}\left(\frac{\vec{\nabla}\varepsilon}{\varepsilon}.\vec{E}\right), \tag{2.10}$$

$$\nabla^2 \vec{H} + k^2 \vec{H} = -\frac{\vec{\nabla}\varepsilon}{\varepsilon} \times \vec{\nabla} \times .\vec{H}\,. \tag{2.11}$$

It can be seen that the three components E_x ,E_y , and E_z for the electric field are generally coupled together because $\vec{\nabla}\varepsilon \neq 0$ in a waveguide. For the same reason, H_x ,H_y , and H_z are also coupled. This fact indicates that the vectorial characteristics of a mode field in a waveguide are strongly dependent on the geometry and refractive index profile of the waveguide.

If the terms on the right-hand sides of (2.10) and (2.11) disappear, then the field components are decoupled. This condition exists only in certain special cases. For example, in the case of a TE mode, $\vec{\nabla}\varepsilon \perp \vec{E}$, so that $\vec{\nabla}\varepsilon.\vec{E} = 0$. As a consequence, each component of the electric field of a TE mode satisfies a homogeneous scalar differential equation. The magnetic field components of a TE mode are still coupled because the right-hand term of (2.11) does not disappear.

The index profile of a step-index waveguide is piecewise constant. A homogeneous wave equation can be separately written for each region of constant ε because $\vec{\nabla}\varepsilon = 0$ within each region. By taking $\vec{E}$ and $\vec{H}$ in the forms of (2.2a) and (2.2b) respectively, and using (2.10) and (2.11) with $\vec{\nabla}\varepsilon = 0$ for each region of constant ε, we obtain,

$$\frac{\partial^2 E_z}{\partial x^2} + \frac{\partial^2 E_z}{\partial y^2} + \left(k_i{}^2 - \beta^2\right) E_z = 0\,, \tag{2.12}$$

$$\frac{\partial^2 H_z}{\partial x^2} + \frac{\partial^2 H_z}{\partial y^2} + \left(k_i{}^2 - \beta^2\right) H_z = 0\,. \tag{2.13}$$

where,

$$k_i^2 = \omega^2 \mu_0 \varepsilon_i = n_i^2 \frac{\omega^2}{c^2} \tag{2.14}$$

is a constant for region *i*, which has a constant index of refraction n_i. Similarly, a homogeneous equation can be written for each of the four field components, E_x ,E_y ,H_x , and H_y. However, it is not necessary to solve the wave equations for all field components because the transverse field components can be found from E_z and H_z using the relations in (2.9a) to (2.9d), once E_z and H_z are found. Therefore, the mode field pattern can be obtained by solving only (2.12) and (2.13) for each region of constant index and by requiring the fields to satisfy the boundary conditions at the interfaces between neighboring regions. Clearly, this approach does not work for graded-index waveguides because (2.12) and (2.13) are not valid for such waveguides.

2.2 Step-Index Planar Waveguides

A step-index planar waveguide is also called a slab waveguide. The structure and parameters of the three-layer slab waveguide assumed for discussion here in this section is shown in Fig. 2.3. The mode properties of a waveguide are commonly characterized in terms of a few dimensionless normalized waveguide parameters. The normalized frequency and waveguide thickness, also known as the *V* number, of a step-index planar waveguide is defined as follows:

$$V = \frac{2\pi}{\lambda} d\sqrt{n_1^2 - n_2^2} = \frac{\omega}{c} d\sqrt{n_1^2 - n_2^2}\,, \tag{2.15}$$

where, *d* is the thickness of the waveguide core. The propagation constant β can be represented by the following normalized guide index:

$$b = \frac{\beta^2 - k_2^2}{k_1^2 - k_2^2} = \frac{n_\beta^2 - n_2^2}{n_1^2 - n_2^2}, \tag{2.16}$$

where $n_\beta = c\beta/\omega = \beta\lambda/2\pi$ is the effective refractive index of the waveguide mode that has a propagation constant β. The measure of the asymmetry of the waveguide is represented by an asymmetry factor a, which depends on the polarization of the mode under consideration.

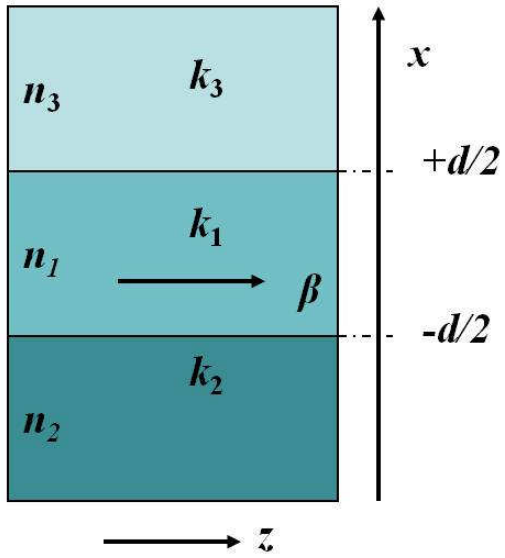

Figure 2.3. Three-layer planar slab waveguide

For TE modes, we have,

$$a_E = \frac{n_2^2 - n_3^2}{n_1^2 - n_2^2}. \tag{2.17}$$

Similarly, for TM modes, we have,

$$a_M = \frac{n_1^4}{n_3^4}\frac{n_2^2 - n_3^2}{n_1^2 - n_2^2}. \tag{2.18}$$

For a given asymmetric structure, the asymmetry factor for TM mode is greater than for TE mode i.e. $a_M > a_E$. For symmetric waveguides, the refractive index of upper and lower layers is same i.e. $n_3 = n_2$ and as a result, $a_E = a_M = 0$.

As discussed earlier in section 2.1 for a guided mode, the allowed values of β are $k_1 > \beta > k_2 > k_3$. Therefore, positive real parameters h_1, γ_2, and γ_3 exist such that,

$$k_1^2 - \beta^2 = h_1^2, \tag{2.19}$$

$$\beta^2 - k_2^2 = \gamma_2^2, \tag{2.20}$$

$$\beta^2 - k_3^2 = \gamma_3^2. \tag{2.21}$$

As per the discussions leading to (2.5), it can be seen from (2.19) that $h_1 = k_1 \cos\theta$, which has the meaning of the transverse component of the wave-vector in the core region of a refractive index n_1.

For a guided mode, the transverse components of the wave-vectors in the substrate and cover regions given by,

$$h_2^2 = k_2^2 - \beta^2, \tag{2.22}$$

and,

$$h_3^2 = k_3^2 - \beta^2, \tag{2.23}$$

respectively, are purely imaginary because $\beta > k_2 > k_3$. The field of the guided mode has to decay exponentially in the transverse direction in the substrate and cover regions with $\gamma_2 = |h_2|$ and $\gamma_3 = |h_3|$ being the decay constants in these regions. For a substrate radiation mode, $k_1 > k_2 > \beta > k_3$. Then h_2 can be chosen to be real and positive and (2.20) is replaced by (2.22) while (2.21) is still valid in this case. For a substrate–cover radiation mode, $k_1 > k_2 > k_3 > \beta$. Then both h_2 and h_3 are real and positive. In this case, in addition to replacing (2.20) with (2.22), (2.21) is replaced by (2.23).

The transverse field pattern of a mode is characterized by the transverse parameters h_1, γ_2 (or h_2), and γ_3 (or h_3). Because k_1, k_2, and k_3 are well-defined parameters of a given waveguide, the only parameter that has to be determined for a particular waveguide mode is the longitudinal propagation constant β. Therefore, a waveguide mode is completely specified by

its β. Alternatively, if any one of its transverse parameters, such as h_1 is determined, the value of its β is also determined, by (2.19), and the mode is completely specified.

2.3 Guided TE and TM modes

Homogeneous wave equations exist for planar waveguides of any index profile $n(x)$. For a planar waveguide, the modes are either TE or TM. Furthermore, it is assumed that the waveguide is infinite in extent along y-axis and $\partial/\partial y = 0$, because the index profile is independent of the y coordinate. The wave equations thus become substantially simplified.

For any TE mode of a planar waveguide, $E_z = 0$. It can be seen from (2.9a) to (2.9d) that $E_x = H_y = 0$ as well because $\partial H_z/\partial y = 0$. The only non-disappearing field components are H_x , E_y , and H_z . Because E_y is the only non-disappearing electric field component, the wave equation for E_y is decoupled from the other field components. Therefore, we have

$$\frac{\partial^2 E_y}{\partial x^2} + (k^2 - \beta^2)E_y = 0\,, \tag{2.24}$$

where,

$$k^2 = \omega^2 \mu_0 \varepsilon(x) = \frac{\omega^2}{c^2} n^2(x)\,. \tag{2.25}$$

Using (2.7a) and (2.7c), the other two non-disappearing field components that can be obtained from E_y are,

$$H_x = -\frac{\beta}{\omega\mu_0} E_y\,, \tag{2.26}$$

$$H_z = -\frac{1}{i\omega\mu_0}\frac{\partial E_y}{\partial x}\,. \tag{2.27}$$

The fields of a TE mode are obtained by solving (2.24) for E_y and by using (2.26) and (2.27) for H_x and H_z, respectively. The boundary conditions require that E_y, H_x, and H_z be continuous at the interfaces at $x = \pm d/2$ between layers of different refractive indices as

shown in Fig. 2.3. From (2.26) and (2.27), it can be seen that this is equivalent to requiring E_y and $\partial E_y/\partial x$ be continuous at these interfaces.

For a guided mode, h_1, γ_2, and γ_3 defined in section 2.2 have to be used, for the transverse field parameters in the core, substrate, and cover regions, respectively. The solutions of (2.24) and the requirement of the boundary conditions yield the following mode field distribution:

$$\hat{E}_y = C_{TE}\begin{cases}\cos(h_1 d/2-\psi)\exp[\gamma_3(d/2-x)], & x > d/2,\\ \cos(h_1 x-\psi), & -d/2 < x < d/2,\\ \cos(h_1 d/2+\psi)\exp[\gamma_2(d/2+x)], & x < -d/2,\end{cases} \tag{2.28}$$

and, the following eigenvalue equations

$$\tan h_1 d = \frac{h_1(\gamma_2+\gamma_3)}{h_1^2-\gamma_2\gamma_3}, \tag{2.29}$$

and,

$$\tan 2\psi = \frac{h_1(\gamma_2-\gamma_3)}{h_1^2+\gamma_2\gamma_3}. \tag{2.30}$$

where, ψ represents spatial phase of mode-field distribution in radians. Normalization of the mode field in (2.28) yields,

$$C_{TE} = \sqrt{\frac{\omega\mu_0}{\beta d_E}}, \tag{2.31}$$

where,

$$d_E = d + \frac{1}{\gamma_2} + \frac{1}{\gamma_3} \tag{2.32}$$

is the effective waveguide thickness for a guided TE mode.

For any TM mode of a planar waveguide, $H_z = 0$. Then, $H_x = E_y = 0$ because $\partial E_z/\partial y = 0$. The only non-disappearing field components are E_x, H_y, and E_z. Similar to the case of TE mode, H_y is the only non-disappearing magnetic field component, and the wave equation for H_y is decoupled from the other field components. From (2.11), we have

$$\frac{\partial^2 H_y}{\partial x^2} + (k^2 - \beta^2) H_y = \frac{1}{\varepsilon}\frac{d\varepsilon}{dx}\frac{\partial H_y}{\partial x}, \tag{2.33}$$

where $k^2 = k^2(x)$ is the same as defined by (2.25). The other two non-disappearing field components can be obtained from H_y:

$$E_x = \frac{\beta}{\omega\varepsilon} H_y, \tag{2.34}$$

$$E_z = -\frac{1}{i\omega\varepsilon}\frac{\partial H_y}{\partial x}. \tag{2.35}$$

In the case of a planar waveguide, it is convenient to solve for the unique transverse field component first: E_y for a TE mode and H_y for a TM mode. The other field components, including the longitudinal component, then follow directly. Although there is only one non-disappearing longitudinal field component for each type of mode in a planar waveguide, it is coupled to a transverse field component. For example, H_z of a TE mode is coupled to H_x and is not described by a simple equation of the form of (2.24).

The fields of a TM mode are obtained by solving (2.33) for H_y and by using (2.34) and (2.35) for E_x and E_z, respectively. Note that for the step-index waveguide considered here, $d\varepsilon/dx = 0$ in each waveguide layer except at the boundaries. The boundary conditions require that H_y, εE_x, and E_z be continuous at the interfaces at $x = \pm d/2$ between layers of different refractive indices as shown in Fig. 2.3. Note that E_x is not continuous because it is the electric field component normal to the interfaces where discontinuities in ε occur. Similarly, $\partial H_y/\partial x$ is not continuous at the interfaces. Rather, it is $\varepsilon^{-1}\partial H_y/\partial x$, or $n^{-2}\partial H_y/\partial x$, that is continuous at the interfaces. Therefore, the boundary conditions are simply that H_y and $n^{-2}\partial H_y/\partial x$ are continuous at the interfaces.

For a guided TM mode, the solutions of (2.33) and the boundary conditions yield the following mode field distribution:

$$\hat{H}_y = C_{TM}\begin{cases}\cos(h_1 d/2-\psi)\exp[\gamma_3(d/2-x)], & x > d/2,\\ \cos(h_1 x-\psi), & -d/2 < x < d/2,\\ \cos(h_1 d/2+\psi)\exp[\gamma_2(d/2+x)], & x < -d/2,\end{cases} \tag{2.36}$$

and, the following eigenvalue equations:

$$\tan h_1 d = \frac{(h_1/n_1^2)(\gamma_2/n_2^2+\gamma_3/n_3^2)}{(h_1/n_1^2)^2-\gamma_2\gamma_3/n_2^2 n_3^2}, \tag{2.37}$$

and,

$$\tan 2\psi = \frac{(h_1/n_1^2)(\gamma_2/n_2^2-\gamma_3/n_3^2)}{(h_1/n_1^2)^2+\gamma_2\gamma_3/n_2^2 n_3^2}. \tag{2.38}$$

Normalization of the mode field in (2.36) yields,

$$C_{TM} = \sqrt{\frac{\omega\varepsilon_0 n_1^2}{\beta d_M}}, \tag{2.39}$$

where, the effective waveguide thickness for a guided TM mode is,

$$d_M = d + \frac{1}{\gamma_2 q_2} + \frac{1}{\gamma_3 q_3}, \tag{2.40}$$

and,

$$q_2 = \frac{\beta^2}{k_1^2} + \frac{\beta^2}{k_2^2} - 1, \tag{2.41}$$

$$q_3 = \frac{\beta^2}{k_1^2} + \frac{\beta^2}{k_3^2} - 1. \tag{2.42}$$

2.4 Modal Dispersion

Guided modes have discrete allowed values of β and are determined by the allowed values of h_1 as β and h_1 are directly related to each other through (2.19). Because γ_2 and γ_3 are uniquely determined by β through (2.20) and (2.21), respectively, they are also uniquely determined by h_1. In terms of the normalized waveguide parameters, we have

$$\gamma_2^2 d^2 = \beta^2 d^2 - k_2^2 d^2 = V^2 - h_1^2 d^2, \tag{2.43}$$

$$\gamma_3^2 d^2 = \beta^2 d^2 - k_3^2 d^2 = (1 + a_E) V^2 - h_1^2 d^2, \tag{2.44}$$

Therefore, there is only one independent variable h_1 in the eigenvalue equations, (2.29) for TE modes and (2.37) for TM modes. The solutions of (2.29) yield the allowed parameters for guided TE modes, while those of (2.37) yield the parameters for guided TM modes. A transcendental equation such as (2.29) or (2.37) is usually solved graphically by plotting its left- and right-hand sides as a function of $h_1 d$ while using (2.43) and (2.44) to replace γ_2 and γ_3 by expressions in terms of $h_1 d$. The solutions yield the allowed values of β, or the normalized guide index b, as a function of the parameters a and V.

Typical Modal-dispersion curves (Kogelnik 1974) that reflects normalized guide index b as a function of normalized frequency V for the lowest three TE mode orders for various degrees of asymmetry i.e for various values of a_E are shown in Fig. 2.4. The plot of V versus b with a as a parameter provides a universal plot for any waveguide. The values of b can be obtained by substituting effective index in (2.16). Higher values of b indicate stronger guidance of mode, while $b = 0$ represents the cut-off condition for the mode.

For a given waveguide, a guided TE mode has a larger propagation constant than the corresponding TM mode of the same order:

$$\beta_m^{TE} > \beta_m^{TM} \tag{2.45}$$

However, for ordinary dielectric waveguides where $n_1 - n_2 << n_1$, the difference is very small. This simplification is known as weak-guidance approximation. Generally, waveguides have a slight variation of the refractive index over their cross-sections, hence index

difference forming the guide is small in practical guides, especially for the two-dimensional refractive index distributions that occur in channel waveguides or optical fibers. Then Fig. 2.4 can be used approximately for TM modes with $a = a_M$.

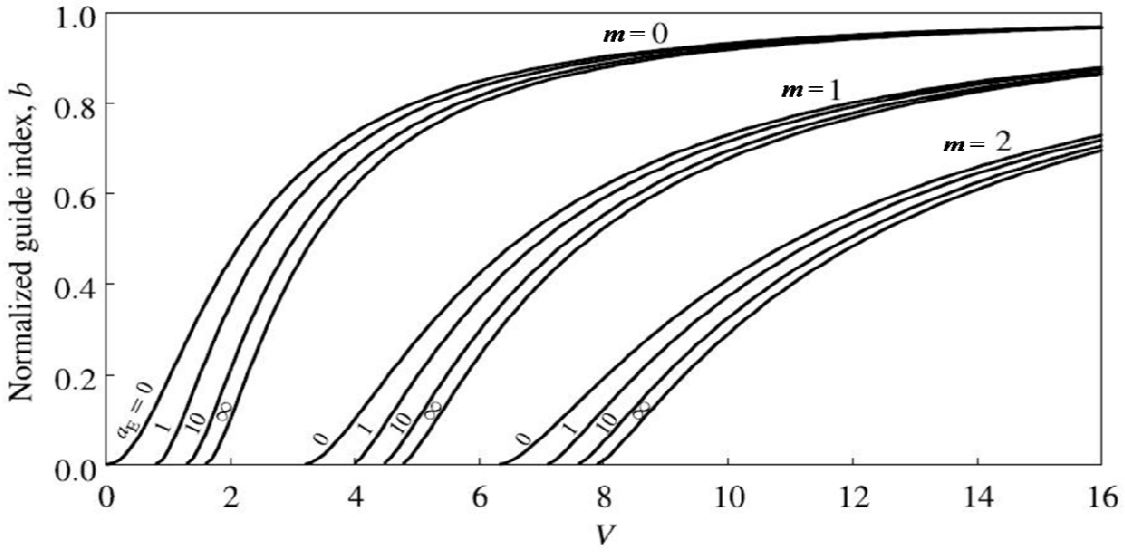

Figure 2.4: Normalized dispersion *V*-*b* curves for TE modes.

For a given waveguide, the values of a_E and a_M, as well as those of d and $n_1^2 - n_2^2$, are fixed. Then, β is a function of optical frequency ω because V depends on ω. Comparing β, k_1, and k_2, it is seen that the propagation constant of a waveguide mode has a frequency dependence contributed by the structure of the waveguide in addition to that due to material dispersion. This extra contribution also causes different modes to have different dispersion properties, resulting in the phenomenon of modal dispersion. Polarization dispersion also exists because TE and TM modes generally have different propagation constants. Polarization dispersion is very small in weakly guiding waveguides where $n_1 - n_2 << n_1$.

2.5 Cut-off Conditions

As discussed in section 2.2, γ_2 and γ_3 are real and positive for a guided mode, so that the fields of the mode decay exponentially in the transverse direction outside the core region and remain bound to the core. This is equivalent to the condition that the optical wave in the core is totally reflected by both interfaces i.e. $\theta > \theta_{c2} > \theta_{c3}$ as illustrated in Fig. 2.2. Because $\theta_{c2} > \theta_{c3}$, the transition from a guided mode to an unguided radiation mode occurs when $\theta = \theta_{c2}$.

This corresponds to the condition that $\beta = k_2$ and $\gamma_2 = 0$. As can be seen from the mode field solutions in (2.28) and (2.36), the fields extend to infinity on the substrate side for $\gamma_2 = 0$. This defines the cutoff condition for guided modes. The cutoff condition is determined by $\gamma_2 = 0$, rather than by $\gamma_3 = 0$, because $\gamma_3 > \gamma_2$ and γ_2 reaches zero first as their values are reduced. The cutoff value V_c for a guided mode is the value of V at the point where the b versus V curve shown in Fig. 2.4 intersects with the horizontal axis $b = 0$.

From (2.43) and (2.44), we find by setting $\gamma_2 = 0$ that,

$$h_1 d = V_c \text{ and } \gamma_3 d = \sqrt{a_E} V_c , \tag{2.46}$$

at cutoff. Substitution of (2.46) and $\gamma_2 = 0$ in (2.29) for a guided TE mode yields,

$$\tan V_c = \sqrt{a_E} . \tag{2.47}$$

Therefore, the cutoff condition for the m^{th} guided TE mode is,

$$V_m^c = \tan^{-1} \sqrt{a_E} + m\pi , \text{ m = 0, 1, 2,…} \tag{2.48}$$

Similarly, the cutoff condition for the m^{th} guided TM mode can be derived as follows:

$$V_m^c = \tan^{-1} \sqrt{a_M} + m\pi , \text{ m = 0, 1, 2,…} \tag{2.49}$$

Because $a_M > a_E$ for a given asymmetric waveguide, the value of V_c for a TM mode is larger than that for a TE mode of the same order.

Using (2.15), we can write,

$$V_m^c = \frac{2\pi}{\lambda_m^c} d\sqrt{n_1^2 - n_2^2} = \frac{\omega_m^c}{c} d\sqrt{n_1^2 - n_2^2} \tag{2.50}$$

where, λ_m^c is the cutoff wavelength and ω_m^c is the cutoff frequency of the m^{th} mode. The m^{th} mode is not guided at a wavelength longer than λ_m^c, or a frequency lower than ω_m^c. For given waveguide parameters, (2.48) and (2.49) can be used with (2.50) to determine the cutoff wavelengths of TE and TM modes, respectively. For a given optical wavelength, they can be used to determine the waveguide parameters that allow the existence of a particular guided

mode. For given waveguide parameters and optical wavelength, they can be used to determine the number of guided modes for the waveguide. Therefore, for a given optical wavelength and a waveguide with a given V number, the total number of guided TE modes is simply

$$M_{TE} = \left[\frac{V}{\pi} - \frac{1}{\pi} \tan^{-1} \sqrt{a_E} \right]_{\text{int}}, \tag{2.51}$$

while that of the guided TM modes is

$$M_{TM} = \left[\frac{V}{\pi} - \frac{1}{\pi} \tan^{-1} \sqrt{a_M} \right]_{\text{int}} \tag{2.52}$$

where $[\ ]_{\text{int}}$ means the nearest integer larger than the value in the bracket. A waveguide with $M = 1$ that supports only the fundamental TE_0 and/or TM_0 mode is called a single-mode waveguide. A waveguide that supports high-order modes is called a multimode waveguide.

2.6 Symmetric Slab Waveguides

In a symmetric slab waveguide, $n_3 = n_2$ and $a_E = a_M = 0$. In addition, we also have $\gamma_3 = \gamma_2$. Then, it can be seen from (2.28) and (2.38) that $\tan 2\psi = 0$ and

$$\psi = \frac{m\pi}{2}, \; m = 0, 1, 2, \ldots \tag{2.53}$$

for both TE and TM modes. Therefore, the mode field patterns of a symmetric waveguide given by (2.28) and (2.36) are either even functions of x with $\cos h_1 x$ in the region $-d/2 < x < d/2$ for even values of m or odd functions of x with $\sin h_1 x$ in the region $-d/2 < x < d/2$ for odd values of m. This characteristic is expected because the mode field pattern in a symmetric structure is either symmetric or anti-symmetric.

Since $\gamma_3 = \gamma_2$, the eigenvalue equation (2.29) for TE modes can be transformed using basic trigonometric identities to the following two equations:

$$\tan \frac{h_1 d}{2} = \frac{\gamma_2}{h_1}, \text{ for even modes,} \tag{2.54}$$

$$-\cot\frac{h_1 d}{2} = \frac{\gamma_2}{h_1}\ \text{, for odd modes,} \tag{2.55}$$

which yield the allowed parameters of guided TE modes. Equation (2.54) and (2.55) can be combined in one eigenvalue equation for all guided TE modes:

$$\tan\left(\frac{h_1 d}{2} - \frac{m\pi}{2}\right) = \frac{\gamma_2}{h_1} = \frac{\sqrt{V^2 - h_1^2 d^2}}{h_1 d},\ m = 0, 1, 2,\ldots \tag{2.56}$$

where m is the same mode number as the one in (2.53). Using (2.37), a similar procedure yields,

$$\tan\left(\frac{h_1 d}{2} - \frac{m\pi}{2}\right) = \frac{n_1^2}{n_2^2}\frac{\gamma_2}{h_1} = \frac{n_1^2}{n_2^2}\frac{\sqrt{V^2 - h_1^2 d^2}}{h_1 d},\ m = 0, 1, 2,\ldots \tag{2.57}$$

for guided TM modes. The solutions of (2.56) and (2.57) yield the allowed values of $h_1 d$ for a given value of the waveguide parameter V for both even and odd TE modes as well as TM modes, respectively.

Since $a_E = a_M = 0$, TE and TM modes of a symmetric waveguide have the same cutoff condition:

$$V_m^c = m\pi \tag{2.58}$$

for alike m^{th} TE and TM modes. Because $m = 0$ for the fundamental modes, neither fundamental TE nor fundamental TM mode in a symmetric waveguide has cutoff. When $0 < V < \pi$, any symmetric dielectric waveguide supports at least one TE and one TM mode in the waveguide, and the waveguide is referred to as a single mode waveguide. The number of TE and TM modes supported by a given symmetric waveguide is simply

$$M_{TE} = M_{TM} = \left[\frac{V}{\pi}\right]_{\text{int}} \tag{2.59}$$

These conclusions are unique to symmetric waveguides. They are not true for an asymmetric waveguide. For instance, a guided mode for an asymmetric slab waveguide at a given optical

frequency may not exist because both its fundamental TE and TM modes have a nonzero cutoff.

2.7 Channel Waveguides

Till now, we have discussed the characteristics of planar waveguides. Practically, non-planar waveguides are mostly used in device applications. The index profile $n(x, y)$ of a non-planar waveguide is a function of both transverse coordinates x and y. There are different types of non-planar waveguides that have distinct index profiles or cross-sectional geometries. Two examples of non-planar waveguides are optical fibers of circular cross-section and rectangular cross-section channel waveguides. The latter is dealt in this thesis work, hence, is discussed in detail in the following paragraphs.

A channel waveguide offers two-dimensional confinement of light in x- and y-directions as opposed to one dimensional light-confinement in only x-direction offered by planar or slab waveguides. Various types of channel waveguides with rectangular cross-section may be developed such as buried channel waveguide, the strip-loaded waveguide, the ridge waveguide, the rib waveguide, and the embedded waveguide. Cross-sections of the channel waveguides just mentioned above are depicted in Fig. 2.5. Types of waveguides shown collectively in Fig. 2.5 usually classify as rectangular waveguides with a thickness d in the x direction and a width w in the y direction, though their shapes practically are not exactly rectangular. A buried channel waveguide is formed with a high-index core buried in a low-index surrounding medium. The core can have any cross-sectional geometry though it is often intended to have a rectangular shape, as shown in Fig. 2.5(a). A strip-loaded waveguide is formed by loading a planar waveguide, which already provides optical confinement in the x direction, with a dielectric of index $n_3 < n_1$ as shown in Fig. 2.5(b). The light guiding core of a strip waveguide is the high-index region n_1 under the loading strip of index $n_2 < n_1$. The thickness h and width of n_1 layer is determined by the thickness d and width w of the loading strip.

A ridge waveguide, shown in Fig. 2.5(c), has a structure that looks like a strip waveguide, but the strip, on top of its planar structure has a high index and is actually the light guiding core. A ridge waveguide has strong optical confinement because it is surrounded on three sides by

low-index n_3 and on one side by low-index n_2. A rib waveguide, shown in Fig. 2.5(d) has a structure similar to that of a strip or ridge waveguide, but the strip has the same index as the high-index planar layer beneath it and is part of the light guiding core. An embedded waveguide shown in Fig. 2.5(e) is formed by creating a high-index region in a substrate through diffusion of dopants, such as a $LiNbO_3$ waveguide with a core formed by Ti diffusion. Because of the diffusion process, the core boundaries in the substrate are not sharply defined. However, an embedded or a diffused waveguide also has a thickness *d* defined by the diffusion depth of the dopant in the *x* direction and a width *w* defined by the distribution of the dopant in the *y* direction.

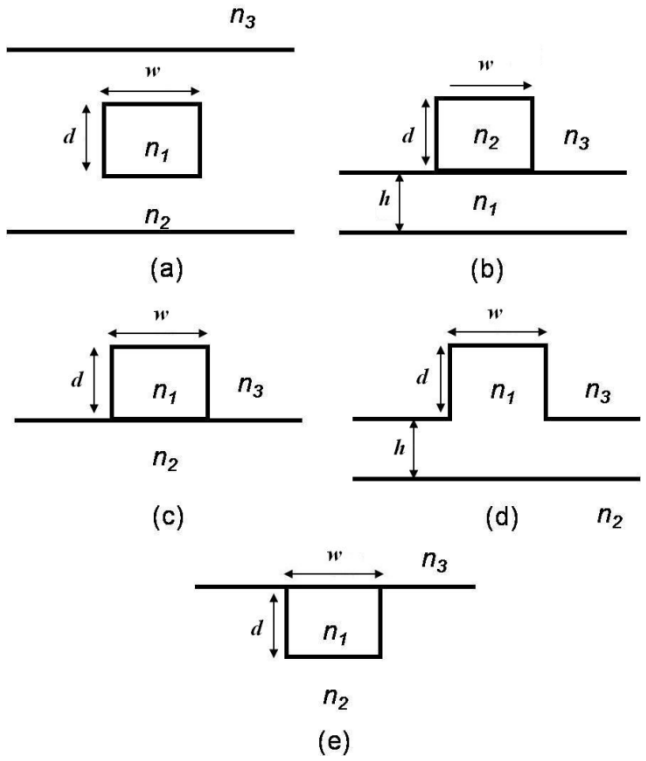

Figure 2.5. Cross-sections of channel waveguides (a) buried-channel guide, (b) strip-loaded guide, (c) ridge guide, (d) rib guide, (e) embedded guide.

Channel waveguides are used mostly in guided-wave devices such as a directional coupler, Y-branch splitter, waveguide laser, guided-wave modulator, waveguide photodetector, waveguide demultiplexer, ring resonator, waveguide filter, etc. Properties of the channel guided-wave mode which are most important to these applications are the effective index, the

attenuation rate, the polarization of the mode, and the evanescent tails. Most channel waveguide devices are a few centimeters or less in length. Thus, unlike optical fibers, any reasonable attenuation rate, such as a few dB/cm or less, may be acceptable in many practical applications.

Different modes superpose with different phase at different values of propagation lengths as a consequence of which the transverse intensity distribution will vary with propagation lengths. There is no transfer of power between the modes and power associated with each mode remains the same as the field propagates. However, at different values of propagation distances, the two modes interfere with different phases, resulting in a varying transverse intensity pattern. Channel waveguide devices often involve one guided-wave mode interacting with another guided-wave mode. Periodic perturbations in waveguide parameters may result in mode-coupling i.e. power transfer between two modes (Ghatak 1998).

2.8 Approximate Analyses of Guided Modes

The dielectric waveguide used in photonic integrated circuits typically need to be single mode, although multimode guides are utilized in many applications too. Thus, modal analysis is a critical part of the design process that provides information on the modes that may propagate; their propagation constants and mode shapes. The most fundamental requirement is to find the optical modes that may propagate in a given waveguide structure. Mode solving techniques are required to address this fundamental requirement. All the mode solvers assume that the waveguide section is uniform in the propagation direction resulting in the assumption that the variation in this direction is $e^{i\beta z}$, where β is the propagation constant. The task of mode solvers for a given waveguide cross-section and a specified value of operating frequency or wavelength is to determine the values of β and the corresponding modal pattern for each desired mode.

Except for those few exhibiting special geometric structures, such as optical fibers with circular cross-sections, non-planar dielectric waveguides with rectangular cross-sections generally do not have analytical solutions for their guided mode characteristics. For the analysis of these channel waveguide modes, one can make use of several approximation and numerical methods. Some of the approximation methods are: Marcatili's method (Marcatili

1969); and the effective index method (EIM) (Knox 1970); out of which due to simplicity, the effective index method shall be discussed in the following section. The effective index method has one advantage over Marcatali's method and that is, the propagation constant is easily obtained by a short calculation. If the field distribution are required as well as the propagation constant, however, Marcatali's method must be chosen (Nishihara 1985).

Nonetheless, there are no exact analytical solutions for the modes of the channel waveguides, even in the limit of the weak-guidance approximation. One has to depend on numerical methods to obtain accurate solutions of the scalar wave equation for waveguides with rectangular core cross-sections. Some of the numerical methods that exist for analyzing channel waveguides include: Fourier decomposition method (FDM) (Henry 1989), finite element method (FEM) (Yeh 1979)(Rahman 1984) and BPM (Feit 1978). BPM simplifies the guided wave problem by reducing the computational complexity and thus, speeding up the computational process. Here, in this work, a commercial optoelectronic CAD software BeamPROP^{TM} (from RSoft Inc., USA) based on the beam propagation method (BPM), was used to evaluate modal characteristics of polymer waveguides.

2.8.1 Effective Index Method

The effective index method is one of the simplest of all the methods and provides reasonably accurate results. The basic concept of the effective index method illustrated in Fig. 2.6 is to convert the problem of a channel waveguide into that of two planar waveguides. The effective index method is a good approximation only if the waveguide satisfies the following two conditions:

(i) the waveguide width is larger than its thickness, i.e., $\frac{w}{d} > 1$; and,

(ii) wave guiding in the *y* direction across its width is not stronger than that in the *x* direction across its thickness.

The effective index method applies to both step-index and graded-index channel waveguides, as long as the above two conditions are satisfied. When these two conditions are satisfied, the characteristics of the guided modes are primarily determined by the layered structure

perpendicular to the x direction, much like a planar waveguide of thickness d, but are modified by a lateral structure of width w. The planar structure defines TE and TM polarizations, but the lateral structure distorts them. Therefore, a mode with its electric field mostly in the y direction parallel to the planar layers is called a TE-like mode, and one with its magnetic field mostly in this direction is called a TM-like mode (Nishihara 1985). One distinctive property of non-planar dielectric waveguides versus planar waveguides is that a non-planar waveguide supports hybrid modes, whereas a planar waveguide supports only TE and TM modes. In principle, guided-wave modes of channel waveguides are hybrid modes, meaning that there are field components in all x, y, and z directions. However, from the effective index analysis, it is clear that guided-wave modes can be considered as total internal reflection of the TE_m (or TM_n) planar guided-wave modes at the y boundaries at a very small propagation angle from the z axis. It means that the polarization of the TE modes still has predominantly an electric field in the y direction and a magnetic field in the x direction. Therefore they are still called TE_{mn} (or TM_{nm}) modes.

The procedure of applying the effective index method is straightforward. Because an effective index is mode dependent, we first decide on the specific mode, either TE_{mn} or TM_{mn}, with specific mode indices m and n, to be analyzed. The waveguide is then divided into three structures for the three vertical regions, I, II, and III, shown in Fig. 2.6. The structure associated with each region is then treated as a planar waveguide to find the propagation constant β_m for the mode m. The x dependence of the y component of the mode field, $E_{m,y}(x)$ in the case of a TE-like mode or $H_{m,y}(x)$ in the case of a TM-like mode, for central waveguide region I is also found through the same procedure.

The propagation constants for the three regions are used to determine the effective indices,

$$n_1 = n_I = c\beta_m^I / \omega = \lambda\beta_m^I / 2\pi,$$

$$n_2 = n_{II} = c\beta_m^{II} / \omega = \lambda\beta_m^{II} / 2\pi, \text{ and}$$

$$n_3 = n_{III} = c\beta_m^{III} / \omega = \lambda\beta_m^{III} / 2\pi, \qquad (2.60)$$

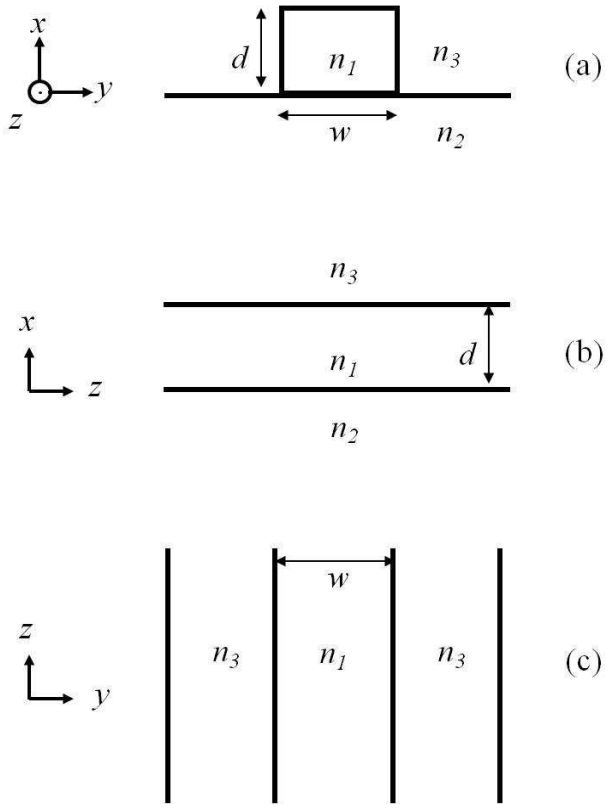

Figure 2.6. Analytical model for the effective index method.

for a vertical planar waveguide of core width w. This structure is then treated as a planar slab waveguide to solve for the propagation constant β_{mn} of the desired mode and for the y dependence of the y component of the mode field, $E_{n,y}(y)$ in the case of a TE-like mode or $H_{n,y}(y)$ in the case of a TM-like mode. Note that $E_{n,y}(y)$ for a TE-like mode of the original channel waveguide is obtained from the E_y component of the TM_n field of the effective vertical planar waveguide, whereas $H_{n,y}(y)$ for a TM-like mode of the original waveguide is obtained from the H_y component of the TE_n field of the effective vertical planar waveguide. Finally, the y component of the total mode field for the original channel waveguide is $E_{mn,y}(x, y) = E_{m,y}(x)E_{n,y}(y)$, in the case when the TE_{mn} mode is considered, or $H_{mn,y}(x, y) = H_{m,y}(x)H_{n,y}(y)$, in the case when the TM_{mn} mode is considered. Other significant field components are found by using (2.26) and (2.27) for a TE-like mode and by using (2.34) and (2.35) for a TM-like mode. The propagation constant is simply β_{mn} found from the effective vertical planar waveguide.

For TE_{00} and TM_{00} modes, when n_1 = 1.57 and n_2 = 1.54 = n_3, for a wavelength of 1550 nm and for a channel waveguide of core thickness of 2.5 μm with aspect ratio of unity, it was found that β = 6.320819, and n_β = 1.559284 for TE_{00} mode and β = 6.319853, n_β = 1.559046 for TM_{00} mode using EIM based 2D mode solver (Hammer 2012). The screenshots of the results obtained from EIM based online 2D mode solver are available in Appendix B. From the mode solver, it was also found that single mode propagation is observed till the aspect ratio is less than 1.25, i.e., till width of the waveguide is 3.1 μm.

2.8.2 Beam Propagation Method

The beam propagation method was first applied to problems of integrated optics by Feit and Fleck (Feit 1978 1979 1980 1983 1985 1990). The BPM approach is based on the approximation of the exact wave equation for monochromatic waves and the numerical solution of the resulting equations. An overview of the basic BPM theory as described by (Rsoft 1993) (Scarmozzino 2001) is presented in this section.

In the basic form of BPM, the electric field is represented as a scalar value instead of a vector value. As a result, polarization effects can be neglected and the propagation is assumed to be paraxial (i.e. confined to a narrow range of angles). The scalar field assumption allows the wave equation to be written in the form of the Helmholtz equation for monochromatic waves:

$$\nabla^2\phi(x,y,z) + k(x,y,z)^2\phi = 0 \tag{2.61}$$

where

$$\nabla^2\phi(x,y,z) = \frac{\partial^2\phi}{\partial^2 x^2} + \frac{\partial^2\phi}{\partial^2 y^2} + \frac{\partial^2\phi}{\partial^2 z^2}; \tag{2.62}$$

Here, the scalar electric field is written as

$$E(x,y,z,t) = \phi(x,y,z)e^{-i\omega t}, \tag{2.63}$$

and the notation $k(x,y,z) = k_0 n(x,y,z)$ is the spatially dependent wave number, with $k_0 = \frac{2\pi}{\lambda}$ is the wave number in free space. It can be seen that the refractive index distribution

$n(x, y, z)$ defines the geometry of the problem. Aside from the scalar equation, (2.61) is exact.

For typical guided wave problems, the phase variation due to propagation along the guided axis (i.e. the *z* axis) gives the most rapid variation in the field ϕ. To enhance the efficiency of the technique, this rapid phase variation is factored out of the problem with the introduction of a slowly varying field *u*, where:

$$\phi(x, y, z) = u(x, y, z)e^{i\bar{k}z} \tag{2.64}$$

where $\bar{k}$ is a reference wave number, a constant representing the average phase variation of the field ϕ; and is frequently expressed in terms of a reference refractive index $\bar{n}$, where $\bar{k} = k_0\bar{n}$. In this approximation, the slowly varying field can be represented numerically on a longitudinal grid that is much coarser than the wavelength for many problems, thus increasing the efficiency of the technique. However, this approximation can only be applied to paraxial fields (i.e. the field is propagating mainly along the z axis).

Substitution of (2.64) into (2.61) yields the following equation for the slowly varying field:

$$\frac{\partial^2 u}{\partial^2 z^2} + 2i\bar{k}\frac{\partial u}{\partial z} + \frac{\partial^2 u}{\partial^2 x^2} + \frac{\partial^2 u}{\partial^2 y^2} + (k^2 - \bar{k}^2)u = 0 \tag{2.65}$$

Assuming that the variation *u* with *z* is sufficiently slow, the second derivative term in *z* may be neglected. This is known as the paraxial or parabolic approximation, which reduces the guided wave problem from a second-order boundary value problem requiring eigenvalue analysis, to a first-order initial value problem that can be simply solved by integration. Equation (2.65) then becomes:

$$\frac{\partial u}{\partial z} = \frac{i}{2\bar{k}}\left(\frac{\partial^2 u}{\partial^2 x^2} + \frac{\partial^2 u}{\partial^2 y^2} + (k^2 - \bar{k}^2)u\right) \tag{2.66}$$

Equation (2.66) is the basic BPM equation in three dimensions which is also known as the scalar, paraxial BPM. This basic form of BPM models the continuous wave (CW) optical fields propagating in the *z*-direction. However, it is important to note that the direct

consequence of the elimination of the second derivative is that devices where reflections are significant (i.e. backward travelling wave solutions) cannot be accurately modeled based on the basic BPM equation. Improved efficiency of BPM has not been achieved without a price. Fields that have a complicating superposition of phase variation, such as exist in multimode devices, may not be modeled accurately. Also, the possibility for backward traveling wave solutions gets eliminated, thus devices for reflections are significant may not be modeled accurately.

By discretizing the cross-section of a waveguide structure into grid points, the BPM works by decomposing a spatial mode into a superposition of plane waves using the above equation (2.66) in the *z*-direction, with each next plane at $z + \Delta z$ being mathematically dependent on the current plane at *z*. This process is repeated until the wave has propagated through the entire structure. The effects of propagating and local index at continuously on the phase as the wave travels but BPM numerically simulate this process in a series of small steps, i.e., BPM uses a split-step process. Equation (2.66) is a parabolic partial differential equation that can be integrated forward in z by a number of standard numerical techniques. The BPM is a numerical simulation of the field in a guide, not an approximate solution to the exact wave equation. The BPM can help us determine the mode profile in a unusual waveguide and can determine the dynamic behavior of a mode as the index profile changes along z, commonly found in a tapered guide or in a guide perturbed by a other nearby guide. Early BPM employed a split-fourier method (Feit 1978), and later an implicit finite-difference approach based on Crank-Nicholson scheme was found superior (Yevick 1990) (Chung 1990a) (Scarmozzino 1991). This approach and its derivatives have become the standard and are frequently denoted as Finite Difference BPM (FD-BPM) in the literature.

2.8.3 Mode Solving Via BeamPROP^{TM}

Simulation of guided-wave photonic devices by means of the beam propagation method (BPM) has become one of the most common and widespread strategies used to design planar lightwave circuits (Marz 1995) (Hoekstra 1997) (Yamauchi 2003). Computer-aided design and modeling software has in many ways spurred the development of lightwave components and systems. With these softwares, new device concepts can be easily evaluated; designs can be optimized and the design cycle can be shortened significantly. BeamPROP^{TM} is design

tool that is part of the Rsoft Photonics Component Design Suite from RSoft Inc., USA. BeamPROP^{TM} is based on the BPM for the design and simulation of integrated and fiber-optic waveguide devices and circuits. The BPM incorporates techniques that utilizes an implicit finite-difference scheme, however it is only suited for a planar topology (Lifante 2003). The flexibility of the software allows users to create schematic designs of photonic devices and circuits as well as fundamental objects such as straight, tapered, curved, and branching waveguide segments. Each individual component has its own set of properties that can easily be accessed to be defined or modified by the user. BeamPROP^{TM} allows the user to manually create photonic structures, but it also contains several built-in utilities to automatically create complicated structures. Utilities are available for common periodic structures, grating structures, and arrayed waveguide grating (AWG) structures. Rsoft CAD with related utilities also allows for the creation of customized components using mathematical equations or data files. BeamPROP^{TM} includes BPM-based mode solvers which allow the calculation of modal propagation constants and profiles of both guided and radiation modes for any arbitrary 2D or 3D geometry (Rsoft 1993).

Once the width and height of the waveguide are decided to allow only a single mode, they can be applied to design a variety of devices such as the elementary straight channel waveguide, power splitter, directional coupler, etc. In this work, optical power splitters based on Y-branch waveguides have been designed and fabricated. The optical power splitter is a fundamental element in PICs. Power splitters with smaller footprints and lower excess losses are need of the hour to allow high device density in polymer-based PICs. Additionally, wide optical bandwidth and splitting-ratio tunability are critical. The targeted waveguides are single-moded at telecommunication wavelengths. With this in mind, design of slab waveguides single-moded at 1550 nm was first undertaken. The results provided the inputs for designing single-moded channel waveguides, which form the backbone of the final device.

Single mode slab waveguides were designed using the standard equations for TE and TM mode propagation in planar rectangular waveguides. Well known UV sensitive photoresist SU-8 with a refractive index of 1.57 at 1550nm was chosen as the material for the waveguide core while Norland Optical Adhesive NOA 61 was used as underclad as well as overclad in

order to fabricate a symmetric waveguide. It must be mentioned that NOA 61 has a refractive index of 1.54 at 1550nm. These refractive indices were also independently verified by fabricating planar SU-8 and NOA 61 waveguides and carrying out measurements on a prism coupler (refer to Chapter 4 for details).

To support fundamental mode in a symmetric waveguide, i.e., $a_E = a_M = 0$, we know from (2.51), (2.52) and (2.59) that, $M_{TE} = M_{TM} = \left[\frac{V}{\pi}\right]_{\text{int}} = 1$.

Hence, $V = \pi$, for the fundamental mode. With $V = \pi$, we get, $d = 2.54$ μm using (2.15), where, $n_1 = 1.57$; $n_2 = 1.54$ and $\lambda = 1550$ nm. With a thickness of 2.5 μm, recalculating using (2.15), we get, $V = 3.096$. Since, the propagation angle for the second mode will be less than for the fundamental mode, for all angles greater than the critical angle, the waveguide will be monomode, i.e., from monomode condition (Pavesi 2006), $\theta_c < \cos^{-1}\left(\frac{\lambda_0}{2n_1 d}\right)$, where $\theta_c = \sin^{-1}\left(\frac{n_2}{n_1}\right) = 78.78^\circ$ for $n_1 = 1.57$ and $n_2 = 1.54$. This, again, yields $d = 2.54$ μm for a wavelength of 1550 nm. Hence, for a given symmetric waveguide, a guide thickness of 2.5 μm was chosen to ensure single mode operation at 1550 nm wavelength.

Having fixed the guide thickness, in order to make single mode channel waveguides it is also important to use appropriate channel width. The propagation constant β and n_β has already been specified in section 2.8.1 for TE_{00} and TM_{00} modes. The values of β and n_β with (2.16) yields the value of normalized guide index, $b = 0.6592$. This value of b can also be observed from Fig. 2.4 as for a value of $V = 3.096$, $b \approx 0.66$ for the V-b curve with $m = 0$ and $a = 0$. The value of $b = 0.6592$ and $V = 3.096$ can be used in a condition (Nishihara 1985): $0 < \frac{w}{d} \le \frac{\pi}{\sqrt{b}.V}$. The condition corresponds to a maximum aspect ratio of 1.249, as a result, limits the waveguide width to 3.1 μm. This is the same value of width of waveguide over which higher modes exist in EIM based 2D Mode solver discussed in section 2.8.1.

All waveguide structures that were simulated were channel waveguides that used a slab mode beam with a wavelength of 1550nm. The simulation, thus, used a launch beam that had same

dimensions as the waveguide under test. Initially to estimate the number of modes in the interconnection structures, mode calculations were performed with the waveguide width and height of 2.5 × 2.5 μm. The core and cladding refractive indices of the two materials mentioned earlier were used in the simulation. The refractive index profile of this structure and the field profile of the fundamental mode are shown in Fig. 2.7(a) and (b) respectively. Again, note that the effective index evaluated by BPM during a 2D simulation as shown in Fig. 2.7(b) is very close to that evaluated using EIM based 2D mode solver discussed in Section 2.8.1.

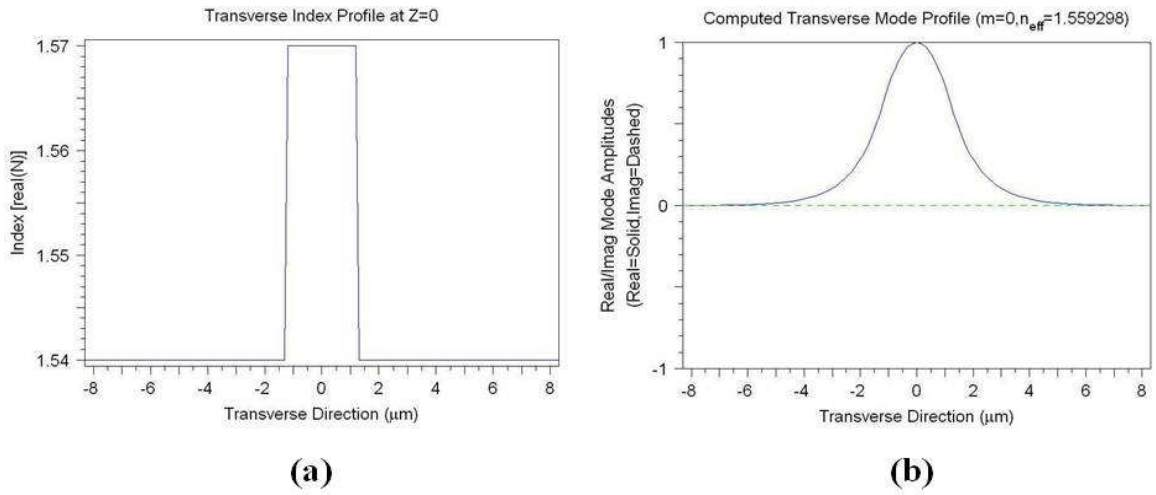

Figure 2.7. 2D (a) Refractive Index Profile and (b) Mode profile.

2.9 Source-to-Waveguide Coupling

Coupling between source and the optical waveguide is based on a modal description of the waveguide and depends on alignment, dimensional differences and geometrical shape (Pollock 1995). There can be significant loss in optical connections due to misalignment or mismatch of the modes between the source and the waveguide. Misalignment between a source and a single mode waveguide by dimension less than 1 μm can cause a coupling loss exceeding 1 dB. Coupling problems are exaggerated by the small dimension of typical optical waveguides and sources which makes alignment a critical and challenging task.

The most efficient coupling between a waveguide an optical source occurs when the source is butted up against the cleaved end face of the waveguide. This is called the butt coupling. The

other way to couple an external beam directly to a waveguide is end-fire coupling, where the beam is focused on to the end of the waveguide. This method works well, if a clean end-face of the waveguide is optically accessible and if one has a ability to tightly focus and position the external light beam The numerical aperture, *NA*, is a critical parameter in coupling as power coupled is proportional to the square of *NA* (Pollock 1995). High is the value of *NA*, more efficient is source-to-waveguide coupling. Lenses can be used in certain circumstances to improve coupling efficiency compared to butt coupling between a waveguide and a source.

In order to employ and integrated optic component in a fiber optical communication system, it is important to provide a fiber pigtail(s) for light input and light output from the device. In order to do this, such devices are usually pigtailed with single mode optical fibers. In such a case, an important parameter to consider is the matching of the mode field diameters of the mode propagating in the integrated optic device and single mode fibers that would be pigtailed to the device. Mode field diameter (MFD) is an expression of distribution of optical power across the end-face of a single mode fiber. For a Gaussian intensity, MFD is the diameter at which the power density is reduced to $1/e^2$ of the maximum power density. The guassian mode profile shown in Fig. 2.7b indicates the mode field diameter for the 2.5 × 2.5 μm cross-section rectangular waveguide will be 4.8 ± 0.5 μm at 1550 nm. Commercially available low-loss fiber e.g. Corning SMF-28e+ LL has a MFD of 10.4 ± 0.5 μm at 1550 nm. The coupling efficiency will be less than 25% if the differences between the mode field diameters is 100% or above (Pollock 1995). For higher efficiency, a better option will be choosing a high-*NA* fiber with MFD almost equal to that of the given waveguide for fiber pigtails. Commercially available, Nufern PWG1-XP fiber is such an option with a MFD of 4.8 ± 0.5 μm at 1550 nm. The specification sheet of Nufern PWG1-XP fiber is available in Appendix A.

2.10 Conclusion

The chapter presented an overview of guided-mode theory for planar waveguides, following which non-planar waveguides, i.e., rectangular channel waveguides were analyzed. The wave equations for solving planar waveguides are derived from Maxwell's equations and its solution can be made about the nature of the propagating field. The analysis of the planar and rectangular channel waveguides involves finding the propagation constants and field profiles

of all the modes that the waveguide supports. The approximate analytical method using effective index approximation was discussed with numerical methods like beam-propagation method in the chapter. A 2D EIM based Mode Solver was used to find the propagation constants for the fundamental mode. The waveguide thickness was chosen to be 2.5 μm to support the fundamental mode only. The aspect ratio lie between unity to 1.25, insisting to a maximum channel width of 3.1 μm, ensuring single-mode propagation. A suitable fiber, Nufern PWG1-XP, was selected to ensure maximum coupling efficiency for fiber-pigtails after studying the Gaussian mode profile derived using a commercial software BeamPROP^{TM} based on beam-propagation method, of the proposed 2.5 × 2.5 μm waveguide.

CHAPTER 3

Y-BRANCH SPLITTER - DESIGN AND FABRICATION

The ever increasing demand for voice, data, and video services in optical access networks will require broadband optical splitters capable of broadcasting and distributing optical signals from the central office to many users (Okada 1997). The broad-band passive optical network (PON) is an important access infrastructure that provides a cost-effective fiber-to-the-home service (Maeda 2001). A PLC-based dynamic optical splitter for PON/fiber-to-the-premise networks was reported and aimed at providing carriers with the flexibility to add new subscribers to an optical network without the need for traffic disruption that usually results from upgrading optical splitters (Queller 2004). In the subscriber network of a PON, a power splitter is used to distribute optical power from one input channel into several output ones. Multiport power splitters are routinely used in WDM systems. For economical reasons, it is desirable to use passive components for optical signal distribution in broadband WDM communication systems. Power splitters based on branching waveguides are key components for optical signal distribution in hybrid or fully optical access networks (Ueda 2001).

A Y-branch waveguide is a fundamental element utilized in deciding the structure and shape of photonic devices and can be symmetric or asymmetric according to the required branching ratio. Y-branch waveguides are essential in PICs both for signal routing and signal processing. They are utilized as power splitters/ combiners in modulators, switches, interferometric devices and semiconductor laser arrays. For the case of symmetric Y-branch, many new structures have been proposed to achieve a low excess loss (Chaudhari 2001) (Yabu 2001) (Hu 1997) (Chung 1990b) (Seino 1987). For the asymmetric case, a wide range of branching ratio with less losses is required (Suzuki 1996) (Lin 1999a). Various passive and active splitter designs have been proposed previously, including a tree of Y-branches PLC splitter (Takahashi 1993), active splitters (Choi 2000) (Jaouen 1999) (Ratovelomanana 1995) using post-amplification to compensate for the splitting loss. Splitters have been realized with Y-branch waveguides (Tao 2008), multimode interference waveguides (Wang 2004), directional couplers (Kiyat 2005), photonic crystals (Frandsen 2004), and others (Chung 2006) (Schuller 2007).

A branching waveguide that has a low branching loss, small and compact overall size, and is easy to fabricate without critical fabrication requirements is said to be an optimum and an efficient structure. In the design of a power splitter reported in this work, the key design parameters considered in device simulation were the branching angle, the type of bend and its length, the overall device length, the final separation of the output ports, etc., which governed the device performance. Both device length and radiation loss of optical waveguide devices are critically determined by the bend and branch requirements. Design and realization of compact and low-loss branches are of great interest in several integrated optics applications.

This chapter discuss the design and fabrication of Y-branch waveguide which is the basis of the optical power splitter. The conventional Y-branch design for a 1 × 4 power splitter is presented in the chapter. The design of mask for fabrication of 1 × N splitters using L-Edit (Tanner Tools) is presented here. The chapter also describes an overview of the micro-fabrication procedures and techniques for polymer waveguides. Finally the details of fabrication process used in this work is presented in the chapter.

3.1 Y-Structure Design and Optimization

Optical power splitters, other than cascaded Y-branch (Burns 1990), are commonly implemented using fiber couplers and multimode interferometers (MMI) (Wang 2002) (Huang 1997) (Huang 1998). However, splitters based on evanescent field coupling and MMI principles suffer from the problem of strong wavelength and polarization dependence if using low index contrast material such as polymer, and therefore they are not suitable for broadband applications (Huang 1997) (Huang 1998). On the other hand, although Y-junction optical power splitters are less wavelength and polarization dependent, they suffer from excess loss due to the mode field/wave-front mismatch between the output and input branches (Yulianti 2010). Splitters based on Y-branch waveguides however, are widely used as the structure is simple and the excess loss caused by optical power splitting is low. Optical outputs of a Y-splitter have a uniform splitting ratio when the splitter is fabricated based on a symmetric structure. Splitters with variable optical power splitting ratio find applications in dynamic control and efficient management of optical power in photonic applications. For

example, the asymmetric power splitters can be used in optical communications to actively distribute light to optical components that consume varying and uneven optical powers.

A conventional 1 × 2 splitter is simply a Y-branch waveguide where two output waveguides are connected to a linear input waveguide. In conventional 1 × N power splitters constructed by cascading Y-branch waveguides (Chaudhari 2001) (Yabu 2001), the overall physical dimensions of the optical power splitter becomes very large as the number of output ports increases. Consequently, it is desirable to develop a new structure for compact, multi-branch, planar power splitters. It must be noted that Y-branch based 1×N splitters (Beguin 1988) (Nourshargh 1989) (Haux 1989) have the advantages of wavelength independence and small insertion loss deviation between output ports when compared with directional coupler type splitters. The performance requirements for the splitters include a low insertion loss, a wide operational wavelength range, a uniform splitting ratio, a low polarization-dependent loss and a compact size. However, the guided wave on a Y branch always loses energy by radiation because of the discontinuous feature of branch structures. Such radiation causes serious problems in circuit performance due to the undesired power coupling or crosstalk with neighboring circuits.

3.1.1 Branching Angle

Burns and Milton introduced a coupled mode equation between branching waveguide modes, and they showed that the Y-branch behaves as a mode-splitter when Y-junction angle is small and it acts as a power divider when the angle is large (Burns 1975). The junction angle should be sufficiently large to avoid coupling of power between output waveguides is negligible. Transmitted power decreases as Y-junction half-angle increases beyond 1º (Anderson 1978). It is well known that Y-branches suffer from severe radiation losses in excess of 3 dB, particularly with a branching angle larger than 2° (Weismann 1989) (Tsutsumi 1988), resulting in poor device performance with respect to contrast ratio and crosstalk. Consequently, for appropriate separation as per standard fiber ribbons between the interacting waveguide arms demands very long dimensions with these narrow branch angles. On the other hand, compact Y-branches that are necessary for high-density integrated optics incur unacceptable losses. The power of the guided mode is divided into branching

waveguides with relatively small losses when the refractive index difference between the core and the cladding is large (Anderson 1978).

A typical loss figure for a conventional Y-junction splitter is 1 dB with a branching angle of 1° (Yabu 2001). In order to minimize the loss, this angle has to be less than 1°. This then makes the Y-junction to be very long in order to achieve a standard full-pitch spacing of 127 μm between its two output branches. Various methods were recently reported to compensate for such a mismatch (Hung 1988) (Belanger 1983) (Lin 1994) (Lin 1999b) (Gamet 2004) (Wang 2003) (Chan 1996) in order to reduce the junction excess loss with a larger branching angle. In summary, there are two basic approaches to tackle this problem. The first approach is achieved by introducing a wave-front accelerator/microprism in order to compensate the mismatch loss (Hsu 1998). However, this requires more than two different types of index materials and may result in higher fabrication cost. As a result, the fabrication cost would be much higher. The second approach is to modify the physical geometry of the Y-junction directly but, the reduction of loss is not so significant in this case especially at large branching angles.

3.1.2 Output waveguide-bends

Standard splitters that are realized based on Y-junctions design suffer from high reflection and radiation loss due to branching complexity (Chan 1996). It is well known that optical devices using Y-branch structures with abrupt-bend and relatively large branching angles suffer large radiation losses when the refractive index difference between the core and the cladding is small. However, a large index difference makes the fabrication difficult. Also there have been situations where Y-branches with small index difference are found more suitable from the viewpoint of coupling efficiency with other optical devices in integrated optics (Min 1997). Studies have been performed showing the relationship between the angle of the bend and the losses encountered. Bends of less than 3° exhibited losses of less than 1dB, while bend angles 4° and higher showed exponentially growing losses of greater than 1dB (Eldada 1996).

A more compact Y-branching waveguide results with the introduction of some curvature in the arms in the form of an S-bend segment. If such S-bend segments were replaced by linear

segments, such a waveguide design would be arbitrarily long (Ladouceur 1996). The types of S-bend structures available in the opto-electronic CAD software BeamPROP^{TM} include the arc type S-bend, Cosine type S-bend and the raised Sine S-bend. For the design of a low-loss Y-branching waveguide, one has to investigate the dependence of the type of S-bend. From the parameter scans of the type of S-bend, optimized designs for Y-branching waveguides were obtained. The Cosine type S-bend gives the lowest branching loss and the largest output power in its arms (Sum 2004).

The performance of Y-branches, is also affected by interference effects between the guided mode and the field radiated from distortions in the input section, e.g., a fiber-waveguide interface or a bend in the input waveguide as required in cascaded splitter devices. These effects impart an oscillatory dependence to the splitting ratio on wavelength and have been noted both theoretically and experimentally (Munowitz 1992) (Chu 1991) (Deri 1988) (Johnson 1984). The interference effects can be minimized by using long straight waveguides for the input section, as the intensity of radiated modes decreases with growing distance from the perturbation. Long input waveguides, however, result in an inacceptable length of complex devices. An optimal splitter design should combine a short length with a low loss and low sensitivity to distortions like those described above.

3.1.3 BPM Simulation: 1 × N Splitters

A conventional Y-branch waveguide structure consists of a single input wave guide and two output waveguides. Y-branches used for power division are easy to design and are fairly insensitive to patterning tolerances (Tsai 2003). Fig. 3.1 shows a Y-branch schematic. It follows from the symmetry of the Y-branch structure that it will act as a symmetrical power divider between the output waveguides. Thus, for each of the two output arms the theoretical power splitting ratio is 50:50. The refractive indices of the polymer materials SU-8 2002 and NOA 61 were used as inputs to the BPM software. It is required to find the power transmitted to the output waveguides, the power reflected in the input waveguide and the power radiated from the junction into the surrounding medium. BPM simulations do not involve reflective power measurements, hence we have to restrict the discussion to power transmitted to output waveguides and power radiated at the Y-junction. Also, transmission loss is predominantly due to radiation (Anderson 1978).

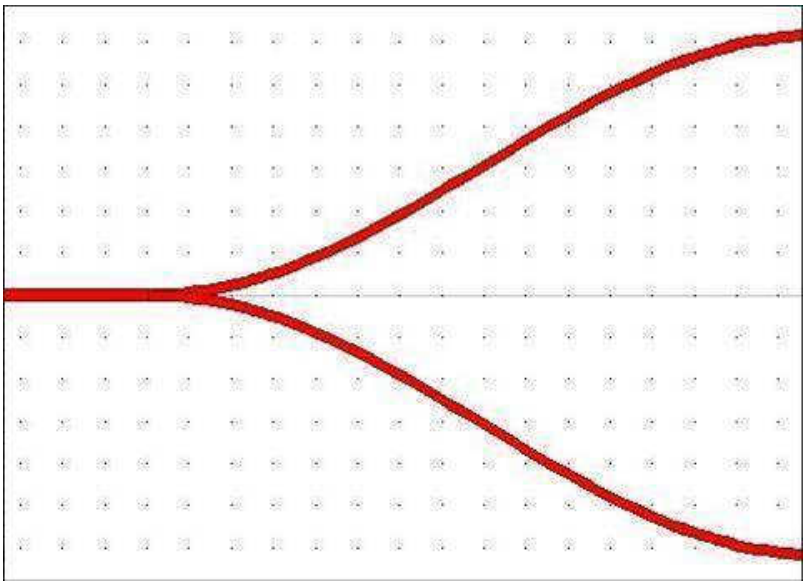

Figure 3.1. RSoft CAD schematic of the Y-branch device.

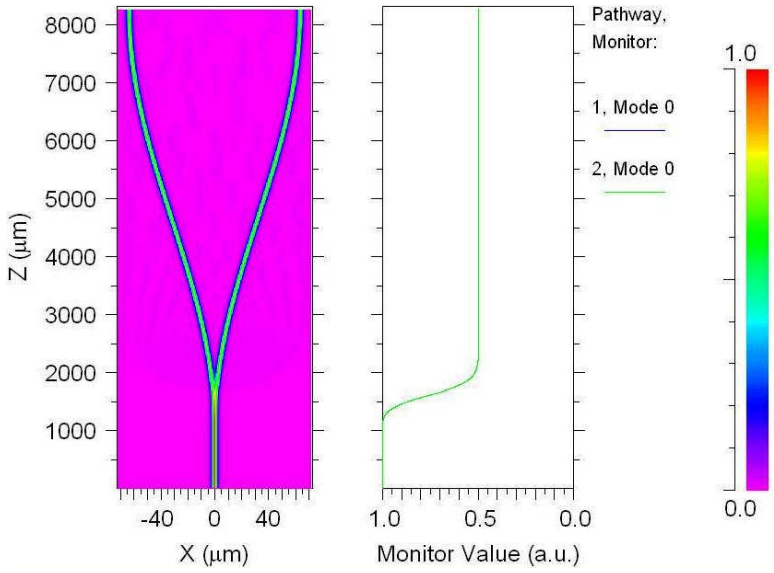

(a) (b)

Figure 3.2. Simulation of a 3-dB, 2° Y-branch (a) Designed Y-branch, (b) Performance of the Y-branch.

We examine here the transmission performance of a 2D single mode symmetrical Y-junction formed on two cosine-bend waveguides that are connected to a linear input segment using the

BPM software, BeamPROP™. The simulation for a 2° angle for a Y-branch is shown in Fig. 3.2. Fig. 3.2(a) shows a top-down view of the device. Light propagation is along the z-direction and the waveguide width is shown along the x-axis. The performance of the Y-branch is shown in Fig. 3.2(b). The input power and the power in the left arm of the Y-branch are shown in blue and that in the right arm is displayed in green. Even though the input power is set to 1, the simulation shows the effects of the 3-dB power distribution, hence the power monitor in green (overlapping blue) shows approximately 0.50 units of the total input power of 1 unit.

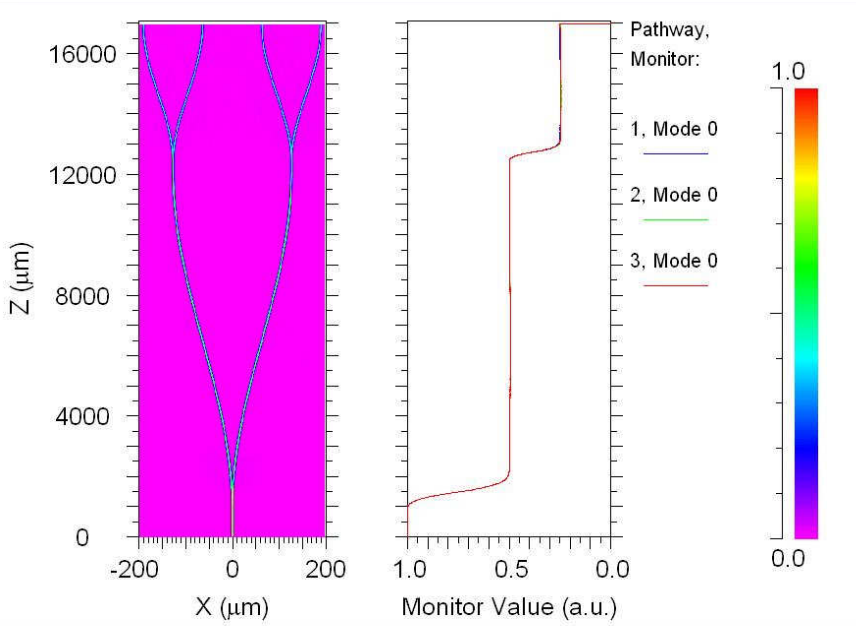

Figure 3.3. Simulated 1 × 4 optical power splitter with the outputs.

Fig. 3.3 show the designed 1 × 4 optical power splitter and its performance. In all Y-branching arms, cosine S-bends were used to minimize the radiation losses at the splitting junction. The splitting ratio of a Y-branch waveguide depends only on the symmetry and is a wavelength independent 3-dB splitter. The port separation at the output has been standardized to 127 μm (center-to-center) so as to match standard fiber ribbon for pigtailing. In designing an S-bend arm, it is well known that longer arm length leads to better results, since the radius of curvature at the waveguide bends is larger leading to lesser bending loss. However, overall device length on a wafer of given dimensions needs to be kept in mind. Since the polymer layers will be deposited by spinning the polymer solution on the wafer, it

can be assumed that the film will be most uniform in the central region. With this in mind, the splitter length was optimized in such a way that the entire device layout would be in the central region of the spun wafer.

Theoretically, an insertion loss of 6 dB is expected for 1 × 4 splitter using this design, and by simulation, it was achieved for the 1 × 4 splitter. The length of the S-bend has been optimized to get the results as close to theoretically predicted ones as possible. The total device length optimal for fabrication on a 4-inch silicon wafer of a 1 × 4 splitter device is about 30 mm (Satyanarayan 2006). However, in practical situation, the device length should be much shorter after optimization. Therefore, in order to achieve an acceptable device-performance with an optimal device-length, a separate simulation was carried out. The device length for 1 × 4 splitter was reduced in order to be suitable for fabrication on 3-inch silicon wafer. The shortened device length (17 mm for 1 × 4 device) shows only a marginal increase in insertion loss, which was 6.03 dB. However, in practical devices, the actual insertion losses will also be influenced by the quality of fiber pigtailing at the input and output ports, matching of the mode field diameters between the mode propagating in the input and output optical fibers and that propagating in the waveguide and also on the quality of the channel waveguide end-facets and several other parameters.

3.2 Mask Design and Development

In contact printing, the resist-coated silicon wafer is brought into physical contact with the glass photomask. The photoresist is exposed with UV light while the wafer is in contact with the mask. Because of the contact between the resist and mask, very high resolution is possible in contact printing. However, a problem with contact printing is that debris, trapped between the resist and the mask, can damage the mask and cause defects in the pattern. The proximity exposure method is similar to contact printing except that a small gap, around 10 microns wide, is maintained between the wafer and the mask during exposure. This gap minimizes (but may not eliminate) mask damage but degrades the resolution that can be achieved from contact-printing. Projection printing (Ashley 1991) (Tumolillo 1991), avoids mask damage entirely. An image of the patterns on the mask is projected onto the resist-coated wafer, which is many centimeters away. In order to achieve high resolution, only a small portion of the mask is imaged. This small image field is scanned or stepped over the

surface of the wafer. Projection printers that step the mask image over the wafer surface are called step-and-repeat systems. Step-and-repeat projection printers are capable of providing good resolution but for best resolution, contact-printing is still the first choice.

The design results from simulations in previous section were converted to GDS-II format in BeamProp™. L-Edit (Tanner Tools) was used to design the mask layout. It may be recalled from section 2.8.3 that for a channel waveguide, aspect ratio (w/d) of 1 – 1.125 was chosen so as to yield channel width in the range 2.5 to 3.1 μm for guide thickness of 2.5 μm. In actual fabrication, it is possible that the actual width of the channel may be different from what is present on the mask. With this in mind, 1 × 4 splitters of different channel widths were made in the mask layout. Various channel widths ranged from 1.8 μm to 2.6 μm. Accompanying every splitter of a given channel width was a straight channel waveguide of same channel width. The straight waveguide may be of use in device characterization. Since the photoresist is a negative tone resist, the appropriate mask used was a dark-field mask. Figure 3.4 shows some portions of masks designed in L-Edit with GDS-II format for 1 × 4 splitters.

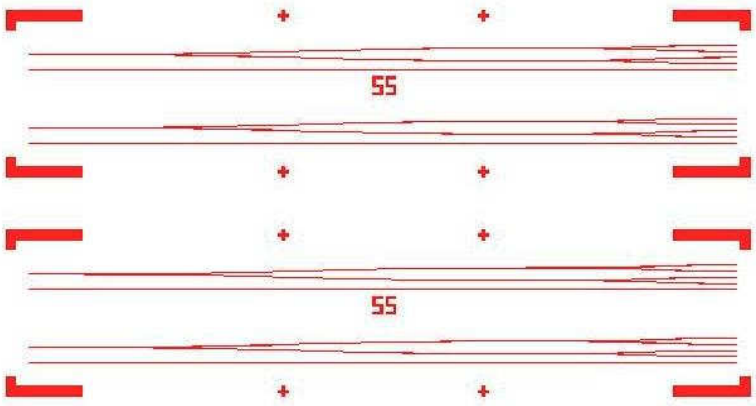

Figure 3.4. Portions of GDS-II mask schematic for a 1 × 4 splitter.

The mask was fabricated by direct-write technique through Laser Pattern Generator (Heidelberg Instruments, Germany) at the Mask Fabrication Facility in CSIR-CEERI, Pilani. The fabricated mask was observed under the microscope to look for defective areas such as pin holes and any other unwanted features.

3.3 Fabrication Techniques for Polymer Waveguides

In this section, various existing and emerging techniques for the fabrication of polymer optical waveguides will be briefly reviewed. The objective of this review is to provide a broad perspective of the different techniques that are available to fabricate polymer waveguides. The techniques can be broadly categorized into: deposition and etching; direct UV photolithography; casting/molding/embossing; and direct-write techniques. Direct write techniques allow rapid prototyping, are flexible, and can afford precise control over different parameters to create novel structures. However they produce low-yields and are not suitable for mass-production of devices. Plasma/Reactive-ion etching and embossing techniques too are multi-step processes and time-consuming, hence cost intensive. UV photolithography is suitable for mass production but need design and production of different masks for different waveguide patterns before they can be fabricated. In general, one of the techniques discussed here in the section or a combination of these techniques may be required for the fabrication of polymer waveguides.

3.3.1 Deposition and Etching

The deposition method is often used to lay down a layer of light-guiding or cladding material on a substrate. For polymer waveguides, spin-coating and dip coating are two methods used to deposit a uniform layer on a substrate. Following deposition of light-guiding layer, techniques such as photolithography and other direct-write methods are used to define the optical pathways (Hikita 1993) (Wang 1994) (Hikitaa 1998). Suitable polymers (usually in powder form) are first dissolved in a suitable solvent before being spun on a substrate in the case of spin-coating. In the case of dip coating, the substrate is dipped into the solvent and then lifted off. After the deposition of the film on the substrate, the coated film is thermally treated to remove the excess solvent and to enhance the adhesiveness of the film to the substrate. Both spin-coating and dip-coating techniques are widely used to deposit thin films of polymeric materials on a substrate (Nishihara 1985) (Madou 2002). Vapor deposition (chemically or thermally) and sputtering are other thin-film deposition techniques popular in microelectronics industry but are not economical compared to techniques employed commonly for polymer material deposition.

The chemical wet etching processes use liquid-phase etchants. The wafer is immersed in a bath of etchant, which must be agitated to achieve good process control. The photographic developer used for photoresist resembles wet etching. Modern VLSI processes avoid wet etching to prevent the disposal of large amounts of toxic waste. For these reasons, they are seldom used in state-of-the-art processes, and use plasma etching instead. Plasma etching is a physio-chemical etching process in which the material is removed from the surface by means of bombardment of ions excited by a plasma (e.g. reactive ion etching). Ions of the reactive element are created in the plasma and an electric field is then used to direct the ions towards the areas to be etched. The optical pathways can be defined by using a mask with conventional photolithography that inhibits the etching. The advantage of reactive ion etching (RIE) is that the process can be used with almost any polymer material (Nguyen 2002). To ensure good quality of waveguide patterns, optimum control over critical etch parameters is required. The etch parameters influence the etching rate and the smoothness of the etched sidewalls. The critical parameters in the etch process are the pressure in the etching chamber, the gas flow of the etching gas and the radio frequency (RF) power of the plasma etching machine. O_2 is generally used as etching gas and different metal layers like chromium, aluminum or gold can serve as etch mask.

Higher RF power results in a higher etch rate. The roughness of the etched sidewalls is improved with higher pressure and lower RF power. However, with higher pressure the anisotropy is inferior due to stronger chemical etching. The process is relatively long, but the individual steps are well known and the results of reproducible quality. A disadvantage of this technology is the inability to fabricate waveguide structures with vertical sidewalls (Nguyen 2002). The influence of the visible sidewall roughness can be reduced by the fact, that the refractive index contrast of the embedded channel waveguide is to be kept small and therefore the scattering losses may diminished. Plasma etching is usually done after material deposition followed by photolithography to fabricate polymeric waveguides (Hikita 1993) (Wang 1994) (Hikitaa 1998). Plasma or ion-etched polymeric materials have been observed to have high surface and sidewall roughness compared to those etched by chemical wet etching with suitable developer.

3.3.2 Direct UV Photolithography

Photolithography is one of the most widely used forms of lithography in micro-electronics industry. Making a choice of suitable low-loss polymer for fabrication of micro-optical components can exploit the same production line already available with the semiconductor industry. The direct UV photolithographic fabrication of optical waveguides, involves film deposition by spin-coating techniques, pattern transfer using lithography, and wet-chemical etching of resist film. Pattern transfer onto the photoresist is achieved by the use of contact masks as discussed in section 3.2. There are two types of photoresist: positive and negative. For negative photoresist, the exposed area remains after development while for a positive photoresist, the exposed area is removed after development.

The wavelengths of the light source ranges from deep ultraviolet (DUV) - i.e. 150 - 300 nm to near UV - i.e. 350 - 500 nm (Madou 2002). In the latter case, the g-line (436 nm) or the i-line (365 nm) of a mercury lamp is used. The sample is exposed to an appropriate dose of UV radiation under a UV lamp through a photomask. Photolithographic process offers very high contrast response allowing the definition of polymer waveguide features with dimensions ranging from few microns to few millimeters with a high degree of accuracy using precise controls.Essentially, photolithography is a two-dimensional process. However, three-dimension polymer waveguides have also been reported by using combined photolithography and reactive ion etching (Garner 1999).

3.3.3 Casting/Molding/Embossing

Casting, molding, hot/cold embossing are few other techniques to fabricate polymer waveguides (Becker 2008) (Mohr 2004). There is a distinct advantage of using polymers over other conventional photonic materials such as glass and semiconductors for fabrication because high throughput techniques are available to the former (Eldada 2000). The tool used comprises of an inverted replica of the structure to be fabricated (i.e. a channel on the tool will become a ridge on the substrate, or vice versa). Waveguides are formed by subsequently either filling the channels or overcladding the ribs formed in the embossing process. In the case for casting or cold embossing, photochemically reactive polymers are required and a UV transparent substrate or a UV-transparent tool is required for processing.

One widely used technique in polymer micro-fabrication is hot embossing. The popularity of this technique can be partially attributed to its simplicity in tool and process setup as compared with other competing techniques, such as micro injection molding (Wiesmann 1996) (Chuang 2005). Embossed polymer devices and systems have demonstrated a great commercial potential, especially for biomedical, telecommunication and optical applications. However, embossing is subjected to some inherent process flaws limiting its capability. One major drawback is caused by the need of keeping the whole polymer material mass in thermal cycling, resulting in a long cycle time. The long dwell time at elevated temperatures could further result in degradation of the embossing polymer. Another drawback lies in the difficulty in reaching high embossing pressure and thus in replicating high aspect ratio features, because by nature hot embossing is an open-die compression molding process.

3.3.4 Direct-Write Techniques

Direct-write lithographic techniques have the advantage of being maskless; thus capable of inexpensive rapid prototyping. However, compared with masked lithography, direct-write techniques can never compete with them in terms of manufacturing throughput. There are several direct-write techniques for the fabrication of optical waveguides. These include electron beam lithography, laser beam direct-writing and proton beam writing.

Electron beam lithography (EBL) technique is inspired from early scanning electron microscopes (Madou 2002). Essentially, it is based on the scanning a beam of electrons across a surface covered with a resist film sensitive to those electrons, thus depositing energy in the desired pattern in the resist film. One of the main advantages of EBL technique is high resolution. However, electrons undergo large angle scattering in a material. Due to the scattering of the electron beam inside the resist and substrate, and backscattering from the substrate, proximity effects are created, resulting in the exposure of the resist up to several microns from the point of impact (Mohammad 2004). This effect can be reduced by either using a thin resist layer and thin substrate support or by using lithography simulation software to optimize the design. Hence, EBL is essentially a surface micromachining technique. Nonetheless, it is capable of sub-10 nm for isolated structures and 30 nm pitch for dense periodic arrays of SiO_2 pillars (Vieu 2000). EBL has been used to fabricate polymer

optical waveguides (Wong 2001) (Nakayama 1997) as well as channel waveguides in silica (Madden 1990) (Blanco 2001).

Laser direct-writing has the advantages of allowing considerable control in focusing, power level and scanning speed. Hence, novel optical structures can be fabricated which cannot be easily done by conventional masked-based photolithographic technique (Eldada 1996). The incident laser beam is focused using a lens and the writing is performed by translating the sample in longitudinal or transverse writing geometries. Both femtosecond laser pulses (Nolte 2003) as well as continuous wave UV exposure methods have been used to fabricate optical waveguides in polymers (Eldada 1996).

Proton-beam writing (p-beam writing) (Watt 2000) is an emerging maskless lithographic technique which uses a focused sub-micron beam of MeV protons to direct-write on a suitable material - e.g. photoresists like PMMA and SU-8. The latent image formed in the former materials is subsequently chemically developed. Three-dimensional, high aspect ratio micro-components with straight and smooth sidewalls have been produced using this maskless technique (van Kan 2001). One of the possible niche areas for this new technique is the fabrication of optical waveguides and components (Sum 2003a) (Sum 2003b) (Bettiol 2003).

3.4 Fabrication Process

In this section, the steps of fabrication process of polymer optical waveguides fabricated and developed in this work are discussed. The organic polymer, SU-8 2002 from MicroChem, USA is the material for the core region in the fabrication of channel waveguides. An economical fabrication method was used to fabricate polymeric optical waveguides on (<100>) silicon wafers. NOA 61 is used as under and over cladding layer. The processing steps required for the fabrication of single mode optical waveguides are presented. To produce acceptable waveguides, the fabrication environment must be taken into consideration. Dust particles on the sample during fabrication lead to adhesion issues and can give problems during photolithography stages while transferring waveguide patterns using a contact mask. For compact device lengths, contamination must be more tightly controlled. Protecting wafers from particles becomes important to ensure good quality optical

waveguides and devices. Therefore, a clean room conditions and practices are critical. The entire studies on waveguide fabrication was carried out in the fabrication facility available in the Semiconductor Devices Fabrication (SDF) Facility of CSIR-CEERI, Pilani.

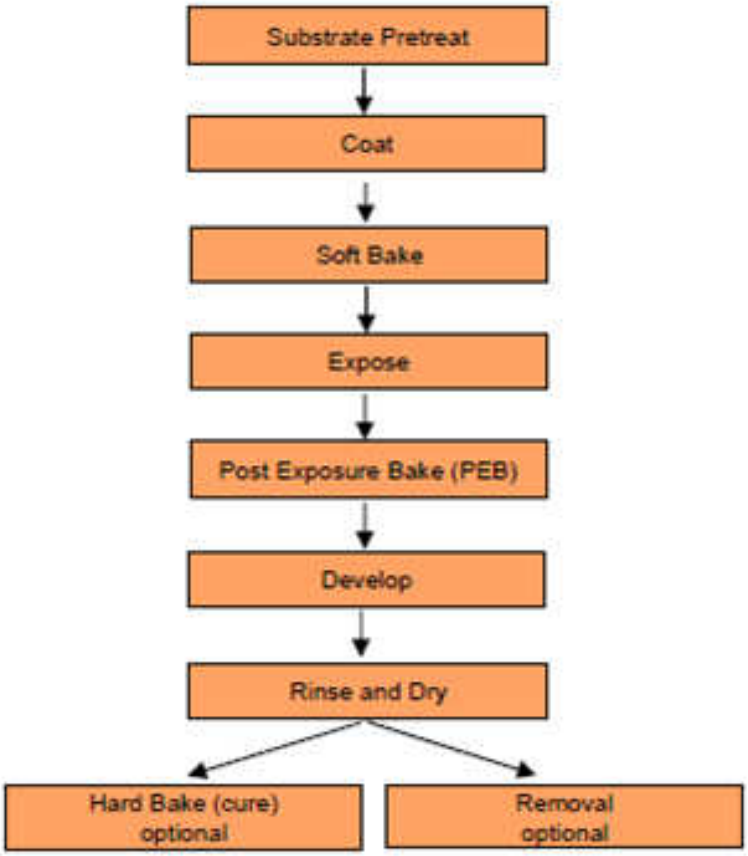

Figure 3.5. Process description for NANO™ SU-8 2000 Series

The NANO™ SU-8 2000 Series are UV-sensitive photopolymers that have been developed for use in microelectronics applications (Microchem 2000). The SU-8 2002 was chosen as the raw material for waveguide fabrication because it follows simple fabrication steps. The SU-8 2002 inherently simplifies the steps of fabrication process and requirement of critical/complex equipments for patterning waveguides is avoided. Fabrication of single mode SU-8 optical waveguides is based on a simple direct UV photolithography process (Tung 2005) (Pelletier 2006) (Yang 2009). Waveguide patterns can be developed simply by direct UV exposure through a photomask containing the pattern using economically

affordable equipments. The fabrication process flow chart (Microchem 2000) is shown in Fig. 3.5.

3.4.1 Material Storage

The photoresist SU-8 and Norland optical adhesive is stored in a refrigerator away from the sunlight between 5 °C to 20 °C as per their material safety datasheets provided by the manufacturers of both products. SU-8 and NOA 61, both need to be equilibrated to room temperature before use.

3.4.2 Substrate Preparation

Silicon wafer was chosen as the substrate material in the polymer based optical waveguide fabrication. Silicon has a good surface quality and a refractive index of 3.48 at 1550nm. The surface preparation of the substrate is extremely important to ensure proper adhesion of the coated film. Typical contamination agents are dust and dirt from shipping or storage, and sample holder or finger prints from handling (Bach 1997). Substrates were ensured free of scratches and pits, clean and dry prior to use. If a light-guiding film is deposited on a scratched or cracked surface, the evanescent wave associated with the light would scatter from the damaged area, as a result the guide will be very lossy (Tamir 1975). The substrate wafers were prepared by piranha etch (H_2SO_4 + H_2O_2) whenever required before rinsing them with de-ionized water in an ultrasonic cleaner for 5 minutes. After that, they were rinsed with ethanol and dried with high pressure nitrogen gun. The cleaned wafers were dehydrated before use at 120-140°C in an oven. Thoroughly dehydrated wafers were critical in providing good adhesion between NOA 61 layer and Silicon wafer surface.

3.4.3 Adhesive Film (Under-Cladding Layer) Deposition

There are a few techniques for film deposition in the waveguide fabrications. They are spin coating, dip coating, thermal vapor deposition, sputtering, chemical vapor deposition (CVD) and polymerization (Nishihara 1985). The Adhesive NOA 61 can be coated on Si-substrate directly without the requirement for any bulky and extremely expensive deposition chamber. The spin coating technique is the simplest and least expensive, but contamination and uniformity of the film needs control and check (Nishihara 1985). Adhesion of NOA 61 layers

to the Si-substrate and core layer are critical issues in thin film fabrication processes. NOA 61 films were spun onto the substrate directly without any adhesion promoter. To obtain a uniformly coated film, formation of air-bubbles were prevented when dispensing the polymer with a syringe or a dropper. The volume of solution dispensed was kept constant for each sample to ensure the uniformity. The spin speed used to deposit the adhesive layer varied according to the final film thickness desired. Spin coater Model PWM-32 PS-R790 SS from Headway Research Inc., USA shown in Fig. 3.6 was used for coating the adhesive. Fig. 3.7 shows the NOA 61 film thickness after UV curing, and final thicknesses obtained after a series of experiments done for the same. A small amount of adhesive depending on the Si-wafer size was dispensed statically at the centre of the wafer in order to spread out the adhesive evenly from the center of the substrate. An under-clad thickness of more than 10 μm over silicon-wafer is required to achieve guidance of light through the SU-8 core as analyzed over a EIM 2D mode solver (Hammer 2012). A typical spin-curve for NOA61 is shown in Fig. 3.7. The spinning speed was kept at 4000 rpm for 30 seconds to achieve the pre-cure thickness above 10 μm as shown in Fig. 3.7.

Figure 3.6. Spin coating unit at CSIR-CEERI, Pilani.

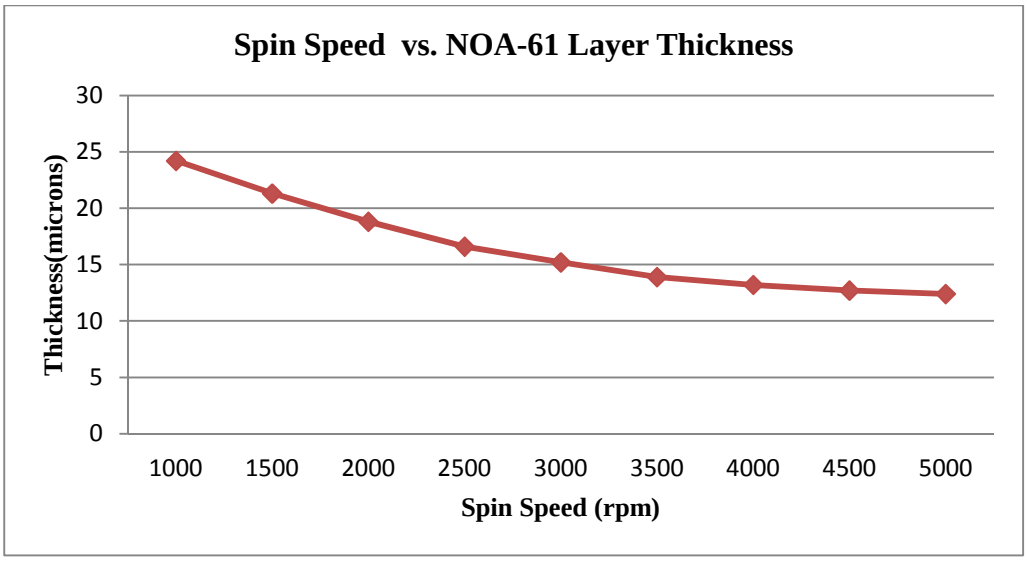

Figure 3.7. Spin Speed vs. Thickness Curve for NOA 61.

3.4.4 UV Cure

The Adhesive NOA 61 gets cross-linked when cured by ultra-violet light. The curing was carried out for 10 minutes at an average intensity of 48 mW cm^{-2} by using a high wattage (400 W) UV lamp (Dymax 5000EC) shown in Fig. 3.8, then left for stabilization at 60°C for next 15 hours. Besides improving adhesion between NOA 61 and Si-wafer, UV curing develops strong adhesion between NOA 61 and SU-8 2002 core layer to be coated over it.

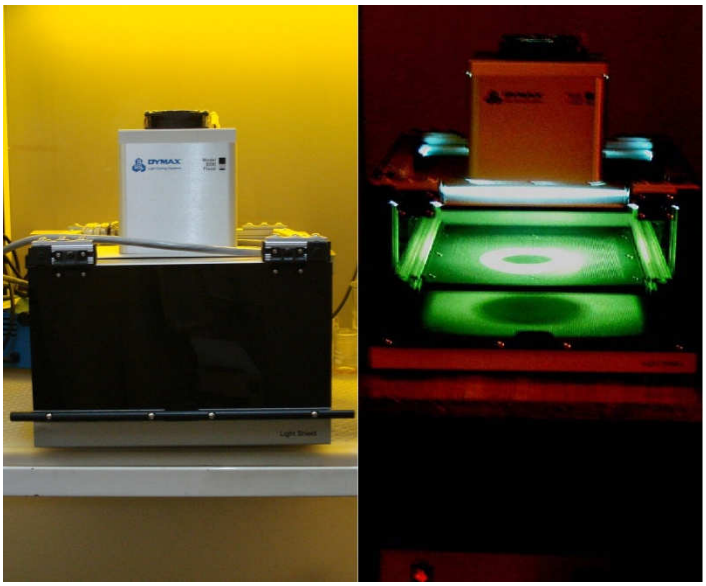

Figure 3.8. Dymax 5000 EC: Set-up (in left), during curing process (in right).

3.4.5 Core (SU-8 2002) Layer Deposition

The most important step in the waveguide fabrication is the light-guiding film deposition, in which a material of slightly higher refractive index is deposited as a thin film on a under-cladding layer of low-refractive index. The SU-8 2002 core material was spun at 1400 rpm for 30 seconds on top of NOA 61 coated Si-wafer, after equilibrating the wafer to room temperature, to achieve a thickness of around 2.5 μm. The thickness of the film deposited decreases in post-spinning baking process. The post-baking thickness of the SU-8 resist was verified by a stylus profiler discussed in section 4.3. Fig. 3.9 shows a typical spin curve for SU-8 2002.

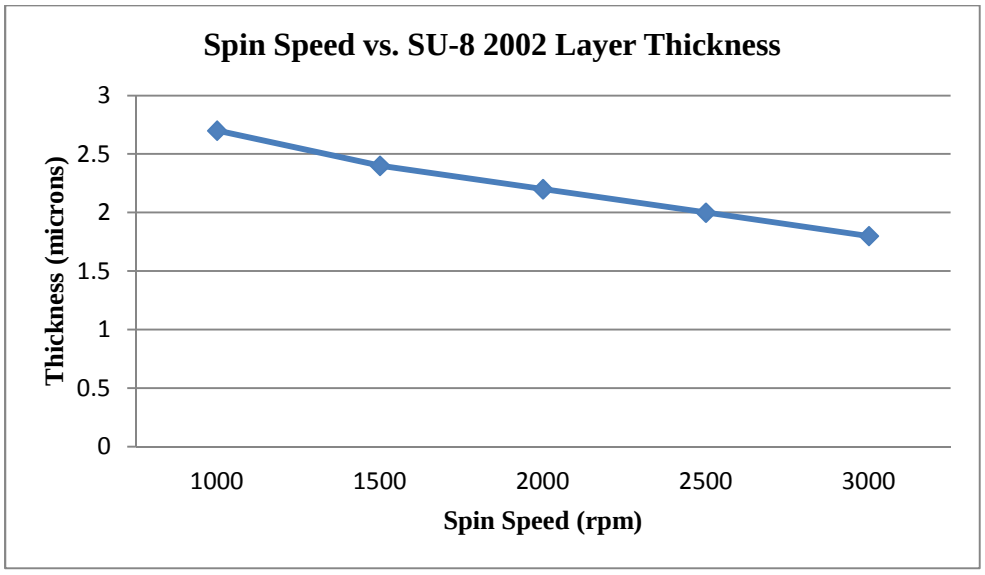

Figure 3.9. Spin Speed vs Thickness Curve for SU-8 2002.

3.4.6 Pre-Exposure Soft Bake

After spin coating, the films were soft-baked using a two-step process for a small duration of time to remove the solvent from the film. The specific time and temperature are dependent on the composition of the substrate as well as the thickness of the film. For SU-8 2002 layer, specification sheet of SU-8 2000 series supplied by manufacturer suggested two-step soft-bake for a duration of 1-2 minutes, first at 60 ºC then at 95 ºC. Pre-exposure bake was done on a hot plate in conjunction with a post-exposure or pre-develop bake. The soft-bake was carried out immediately after spin coating. The uniformity of the film may get altered at

places due to presence of solvent in a fresh-coated film when moved from spin-coater to hot-plate. Therefore, adequate care was taken to keep the substrate in a horizontal position to avoid any change in level while transferring the substrate from spin coater to hotplate during the soft-bake process. The temperature and the duration of soft-bake determine the residual solvent concentration in SU-8 at the moment of UV exposure. For small durations less than 5 min, poor resolution and bad definition of sidewalls was observed while for long durations greater than 1 hour, insufficient cross-linking occurs due to partial development of SU-8 (Keller 2008). Here, a two step-process (65 °C for 5 min and 95 °C for 20 min) was used to remove any traces of solvent before exposure.

3.4.7 UV Photolithography

Photolithography process involves the transference of two-dimensional patterns available on the mask to the polymer film. After being developed, the film has an exact replica of the mask patterns. After the soft bake, the wafers were allowed to cool to room temperature before photolithography. Once the mask and the wafers were appropriately aligned, the exposure process was carried out. The alignment was done keeping in mind that the end-facets of the devices will be prepared by cleaving of the wafers. In order to achieve a better resolution of the image, the mask was placed in physical contact with the wafer also known as hard contact or contact exposure. Unfortunately, physical contact with wafer degrades the mask faster unlike non-contact, and proximity masks, which are few microns above the wafer. The latter method prolongs the mask lifetime but degrades the resolution of the resulting pattern since the separation causes a shadowing effect that increases as the light incidence is less normal. The hard contact method also degrades the uniformity of the film, as the polymer will stick to the mask, in case the film is not fully dried after the pre-exposure soft bake. However, hard contact method was used to ensure better resolution for the patterned waveguides as it was critical to achieve better device performance, as will be discussed in chapter 4. The amount of incident radiation required for an optimum resolution depends on several parameters such as the coating thickness, underlying surface reflectivity, structure size, desired wall profile and also feature uniformity (Gang 2004). SU-8 waveguides were realized by UV exposure for 90 seconds in contact with photomask using a

Karl Suss MA56 mask aligner, shown in Fig. 3.10, with an i-line mercury lamp providing intensity ~10 mW cm^{-2}.

Figure 3.10. Karl Suss MA56 Mask Aligner at CSIR-CEERI, Pilani.

3.4.8 Post-Exposure Bake

After exposure, a post exposure bake ≥ 90 °C is required to cross link the resist. The issue with thin SU-8 films is that this results in cracking or delamination mainly due to thermal stress. One way to overcome the issue is to use high exposure dose as it corresponds to a higher photo-acid concentration and improves cross-linking. For a post exposure bake ≥ 60 ºC, the thickness of the SU-8 layer stays uniform while the tensile stress increases linearly. However, the absolute stress values are considerably low at higher exposure doses. The duration of post exposure bake has only minor influence on the film thickness and stress (Keller 2008). However, high exposure dose has a negative influence on the lithographic resolution. High exposure dose leads to waveguide broadening and a reduced trench width due to optical effects such as diffraction at the mask and reflection on the substrate (Zhang 2004). A post exposure two-step baking process (65 ºC for 2 min and 95 ºC for 5 min) is used to crosslink the polymer.

3.4.9 Waveguides Development

Once the photolithographic process is done followed by a post exposure baking, the next step is selective removal of the film from unexposed areas of the samples with the etching processes. SU-8 2002 can be developed by wet-etching method, which can be done without costly and bulky equipments such as RIE, ICP or plasma etching. By wet etching, it is understood that the elimination of a material is accomplished by its dissolution in an adequate etching solution. It is mainly used for cleaning, shaping and polishing. The drawback of wet chemical etching is the lower quality of sidewall resolution of the waveguides. The wafer was placed in a bowl filled with SU-8 developer, the etching solution: Propylene Glycol Methyl Ether Acetate (PGMEA). Sufficient amount of developer was used to completely immerse the wafer. The wafer was allowed to rest in developer for a pre-determined length of time to allow dissolution of the unexposed areas. The develop time was set as 70 seconds and then rinsed in IPA for 10-15 seconds. Following the rinse, the wafer was blown dry (N_2) to remove the developer solvent and dry the wafer. The waveguide patterns if loosely adhere to the under-clad layer, will get displaced indicating poor adhesion between core and cladding material.

The wafer was observed through a high resolution microscope for inspection of the developed pattern. The etching process was repeated if the waveguide was under etched. Development times were varied to observe the effect of chemical etching on waveguide dimensions and the surface quality. The duration for development was optimized to obtain best possible results. A step of post-develop bake for a small-duration may also be included here as without the post-develop bake, the side wall inconsistencies of the waveguide may occur and hence giving higher scattering losses (Microchem 2000). The post-develop bake can be carried out at 65°C for 60 seconds. Post-develop bake ensures removal of traces of developer from wafer and improves adhesion with over-clad layer to be deposited next.

3.4.10 Adhesive Film (Over-Cladding Layer) Deposition

Coating of NOA 61 layer as over-clad is the final step of waveguide fabrication process. The over-clad deposition is done following the same steps as for the under-clad layer deposition. Following the photolithographic and chemical wet-etching process, an over-cladding layer

was deposited and the layer was UV-cured. The process of deposition of under-clad layer was repeated here to deposit over-cladding layer over the SU-8 waveguides. The fabricated 1 × 4 device is shown in Fig. 3.11. A 1 × 4 device after over-clad deposition is not shown here due to poor visibility of features of waveguide patterns through over-clad layer. Finally, a hard bake at around 120-140 ºC for 60 to 120 minutes is suggested to remove further any traces of solvent or developer left behind. The whole fabrication process (from section 3.4.1 to 3.4.10) is summarized in Fig. 3.12 before concluding this chapter.

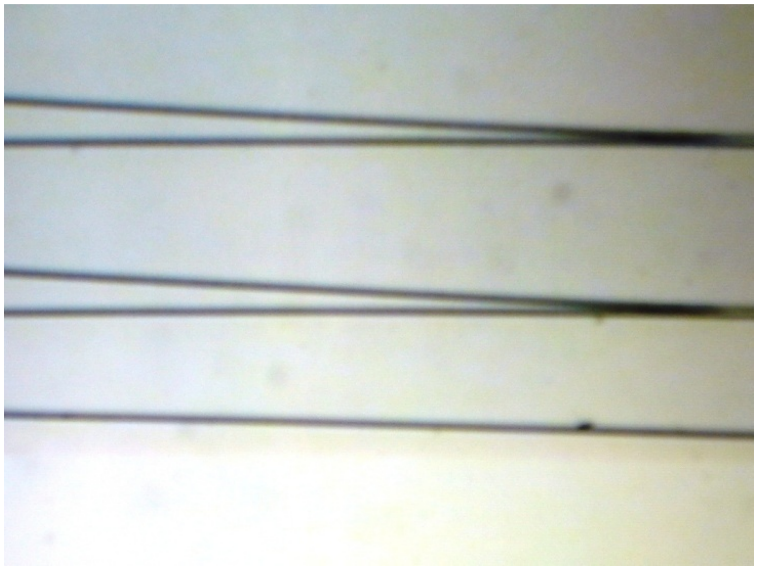

Figure 3.11. Fabricated Conventional 1 × 4 splitter.

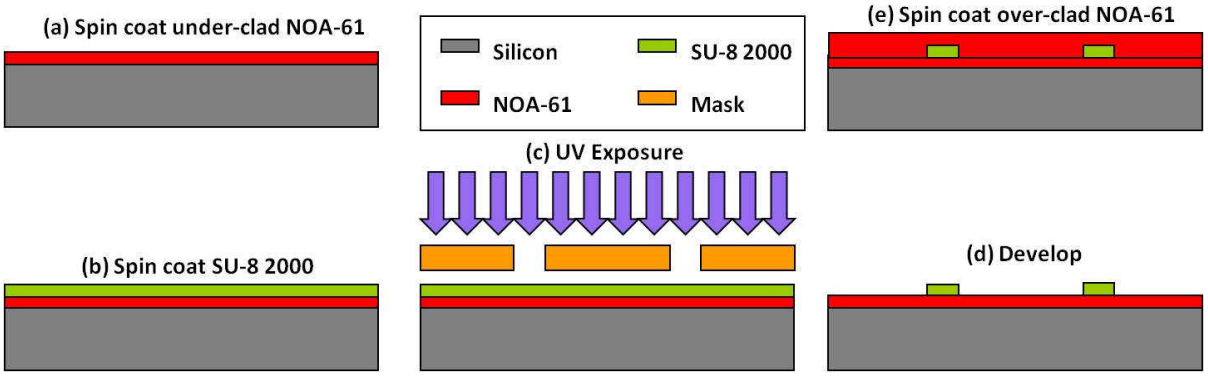

Figure 3.12. Polymer Waveguide Fabrication Process Steps.

3.5 Conclusion

The design and fabrication of Y-branch waveguide which is the basis of the optical power splitter was discussed in the chapter. The conventional Y-branch design for 1 × 4 power splitter was presented in the chapter. The design of mask for fabrication of 1 × N splitters using L-Edit (Tanner Tools) was presented here. An overview of the micro-fabrication procedures and techniques for polymer waveguides was presented in the chapter. Finally the steps of fabrication process used and related issues observed were discussed in the chapter. The substrate surface is coated with NOA 61, followed by UV curing and baking and then left for stabilization at 60ºC for 15 h. The SU-8 2002 core material was spun on top of NOA 61 coated silicon substrate and then soft baked using a two-step process to remove any traces of solvent after exposure. Channel waveguide width of 2.5 μm was realized by UV exposure in contact with a photomask. A post-exposure two-step baking process was used to crosslink the polymer. The photoresist-coated UV-exposed substrate was developed in PGMEA and then rinsed in IPA. An over-clad of NOA 61 was coated on developed SU-8 waveguides. Finally, a hard bake at 140 ◦C for 1 hour, removed the traces of developer or solvent left behind.

CHAPTER 4

WAVEGUIDE CHARACTERIZATION

The characterization of optical waveguides is an essential post-fabrication step in any waveguide development process. It is necessary to evaluate and to confirm that the fabricated waveguide exhibits characteristics, designed for. Simulation and fabrication steps can only be validated when experimental results match with those expected. Thin film optical characterization is needed in order to determine the suitability of the material for fabrication of optical waveguides. The characteristics of a waveguide, designed and fabricated should be evaluated through experiments in which a guided wave is excited. The evaluation of the waveguide characteristics serve as a feedback to improve the design and the fabrication process, as a consequence improves the waveguide or device performance. In this chapter, the optical waveguide characterization techniques used in this work will be elaborated.

In a typical waveguide evaluation experiment, light of a certain power is launched into the waveguide and power of the light output from the waveguide measured. The ratio of the output to the input powers expressed in logarithmic scale (dB) gives the insertion loss of the waveguide. In order to make a choice from optical materials and to schematically design waveguide based devices, it is necessary to know the refractive index of the guiding layer, the layer thickness, guide propagation loss, etc. In order to keep the refractive indices and the waveguide geometry within the required tolerance limits, they have to be measured with suitable methods at appropriate times. Measurements on optical waveguides are useful to assess suitability of the device for a particular application and enabling design optimization of device structures. Such measurements provide important fundamental data to decide whether the waveguide is appropriate for construction of optical integrated circuits. These results are also utilized to specify the reason for any degradation in waveguide characteristics. Techniques, methods or processes to improve performance at waveguide or device level are accomplished through feedback to the design and fabrication processes.

The first step in any waveguide design is to determine if the combination of substrate, guiding region and the cover work as a waveguide at all. This can be done by determining the number of modes supported by a given planar waveguide structure. This information is

valuable in designing a channel waveguide which is the basis for any integrated optic device. Some of the waveguide parameters usually measured are: the waveguide effective index, the refractive index profile, the guide-mode numbers, propagation losses, etc. This chapter includes brief details of facilities utilized for characterization for waveguides available at CSIR-CEERI, Pilani and SAMEER, Mumbai. Refractive index measurements and modal characterization of planar waveguides are discussed in first few sections of the chapter. Planar waveguides fabricated in this work were characterized by prism coupling for number of TE and TM modes supported. Discussion on characterization of planar waveguides is followed by characterization of channel waveguides. Finally, characterization of power splitter based on Y-branch waveguide is presented in the chapter. Effect of residual resist at Y-junction of a conventional 1 × 2 splitter is analyzed through BPM simulation and discussed in last section of the chapter.

4.1 Refractive Index Measurements

The silicon wafers coated with NOA 61 only and with SU-8 over NOA 61 were used to measure the film refractive indices. The measurement was carried out with UV-cured polymers coated on Si-wafer in a commercial prism coupler unit (Metricon 2010) available at CSIR-CEERI Pilani. The measurements for TE mode at 632.8 nm and 1548 nm are shown in Fig. 4.1 (a) and (b) respectively. Measurements on the refractive index of the film indicated that the values of the refractive indices of core and clad polymers at a wavelength of 1550 nm assumed in the simulation were correct. Fig. 4.2 summarizes the measurements carried out. Refractive index measurements of a given material through Metricon 2010 Prism Coupler requires information about the coated film thickness. The film thickness can be estimated through the spin speed versus film thickness curve, or it can be measured through an stylus profilometer e.g. AMBIOS XP-2 after waveguide patterns are developed over silicon wafer. Measurements were carried out using AMBIOS XP-2 stylus profiler for SU-8 waveguides and details of the same are discussed in section 4.4 of the chapter. It must be pointed out here that the film thickness of NOA 61 is difficult to be accurately measured using the stylus profiler. So, the best option was to rely upon the spin-speed versus thickness curve. To avoid guided power penetration towards Si substrate, optimum coating thickness of

NOA 61 is required. Thus, a spin-speed of 4000 rpm was chosen to spin-coat the optical adhesive so as to keep the NOA 61 thickness above 10 microns (See Fig. 3.7 in Chapter 3).

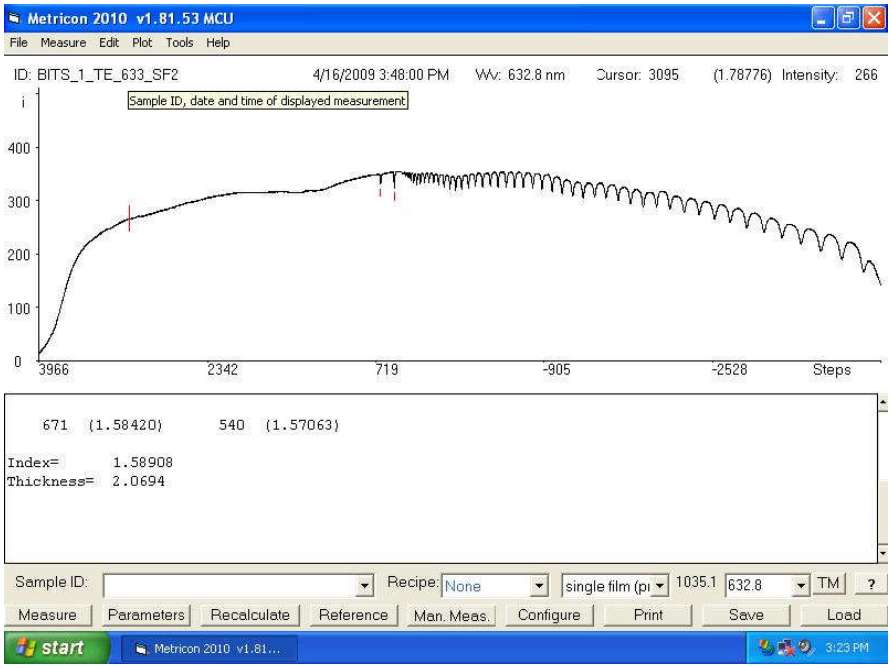

(a)

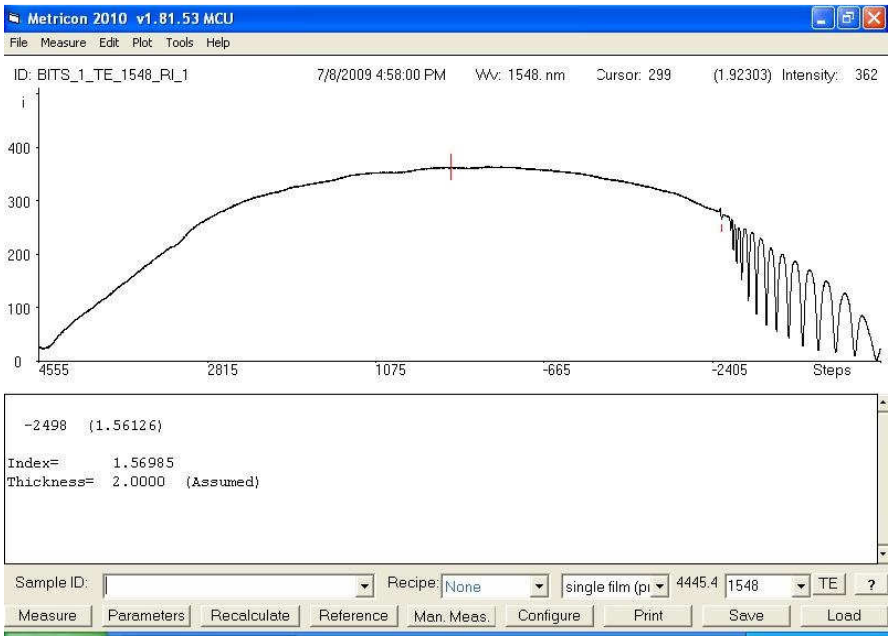

(b)

Figure 4.1. Refractive index measured (a) at 632.8 nm and (b) at 1548 nm.

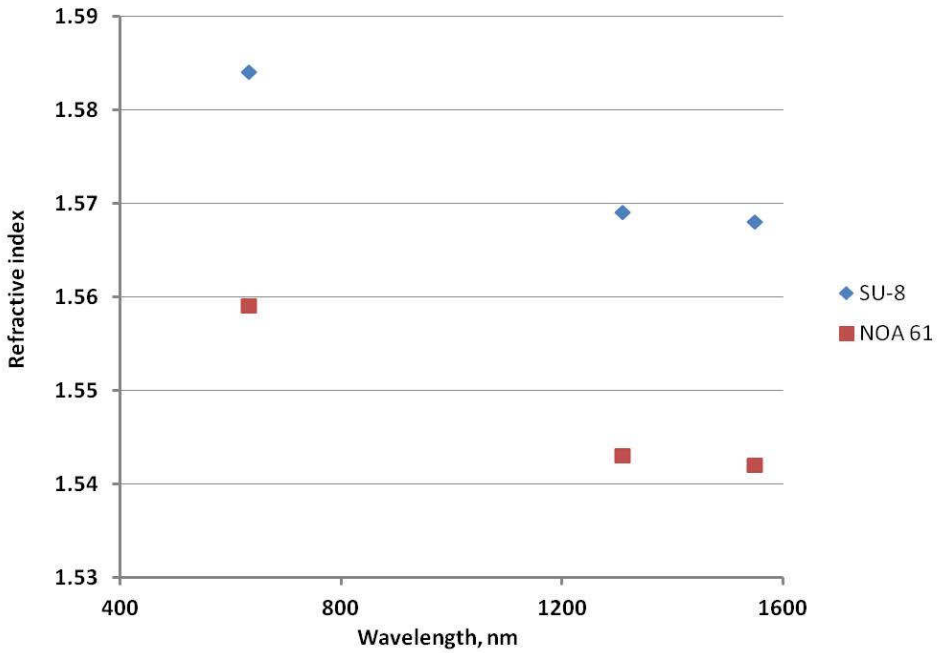

Figure 4.2. Refractive index (TE mode) as a function of wavelength.

4.2 Modal Characterization

Determination of number of guided modes in a planar waveguide is an important characterization. The waveguides in this work were designed to be single-mode at 1550 nm. In multimode waveguides the light intensity couples between the different guided modes. This altered intensity distribution strongly influences the performance of a device, e.g. in bends or in coupling regions. The well known technique of prism coupling (Tien 1971) was used in this work to estimate the number of guided modes. One such prism coupler set-up is shown in Fig. 4.3. The totally reflecting prism coupler technique, also referred to as the m-lines technique, is commonly used to determine the optical properties of thin films (Flory 1996). The refractive index and the thickness as well as the anisotropy of dielectric planar waveguides can also be determined. (Kersten 1975) (Lukosz 1995).

The coupling of a laser beam by a prism into a planar dielectric waveguide is governed by the angle of incidence of the light onto the prism. Under certain conditions, the light energy can be transferred into the waveguide by the evanescent fields that are excited in the gap between the prism and the film. These conditions are: (a) the incident beam must have the proper angle of incidence so the evanescent field in the gap travels with the same phase

velocity as the mode to be excited in the waveguide; (b) the incident beam must have the same polarization as the mode to be excited; (c) the film must be placed close enough to the prism base (typically the gap is in order of half a wavelength). The m-lines appear for the different incident directions corresponding to the coupling of light in the waveguide. As the coupling between the prism and the waveguide increases, the m-lines are broadened and shifted. For m-lines measurements, the coupling is generally considered weak and is neglected as soon as the thickness of the air layer between the prism and the waveguide is greater than about half the wavelength of the coupled beam (Kersten 1975) (Lukosz 1995).

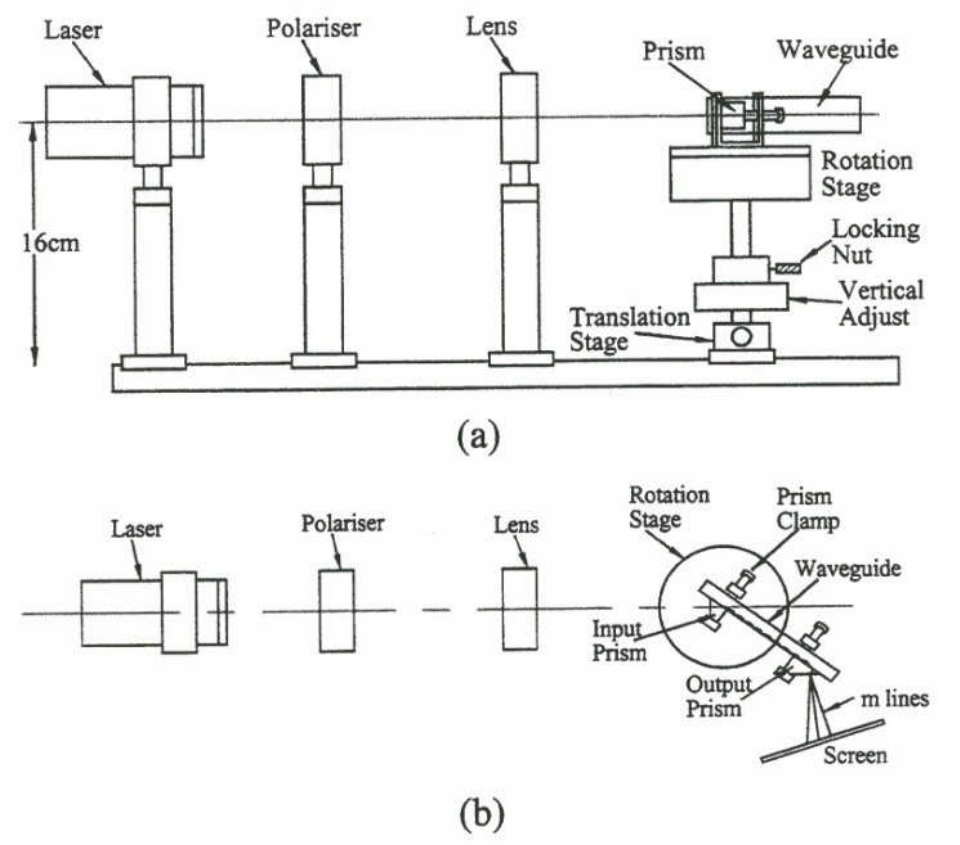

Figure 4.3. Set-up for m-lines (a) Side View (b) Top View.

Figure 4.4 shows the experimental set-up from OPTOSCI Ltd., UK used to analyze the planar waveguide and consisted of the following hardware elements: An optical rail bench fitted with a visible semiconductor diode laser with integral drive electronics plus mount, a polariser with a graduated rotational mount, a mounted lens, a precision graduated rotational table fitted with a high index prism coupling assembly into which the waveguide is mounted.

While changing the incidence angle, the bright lines (so called m-lines because they display the modes of different orders m) appear on the screen only when the laser beam is coupled into a mode of the film.

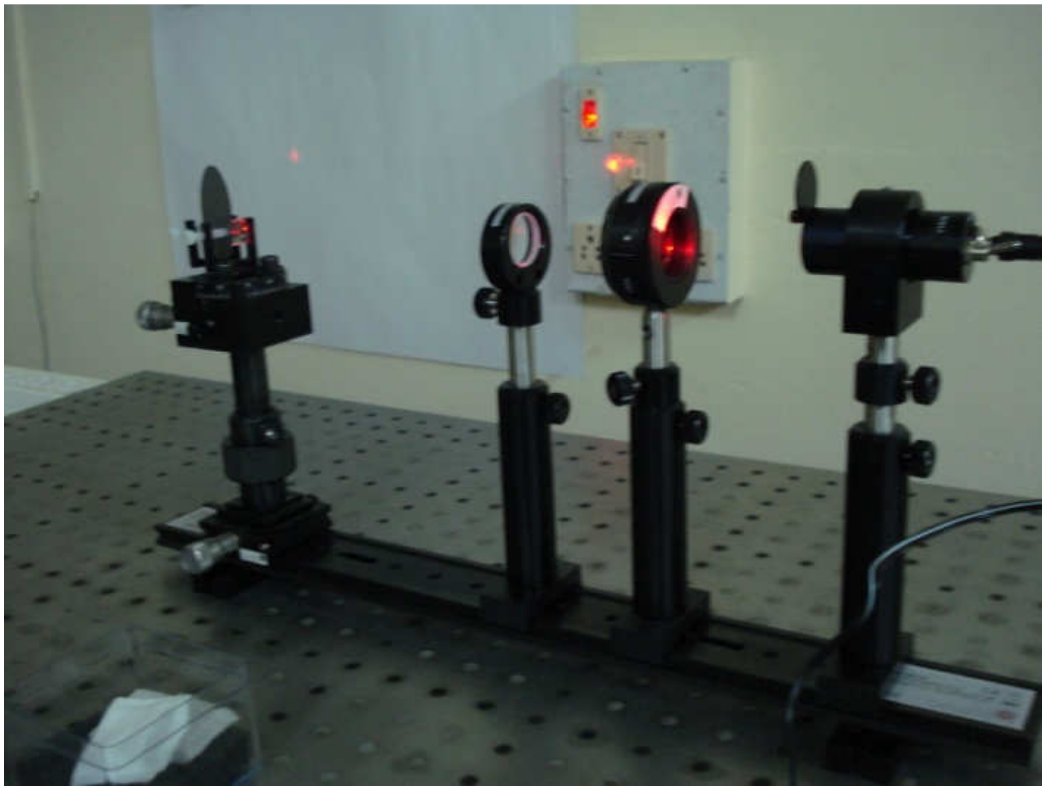

Figure 4.4. Prism Coupler from OPTOSCI Ltd, UK.

The light propagating in that mode is scattered into other directions (in the plane of the film) of the same mode and of the other modes. A fraction of the scattered light is then coupled out again by the prism and produces the bright lines on the screen. In accordance with this explanation it is characteristic for the bright m-lines that they all light up simultaneously when, during rotation of the prism, one of the coupling directions passes through the direction of the input beam. Moreover, in each of these coupling situations, the reflected beam on the screen coincides with one of the m-lines. Identifying the mode number (m = 0, 1, 2…) and corresponding excitation angle, the film index and thickness can be determined. At 632.8 nm, it was observed that m = 0, 1 for a 2.5 μm thick SU-8 planar waveguides with a lower cladding of NOA 61 and no upper cladding layer. Fig. 4.6 shows one such m-line at 632.8 nm.

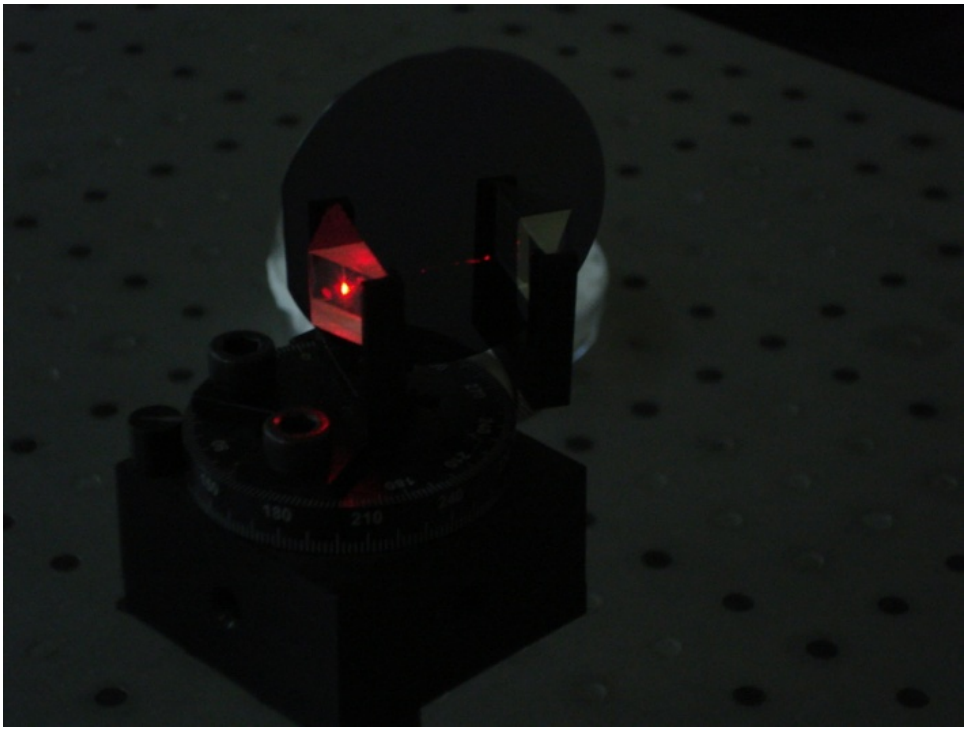

Figure 4.5. Guided mode at 632.8 nm in planar SU-8 waveguide.

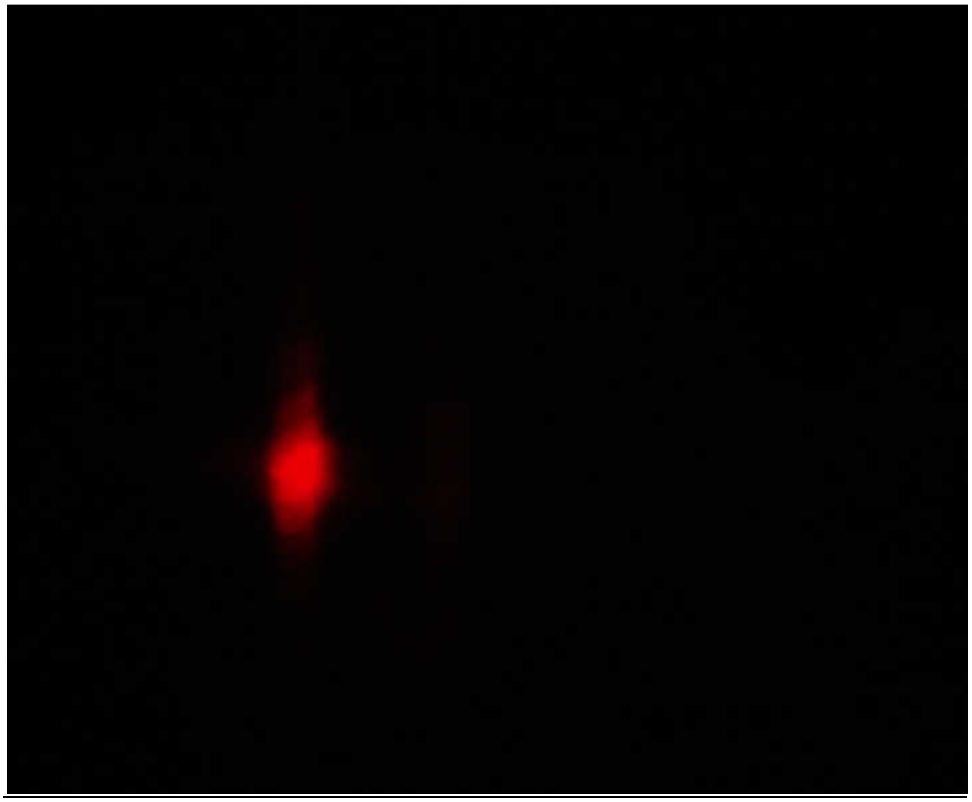

Figure 4.6. Mode-line (m-line for m = 0) at 632.8 nm

Table 4.1: Mode Calculations at 632.8 nm (Theoretical)

Mode Number (m)	**TE mode**		**TM mode**	
	Eff. RI	**Modal Cut-off Thickness (μm)**	**Eff. RI**	**Modal Cut-off Thickness (μm)**
0	1.5663	0.4338	1.5661	0.4832
1	1.5553	1.4696	1.5547	1.519
	$V_{cut\text{-}off} = 1.32$; $V_{Number} = 7.58$		$V_{cut\text{-}off} = 1.47$; $V_{Number} = 7.58$	

Table 4.2. Mode Calculations at 632.8 nm (Experimental)

Mode Number (m)	**Direction (+ve/-ve)**	**Launch Angle**		**Eff. RI**	**Modal Cut-off Thickness (μm)**
		Degrees	**Minutes**		
TE mode					
0	+ve	2	56	1.566	0.434
1	+ve	1	24	1.553	1.471
TM mode					
0	+ve	2	56	1.566	0.483
1	+ve	1	24	1.553	1.52
Film Index: 1.57; Depth: 2.32 μm					

SWAN (MIC) - Software for Waveguide Analysis (Modal Index Calculator) is an Optical Waveguide Analysis Software provided by OPTOSCI for use with, and to complement, OPTOSCI's prism coupling unit. It provides a simple tool for studying planar optical waveguides experimentally and theoretically. As the prism coupling unit is provided with a 632.8 nm laser, modes were calculated theoretically and experimentally for 2.5 μm thick SU-8 planar waveguides at wavelength of 632.8 nm. Initially, the Laser orientation is fixed to provide an output polarization direction at 45º which launches both TE and TM polarization conditions simultaneously. The polarization direction incident may be adjusted simply by rotating the polarizer till its transmission axis is vertical or horizontal as required. The polarizer is fixed in its mount such that its transmission axis is vertical (TE) when the

orientation is set at zero. The theoretical and experimental results are tabulated in Table 4.1 and Table 4.2 respectively.

4.3 Waveguide Surface analysis

High resolution microscopic examination of the planar waveguides is absolutely essential to ensure that the surface of the waveguide is free of any particulate matter, presence of pin holes, etc. Further, it is also important to ensure that the film surface is free of any visible cracks, strains and is of uniform thickness. The coated film of SU-8 2002 over cured NOA 61 on silicon substrate were observed under microscope. The thickness and the topography of the waveguide can also be measured using a stylus surface profiler. Estimates of film thickness, waveguide width and the surface roughness of the coating can be made using the surface profiler. Surface profiling here in this work was done using AMBIOS XP-2 stylus surface profiler. Stylus profiling provides information on both the film thickness as well as film uniformity. However, the stylus of the surface profiler could scratch the waveguide during its scanning on the sample which may be prevented by choosing optimum stylus force. This is a reason why samples used for measurements for optical properties were different from those used for guiding light.

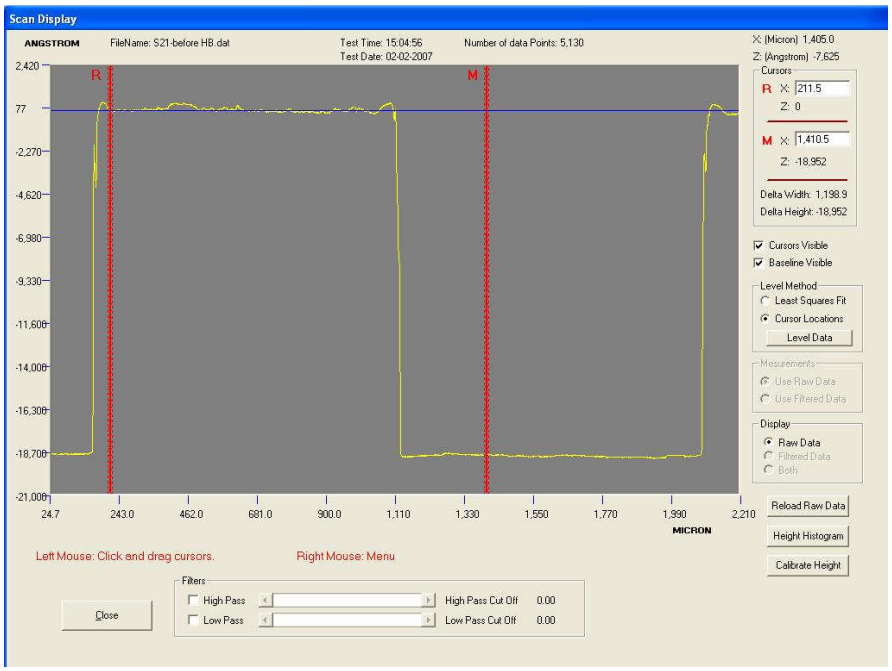

(a)

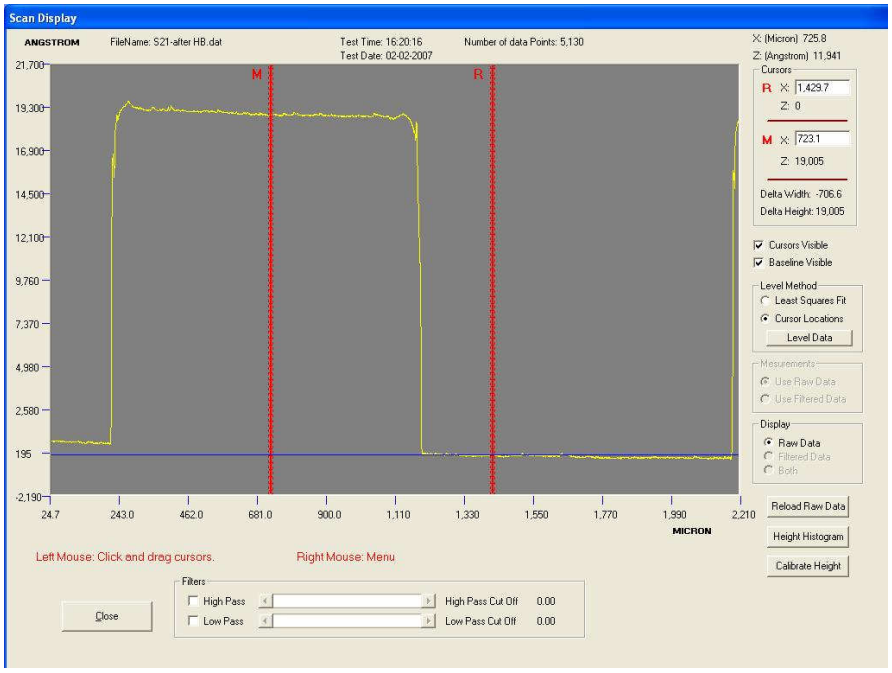

(b)

Figure 4.7. AMBIOS XP-2 surface profile measurements (a) Before hardbake (b) After hardbake.

Channel waveguides with wider cross-section were fabricated to observe thickness of SU-8 films and surface roughness to estimate losses during guiding the light due to the same. Measurements in Fig. 4.7 indicates film thickness of less than 2.5 μm. The surface roughness of the SU-8 thin film captured by the surface profiler can be observed on the top of the cross-section. Decrease in surface roughness after the Hard bake is clearly visible in Fig. 4.7 (b). The average surface roughness was observed to be less than 10 nm.

4.4 Characterization Facility

For channel waveguide, the measurement of output light power with respect to that at the input gives a measure of the insertion loss. The lower the insertion loss, the better is the quality of the channel waveguide. The channel waveguide characterization was carried out at SAMEER, Mumbai. The channel waveguide characterization setup consisted of the following:

a) Laser Systems (e.g., a 632.8 nm , 5 mW He-Ne laser from Melles Griot).

b) Micro-positioning stages to provide precise alignment for end-fire coupling experiments.

c) Microscope objective for coupling in the light, normally a 10X objective.

d) Digital charge coupled device (CCD) camera.

Light was fed into the fabricated channel waveguides by end-fire coupling. End-fire coupling can be achieved by means of a microscope objective lens focused on the input face of the waveguide or butt-coupling an optical fiber with the input face of the waveguide. The guided light from the waveguide end-face is extracted using a long working distance (LWD) microscope objective lens attached to a CCD camera. Though SAMEER, Mumbai had the automatic fiber alignment facility, it was not used because of unpolished cleaved waveguide's input and output end-facets. Therefore, through simple end-fire coupling light was launched into the waveguide and the output beam spots were observed on the screen. One such set-up is shown in Fig. 4.8. Light coupling experiments here, involve the coupling of light into waveguide samples that are simply cleaved without polished facets.

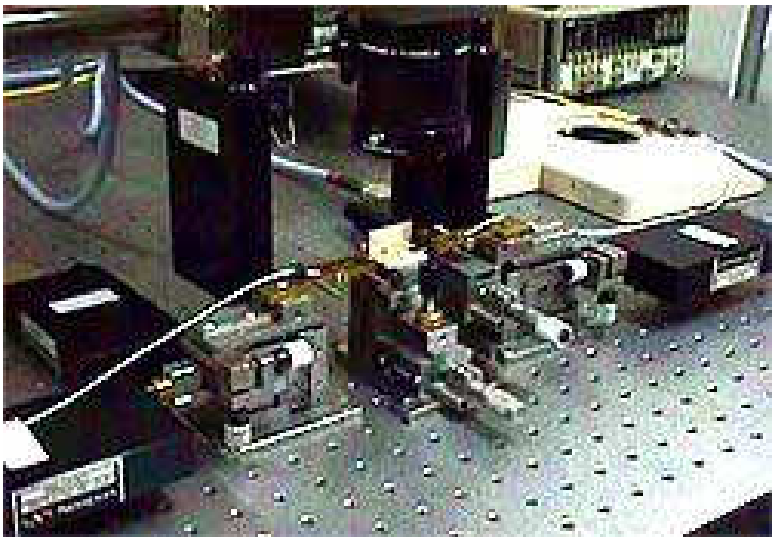

Figure 4.8. Setup at SAMEER Mumbai for end-fire coupling.

The waveguide to be evaluated is kept on precise alignment stages capable of X-, Y- and Z-movements. The input and output components (i.e. the fiber or the input microscope objective and the LWD output microscope objective) and the waveguide sample are

separately mounted on high precision micro-positioners and manipulators to achieve accurate and stable alignment. End-fire coupling experiments were designed for observations of the intensity profiles of waveguide modes. Precise insertion loss measurements could not be made before pigtailing as there is no way to measure the amount of light going into the waveguide in the absence of fiber pigtail at the input and output ends of the waveguide.

4.5 Channel Waveguides Characterization

A similar inspection of the channel waveguides under a high resolution microscope, apart from any non-uniformities in the channel width, defects due to poor lithographic processes, discontinuities in the devices, etc can also give information on the quality of sidewalls, to a certain extent. The thickness of the channel before exposure and hard bake was found to be less than 2.5 μm, and after pattern development before hard bake the height of waveguides was in range 1.8 - 2.2 μm. AMBIOS XP-2 surface profiler was used to measure height of waveguides after pattern development. Figure 4.9 shows one such typical measurement.

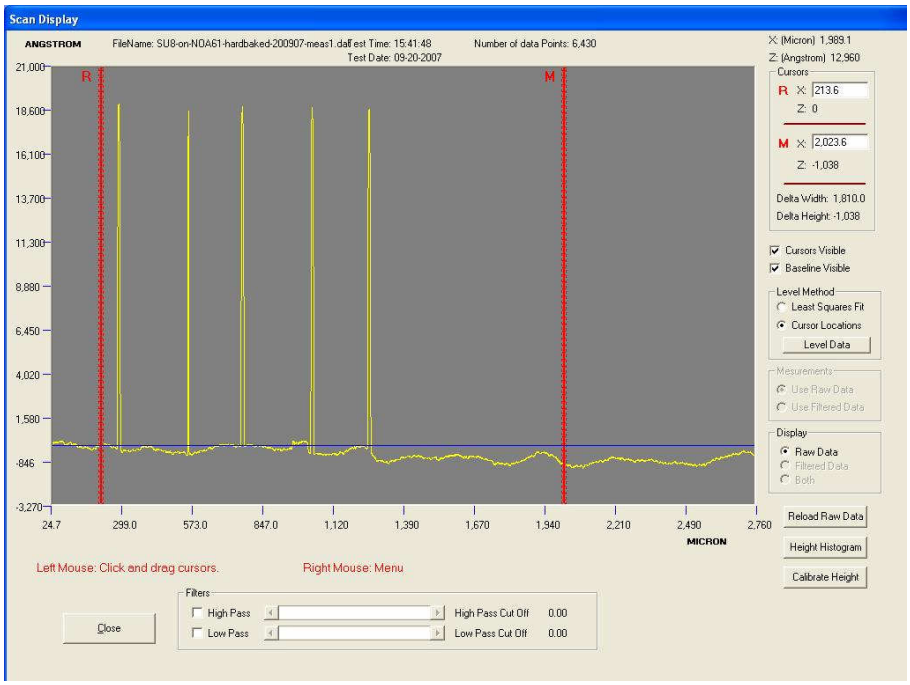

Figure 4.9. AMBIOS XP-2 waveguide height measurements.

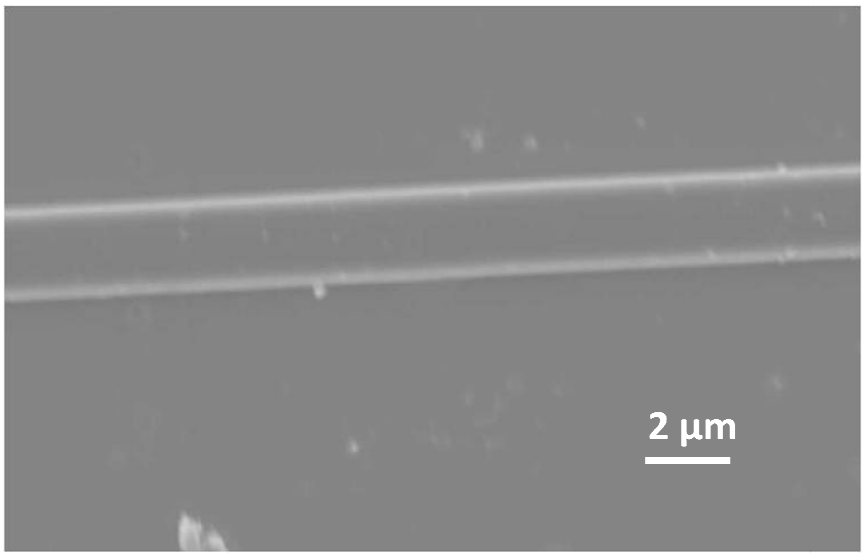

Figure 4.10. SEM of a channel waveguide.

A good evaluation of the sidewall quality can be given by SEM. SEM of a channel waveguide developed using the optimized fabrication process is shown in Fig. 4.10. As is evident from the SEM, the fabricated waveguides were smooth walled and vertical which shows optimal post-exposure etching by the developer. There are neither cracks nor any kind of defects in the fabricated waveguides throughout the device length.

4.7 Waveguide Losses

The attenuation of light propagating through an optical waveguide is a very important parameter in the evaluation of its usefulness for a range of applications. The optical loss of a guided mode is due to absorption, radiation and scattering in the guiding medium. In straight waveguides the absorption and the scattering are dominant. While the absorption may be due to the material itself, the scattering loss is influenced by the quality of the fabrication process. To quantatively describe the magnitude of optical loss, the exponential attenuation coefficients is generally used (Hunsperger 2009). In that case, the intensity (power per area) at any point along the length of the waveguide is given by:

$$I(z) = I_0 e^{-\alpha z} \qquad (4.1)$$

where, I_0 is the initial intensity at the input end of the waveguide i.e. at $z = 0$. $I(z)$ is the transmitted power through the waveguide at a distance z (cm), and α is defined as the

attenuation coefficient of the waveguide, measured in dB/cm. The loss, L in decibels is defined as:

$$L\,(\text{in dB}) = -10\log_{10}\left(\frac{I(z)}{I_0}\right) \tag{4.2}$$

While analyzing the SU-8 planar waveguides for refractive indices, loss measurements were also conducted to understand the propagation loss through planar waveguides at 632.8 nm and 1548 nm. The results obtained are shown in Fig. 4.11.

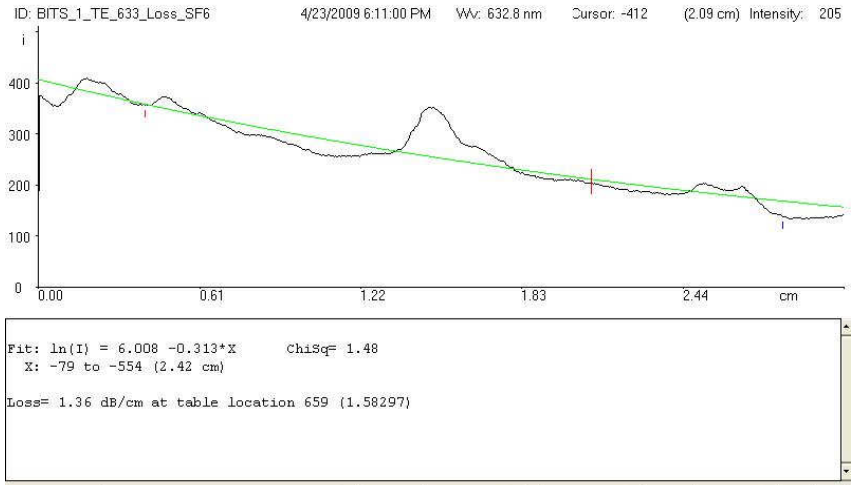

(a)

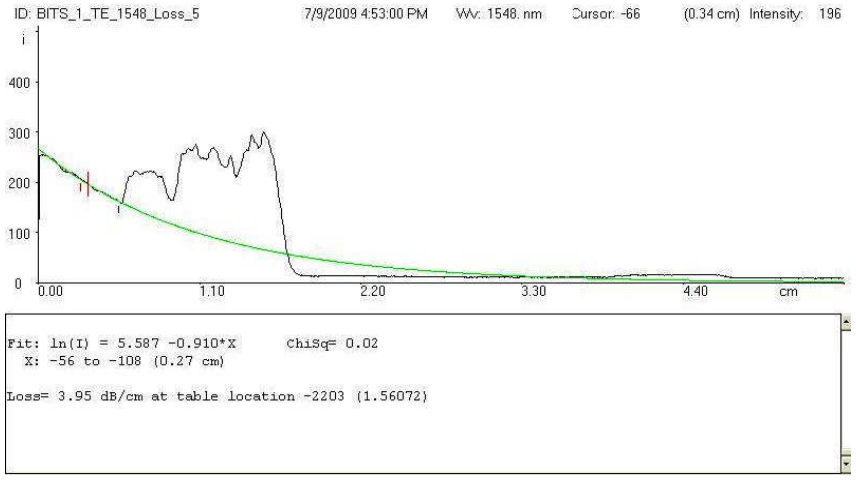

(b)

Figure 4.11. Loss measurements (a) at 632.8 nm (b) at 1550 nm on Metricon 2010

When propagation losses measured for planar waveguides, i.e., Si/NOA 61/SU-8/Air, the losses were found to be 0.39 dB/mm for TE_{00}. Due to small cross-section ~ 2 μm × 2 μm of waveguides, it was very difficult to measure how much light is coupled into the waveguide, unless the input end is pigtailed and the input face of the waveguide is polished to a very high quality. Polishing soft materials such as polymers is very challenging and has not been taken up in this work. The input and output ends of the waveguides were simply prepared by cleaving the Si-wafer on which they were patterned and the guided mode was excited by end-fire coupling. At 1550 nm, the propagation loss was estimated to be 0.125 dB/mm for the TE_{00} mode and 0.171 dB/mm for the TM_{00} mode (Tung 2005). The average insertion loss estimated at chip-level is 11 dB (TE_{00}) for 2-cm waveguide at 1550 nm. Besides 2.5 dB of propagation loss, the coupling losses estimated were 7.4 dB including field mismatch losses of 3.5 dB/port and Fresnel reflection losses of 0.2 dB per port (Tung 2005) (Dai 2009). An additional loss of 1 dB may account for radiation and absorption losses in the waveguides. As a next step, after the evaluation of straight waveguides, simple passive devices were investigated. The performance of a passive device e.g. Y-branch splitter is more sensitive to fabrication quality than a straight waveguide. Hence, a more stringent examination of the fabrication process is possible.

4.8 Power splitters

Y-branch based splitters are the most common type of power splitters or combiners. Generally, they have one input and up to 2^n outputs, where n = 1, 2, 3, 4... The pitch between the outputs is standardized to either 127 μm or 250 μm. Here, in this work we have designed power splitter assuming a pitch of 127 μm between the outputs. The designs need to be optimized for a small insertion loss and symmetric power distribution among the outputs of the splitter. In the present conventional design, to avoid radiation losses due to bends, S-bends were used to define the branches of the Y-splitter. The cosine-shape allows a gentle separation of the branches at the junction. Once the branches are separated, the radius of curvature decreases and the desired pitch is achieved relatively quickly. The final insertion loss in Y-splitter is expected to be larger than obtained in simulations. A general specification for 1 × N splitters regarding the insertion loss (IL) of these devices is given by (Telcordia 2001).

$$IL \text{ (in dB)} = 0.8 + 3.4\log_2 N \quad (4.3)$$

The uniformity (maximum variation of insertion loss between input port and N output ports) should be smaller than (Verizon 2007).

$$\Delta IL \leq 0.6\log_2 N \text{ (in dB)} \quad (4.4)$$

Hence, for a 1 × 4 device as per Telcordia standards, insertion loss should be equal to 7.6 dB and $\Delta IL \leq 1.2$ dB.

4.9 Preparation of Splitter Chips

Before packaging an integrated optic component, it is necessary to test whether the fabricated structure is guiding light. Edge polishing is an important processing step. If the material to be polished has sufficiently high mechanical hardness, conventional lapping and polishing methods can be employed. In the case of polymers, owing to their soft nature, conventional lapping and polishing procedure cannot be directly employed. However, to check if conventional lapping and polishing works in the case of SU-8 based waveguides, a wafer containing the fabricated splitters was diced. The input and output faces of the waveguide were lapped and polished on a Logitech lapping and polishing machine at low speeds. After the polishing process, the wafer was observed under the microscope for possible chipping and delamination which is typical in the case of polymer materials. In this case, dicing at high speed did not cause any chipping of the polymer film. However, attempts to polish it were not successful as the edge of the chip was observed to be not flat but tapered. A typical picture of such an edge is shown in Fig. 4.12. Therefore, it was observed that conventional polishing techniques would not be applicable here.

There have been a large number of reports in literature (Pelletier 2006) (Pelletier 2004) wherein the fabricated devices on silicon wafer were simply cleaved, thus avoiding the complications arising out of dicing and edge polishing. Since polishing was not successful, it was decided to adopt this approach. As mentioned earlier, during fabrication of 1 × 4 power splitters, the pattern on the mask was aligned parallel to the primary flat (<100>) of the wafer so that direct cleaving becomes possible. The following sections describe the cleaving process, chip preparation and device measurement. Since the wafer used in this thesis work

was a (<100>) oriented silicon, it was possible to cleave the wafer at 90º making it possible to prepare small rectangular chips each containing two or more devices.

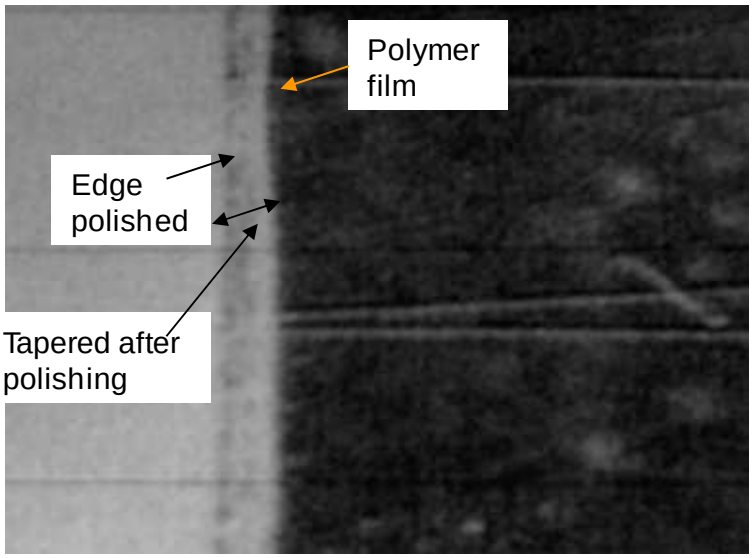

Figure 4.12. Tapered end resulting from polishing the polymer waveguide.

4.10 Cleaving chips for Testing

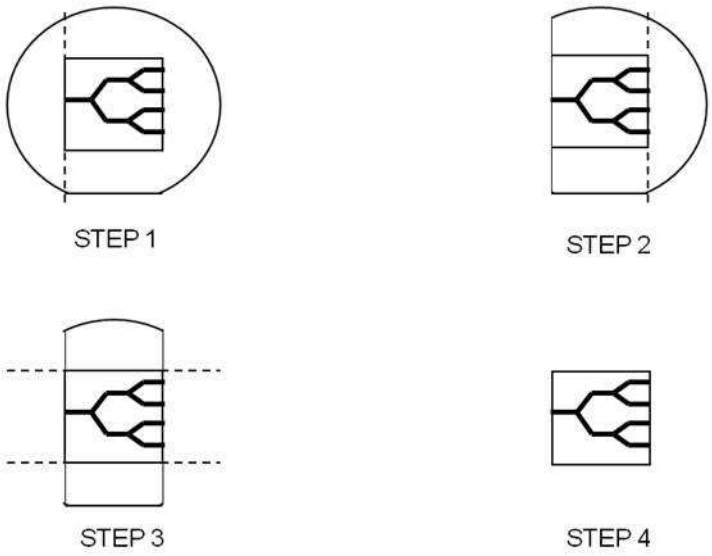

Figure 4.13. Steps involved in cleaving the chips from the wafer.

The wafers containing the fabricated devices were first cleaved before testing. In a typical cleaving experiment, a wafer was placed on a flat surface. Using a sharp tool, such as the

edge of a tweezer, a pointed pressure was applied to the edge of the wafer to initiate the cleaving process. Once initiated, the process terminated as the cleaving point reached the opposite side of the wafer. This is repeated till a rectangular piece of the devices was cleaved out. The process is schematically shown in Fig. 4.13 the dashed lines showing cleaved sides. Individual chips containing one splitter or group of splitters were prepared in this manner. In carrying out this kind of facet preparation, it is extremely important to keep the mirror-like quality of cleaved surfaces. On many occasions, the input end of the device did not terminate in the cleaved facet. Microscopic examination of the cleaved face did show some kind of strain in the polymer layers which either resulted from the cleaving process itself or occurred during the time the cleaved pieces were separated from each other. Getting a cleaved facet exactly perpendicular to the axis of the device critically depended upon how accurately the pattern on the mask is aligned parallel with the primary flat of the wafer.

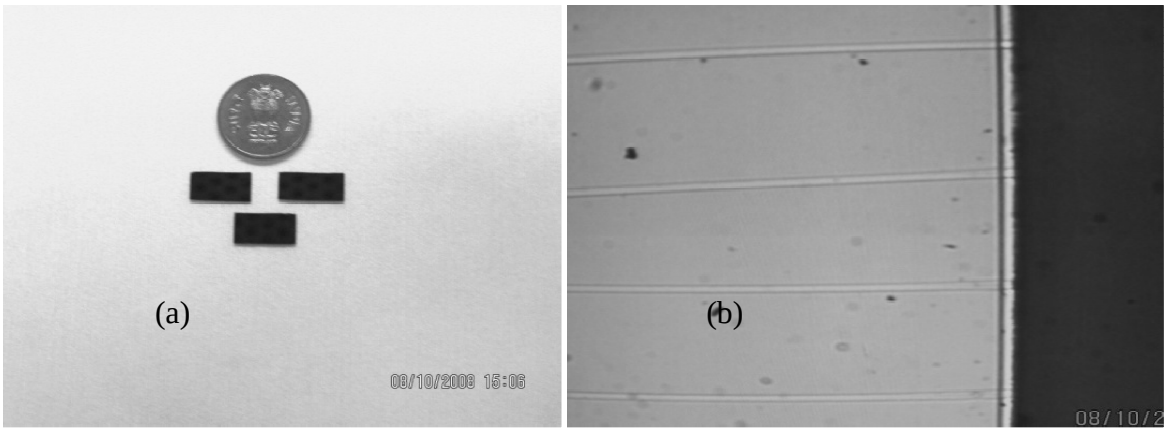

Figure 4.14. (a) Cleaved 1 × 4 chips, (b) Exit face of chip showing the cleaved plane.

Obtaining a mirror-like facet quality was found to be very statistical. Some chips where marginal success was achieved in producing the desired level of cleaving, were used for testing at chip level before packaging (shown in Fig. 4.14). A rough test of light guidance by these devices was done in a conventional test bench containing manual micro-positioning stages. Light at 632.8 nm from a He-Ne laser was injected into the input end of the splitters though an optical fiber. At the output end of the splitter, a microscope objective was used to project the spots on a screen. Fig. 4.15 shows the light guidance through a 1 × 4 splitter. The power in the output ports however is not equal. It is difficult to estimate how much light would have coupled into the 2 μm × 2 μm channel waveguide made in SU-8.

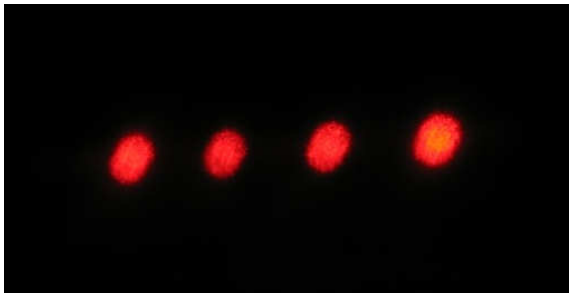

Figure 4.15. 1 × 4 splitter output at 632.8 nm.

In several 1 × 4 devices, it addition to the four output spots a general scattering of light was also observed in the form of streak running through the spots. Testing of 1 × 4 devices at 632.8 nm, 1310 nm as well as 1550 nm before pigtailing was carried out. Table 4.3 shows the result of the testing. It is again seen that the output power in the devices is very unequal, with one port showing a large power compared to the other ports. The experimental results were analyzed. Initial analysis gave important information as to why such unequal splitting could be happening.

Table 4.3: Insertion Loss of fabricated (Conventional)1 × 4 chip.

Wavelength →		**632.8 nm**	**1310 nm**	**1550 nm**
Device No.	**Output Ports**		**Loss (in dB)**	
Dev.2 chip-1	**1**	-24.47	-17.13	-25.12
	2	-22.53	-15.47	-14.76
	3	-25.37	-18.15	-17.84
	4	-18.91	-15.39	-19.57

The special Nufern fiber (PWG-10) was used for pigtailing. This is a high-index optical fiber especially meant for pigtailing integrated optical waveguides. The utility of this special fiber had already been discussed in section 2.9. One of the devices was packaged using v-groove chips procured from OZ Optics, Inc. The fiber was placed in the v-groove chip, epoxied and UV cured. The fiber with the v-groove was then end-polished using standard techniques. The prepared v-groove assembly was then placed in the Newport pigtailing bench to carry out packaging. The v-groove assemblies for the input and output ends of the chips were prepared as mentioned above. The chip to be pigtailed was placed in the pigtailing bench together with the v-groove assemblies and optimally aligned. Owing to poor cleave quality of the output end of the chip, the 4-array fiber assembly could not be optimally placed. The output v-groove assembly was removed and input power to the chips was optimized. The best result for 1 × 4 conventional splitter that could be obtained with this set-up is shown in Table 4.3. The results obtained after characterization of sample devices at SAMEER, Mumbai are listed in Appendix C.

At times, it was found that cleaving actually happened a fraction of a millimeter away from the point where the wafer was pressed. It must be mentioned that in such chips where the cleaved facet was away by a fraction of a millimeter from the input end of the waveguide, hand polishing was carried out on pads charged of 5μ, 3μ and 1μ particle-size in order to let the polished face intersect the input waveguide of the splitter. Extensive damage to the face was observed during microscopic examination of the polished surface. In addition, some chipping of the polymer layers was also observed. If one used water to lubricate, it worsened the situation by attacking the polymer layers. Therefore, it was concluded that any polishing activity involving SU-8 must use non-water based slurry. Ideally, it has to be a combination of chemical and mechanical polish. Chemical-mechanical polishing, however, was not pursued in this work due to lack of such facilities in the country.

4.11 Effect of Remnant Resist on Device Performance: Simulation Results

Polymer residues are usually left behind in the Y-junctions of the Y-branch waveguides. The presence of residual SU-8 resist at the every Y-junction as shown in Fig. 4.16, is the prime reason for unequal power splitting. The remnant SU-8 is due to the limitations with the resolution of the MA-56 mask aligner. The minimum feature size for this aligner is 2 μm.

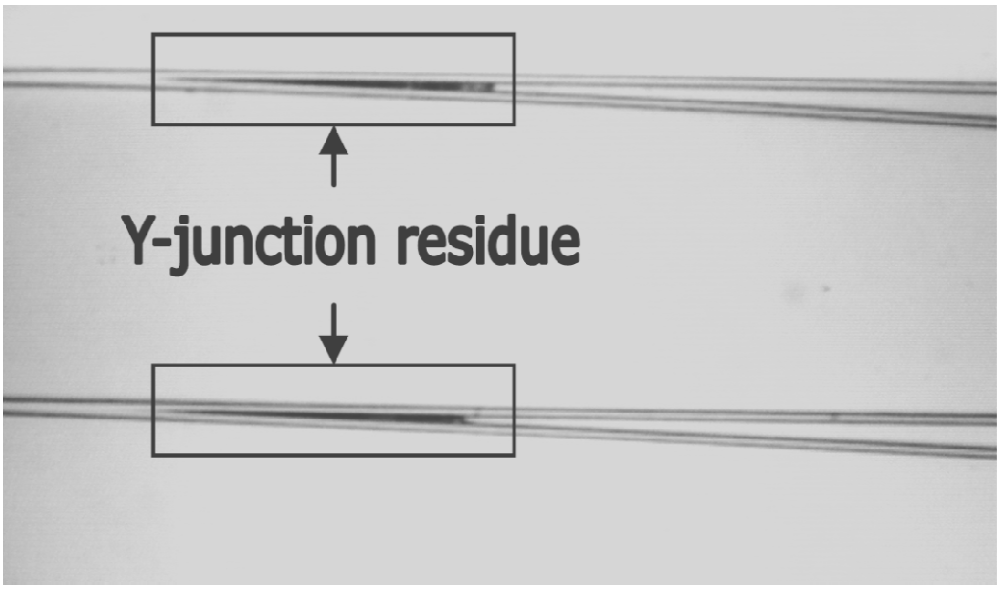

Figure 4.16. Remnant residue at Y-junction.

The initial distance between the output branches of a 1 × 2 splitter is less than the minimum resolvable feature size of the mask aligner. In the earlier fabrication attempts, this was observed consistently and fabrication steps were chosen to minimize it as much as possible. In order to minimize the effect of residual resist on the splitter performance, the splitter design was improved by inserting linear taper and a gap between the output branches at all splitting junctions. The design is proposed and its performance is discussed in detail in chapter 5. It was required to examine the effect of remnant resist on the device performance As a first step, a 1 × 2 splitter was simulated. The basic conventional structure used for the simulation is shown in Fig. 4.17.

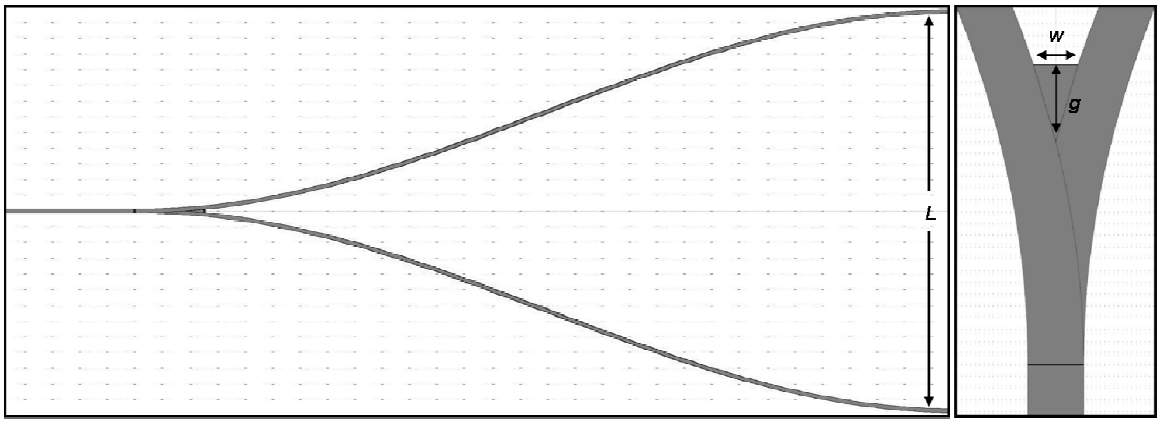

Figure 4.17. Schematic (a) Y-branch waveguide (b) Y-junction with residual polymer.

A conventional Y-branch waveguide as discussed earlier in chapter 3 comprises of a straight guide followed by a Y-branch with cosine S-bend arms (Sum 2004) (Satyanarayan 2006) and is generally referred to as a 1 × 2 power splitter. The conventional 1 × 2 power splitter shown in Fig. 4.17 is different from that shown in Fig. 3.1, in sense that here, resist is included at the Y-junction in the design schematic as shown in Fig. 4.17(b). Also, the output ends of the Y-branch shown in Fig. 4.17 are separated by a distance of 254 μm while in the Y-branch shown in Fig. 3.1, they are separated by 127 μm. A 1 × N power splitter is realized by cascading symmetrical Y-branching guides with residual resist at all Y-junctions of the cascaded structure. The major limitation when designing a conventional Y-branch is transmission loss due to the minimum width of the gap between the two branching waveguides limited by photolithography and etching process (Gamet 2004).

The major losses in a Y-branch power divider occurs at the Y-junction i.e. at the branching point where cosine S-bend branches separate from each other. Here in this work, minimum trench width achievable due to limitation from photolithography was assumed to be $w \sim 2$ μm due the limitation of lithographic resolution of SU-8 and the mask aligner used in fabrication. A parameter denoted as 'g' is defined as the length of residue from the point when $w \sim 0$ to $w \sim 2$ μm. Towards the branching point, g approaches to zero and increases as gap between S-bend branches increases in direction of propagation of light through the device as shown in Fig. 4.17(b). The analysis was performed on BeamProp^{TM} (R-Soft), which is the same simulation tool used to design the splitters. The region that represents the remnant SU-8 has the same refractive index as the guiding region in our simulation. For a 1 × 2 basic splitter as above, it was observed that the simulation yields unequal power splitting.

Due to polymer residue at Y-junction, the evanescent fields of both guides exist in this region between the branches. The overlap of the fields in the two branches causes the power coupling between the two branches. The spread of the evanescent fields of both guides in the region between the branches near the junction is the origin of the radiation loss. More residual polymer if left at Y-junction, leads to more coupling and thus, more is the radiation loss. Fig. 4.18(a) shows the effect of residual resist when it is not present at the branching point of the splitter, while Fig. 4.18(b) shows the effect when it is present.

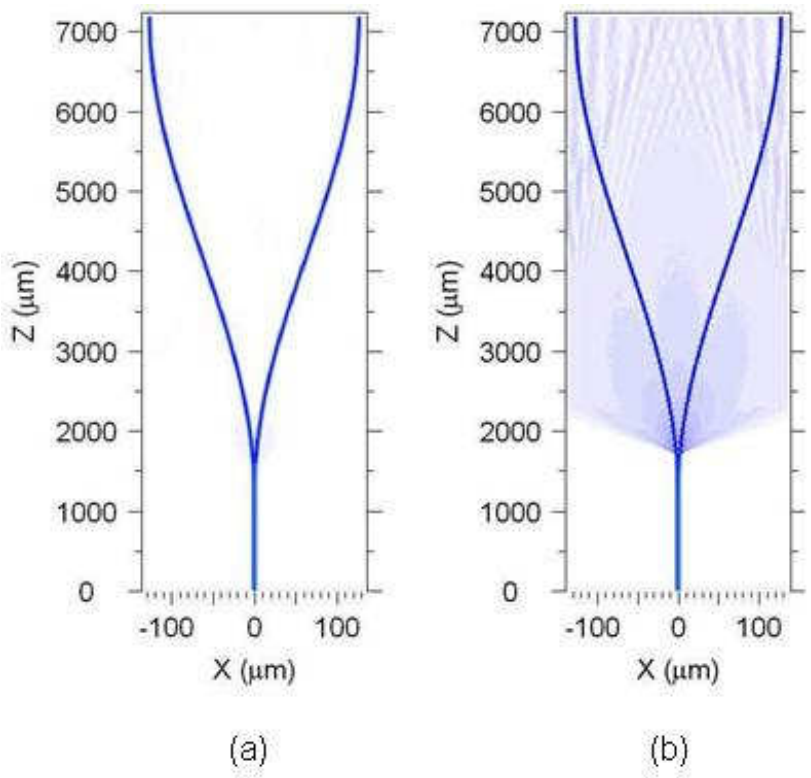

Figure 4.18. BPM Simulation: Radiation loss increases in presence of residue.

An extensive light leakage is clearly observed in the junction in Fig. 4.18(b) when residue is present at the Y-junction of a conventional 1 × 2 splitter. In Fig. 4.18(b), from schematic layout, $0 \leq w \leq 2$ µm, $0 \leq g \leq 130$ µm and $L \sim 254$ µm. The insertion loss (IL) of a 1 × 2 device degrades from 3 dB to 4 dB when the residue-affected area increases from the branching point ($g \sim 0$, $w \sim 0$) to the point when ($g \sim 130$ µm, $w \sim 2$ µm) in as shown in Fig. 4.16.

One of the ways to minimize the radiation loss caused by residue is to optimize the fabrication process to etch out the residual polymer from the Y-junction. As mentioned earlier, g is 130 µm when $w \sim 2$ µm but as the fabrication process is optimized for minimum residual polymer at branching point of Y-waveguide, the length of residue affecting the area decreases from $g = 130$ µm to $g = 90$ µm. At $g \sim 90$ µm, it was observed in Fig. 4.19 that insertion loss is ~ 3.5 dB. An advantage of higher magnitude can be expected from cascaded stages of a high-order 1 × N power splitter. Besides increased insertion loss, the Y-junction residue results in non-uniform splitting ratio.

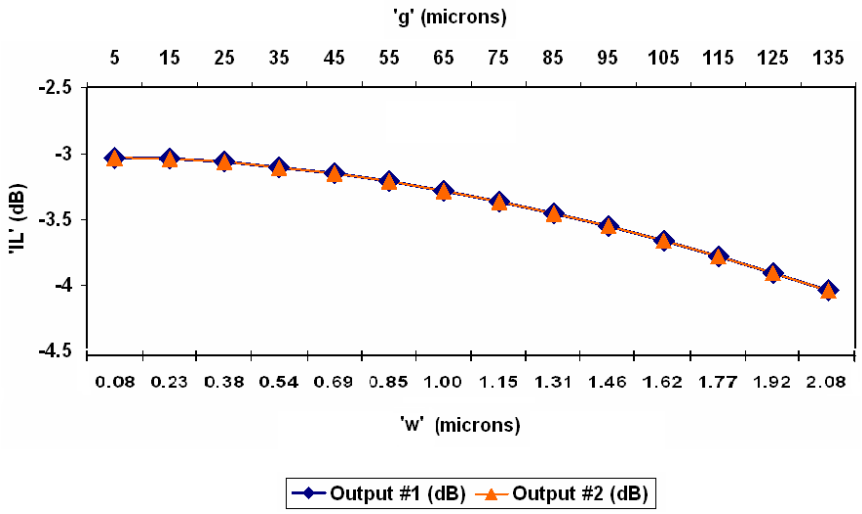

Figure 4.19. BPM Simulation: Insertion Loss vs. '*g*'.

Table 4.4 shows the effect of Y-junction residue on the power distribution among the output ports of a conventional 1 × 4 power splitter using BPM analysis. Besides increase in magnitude of insertion loss, there is non-uniformity in power at the output ends due to the junction residue. The splitters compared in Table 4.4 are of same optimized lengths and geometric features. The device length obtained after optimizing different segment lengths for a conventional design is 1.70 cm. The only difference between the splitters compared is that residue at Y-junction is included in one to measure performance while for other it is not included.

Table 4.4. Loss at outputs of a conventional 1 × 4 splitter (TE mode)

Conventional 1 × 4 power splitter		**No Residue**	**Residue present**
Loss in Output(s) in dB	**1**	6.01	7.47
	2	6.06	8.28
	3	6.04	8.18
	4	6.01	7.51
Average Output with Change (dB)		6.03±0.03	7.86±0.42

The propagation and splitting losses add to give an overall insertion loss of more than 15 dB at 1550 nm as indicated in Table 4.3. As can be seen from the simulated result, the performance of the splitter with residue is indeed inferior compared to the case where there is no junction residue. The residue can be largely minimized by employing a mask aligner which has a better resolution than what was used in this thesis work.

4.12 Conclusion

In this chapter, optical characterization of SU-8 planar and channel waveguides is presented and discussed. Thin film SU-8 waveguides of thickness less than 2.5 μm were characterized for film thickness, refractive indices, modal characteristics, and propagation loss. For a thickness of film 2.5 μm, the refractive index measured at 1550 nm was found to be 1.57. Single mode channel waveguides with a step height of 1.8 to 2.2 μm were realized and characterized. The quality of 1 × N power splitters produced in this work was critically dependent on the limitations imposed by the mask aligner. Polishing of SU-8 based waveguides requires a different approach compared to conventional polishing techniques. The quality of cleaved samples is statistical and is not a reliable process in a production environment. The packaging of the power splitters could have been completed had the chemical-mechanical polishing facility for edge polishing of waveguides been available in the country.

CHAPTER 5

PROPOSED SPLITTER DESIGN

Besides increased insertion loss, the residue left in the Y-junctions of the conventional splitters results in asymmetric distribution of power at device outputs. The remnant residue at the Y-junction of a fabricated 1 × 4 splitter is visible in Fig. 4.16. As is evident from the photomicrographs and SEM of a channel waveguide in Fig. 4.10, the fabricated waveguides were smooth walled. However, a small amount of residual resist remained in the region between the Y-junction guides. The residue left between the Y-junction arms is, in fact, SU-8, which was not removed due to limitations with the resolution of the mask aligner used for photoexposure. As a result, SU-8 in trench near the Y-junction is not etched out well. The mask aligner employed in this work had a resolution of 2 μm, whereas the waveguides are separated by a distance less than the resolution of the mask aligner near to the Y-junction region. The residue can be reduced with an increased UV exposure time during fabrication but an increased exposure time leads to wider waveguides. An analysis of the device performance in the presence of junction residue was presented in chapter 4 and a design to overcome the non-uniformities in output power distribution brought about by the presence of the residue is proposed in this chapter.

During fabrication employing a photomask, the smallest feature size obtainable depends on resolution of the mask aligner used for photolithography. As a result, a small amount of polymer residue may remain at the Y-junction, as shown in Fig. 4.16. The residue length is defined as the distance from the initial point of separation of Y-arms to the end, till the distance between Y-branch arms is equal to the resolution of the mask aligner, in the direction of propagation of light. The residue was shown in schematic used for simulation in Fig. 4.17(b) and 'g' defined the length of the residue. While designing a schematic of a conventional 1 × 4 splitter with overall device length of 1.70 cm, it was observed that the residue lengths were in the range of 140 μm–160 μm in the second stage (i.e., when the output waveguides are separated by a distance of 127 μm) of the device. For the first stage of the same device, the residue lengths were in the range 230 μm–250 μm. It can be observed that g was 130 μm for a 1 × 2 splitter discussed in section 4.11 with 254 μm of separation

between output arms of Y-branch i.e. similar to the separation between the first stage of a 1 × 4 splitter. The difference in residual lengths in both devices is due to the difference in lengths of cosine S-bends optimized for both designs separately. Stages in a cascaded structure have different geometric features, hence, they have different values of residual lengths. Coupling light into a power splitter that contains such residues at all junctions leads to unequal output power distribution, along with increased propagation loss. The more is the length of the residue, more is the degraded performance of the device.

The chapter presents the proposed design that can overcome the non-uniformities in output power distribution brought about by the presence of the remnant residue at Y-junction. The proposed Y-branch with tapered waveguide beam expander is discussed and presented in the chapter. The BPM simulation results of 1 × 4 splitters based on the proposed Y-branch design are presented in the chapter. The fabrication process and characterization steps applied for the conventional design have also been applied to the proposed design. The comparison between the proposed and conventional 1 × 4 splitter is discussed in the chapter.

5.1 Proposed Y-branch

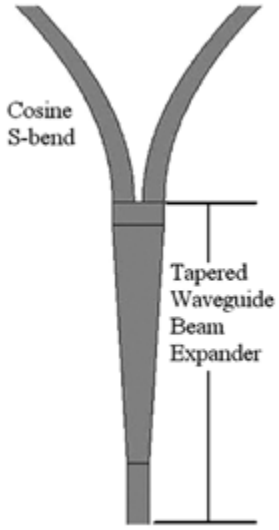

Figure 5.1. Segments of proposed Y-branch.

The proposed design of Y-branch waveguide comprises of a waveguide beam expander (Jamroz 2006) and cosine S-bend segment. Fig. 5.1 shows the Y-branch waveguide

comprising of four segments (from bottom to top): a short straight waveguide, a linear taper, another short straight but a wider waveguide at the end of the taper and cosine S-bend segment. If the fundamental mode is excited at the input, it will split evenly between two branches and the optical power exiting the two branches will be equal. The basic part of waveguide beam expander is a single-dimension linearly tapered waveguide in which the width of channel waveguide is gradually expanded to reduce the effective numerical aperture of the optical beam in the direction of propagation. The linear taper segment allows expansion of the guide width without mode conversion. The tapered waveguide is followed by a straight guide with width equal to the broader end of the taper. A straight waveguide with width equal to broader end of linear taper increases coupling of light to S-bend Y-branches. At the end of each cosine S-bend segment, a straight waveguide is introduced for coupling power to the next stage efficiently, also acting as the input section for the next stage. The width of the waveguide kept was 2.5 μm for single-mode propagation.

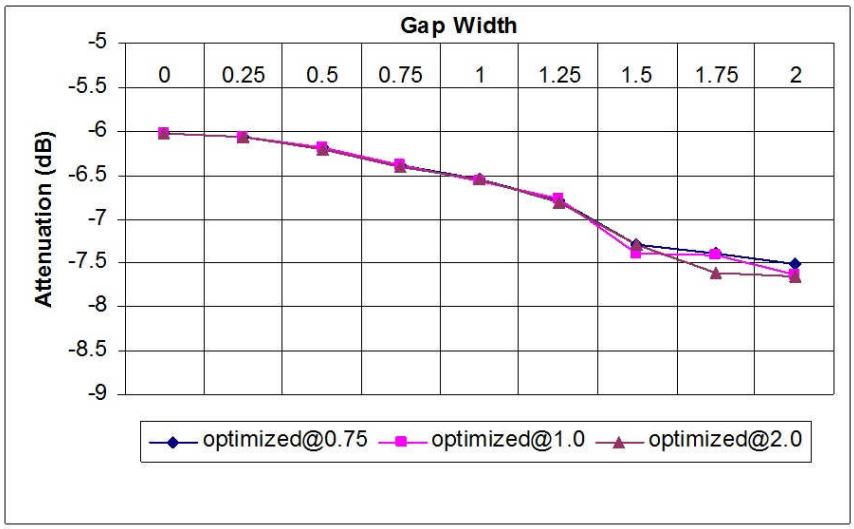

Figure 5.2. 1 × 4 splitter output vs Gap width optimized at different gap widths

A gap was included between the branching waveguides at the splitting junction in the schematic as shown in Fig. 5.1 in order to overcome the fabrication limitations. Post-fabrication, a reduction in area covered by the residual resist was expected due to inclusion of the gap at Y-junction between branching waveguide arms. The inclusion of the gap results in slight degradation in the simulated device output. As the gap width increases, the propagation loss of the 1 × 4 splitters increases, as shown in Fig. 5.2. The loss in output power, when gap

is 2 μm compared to no gap case, is less than 2 dB. A separation of the waveguides larger than 1 μm resulted in increased leakage of light from the broad end of the taper, as expected. As can be observed from Fig. 5.2, the slope of the attenuation curves get steeper after a gap of 1 μm. The separation between the two output waveguides of the proposed Y-branch was varied to obtain an optimum separation of 1 μm. The taper length was also carefully optimized to minimize the loss of light from the junction.

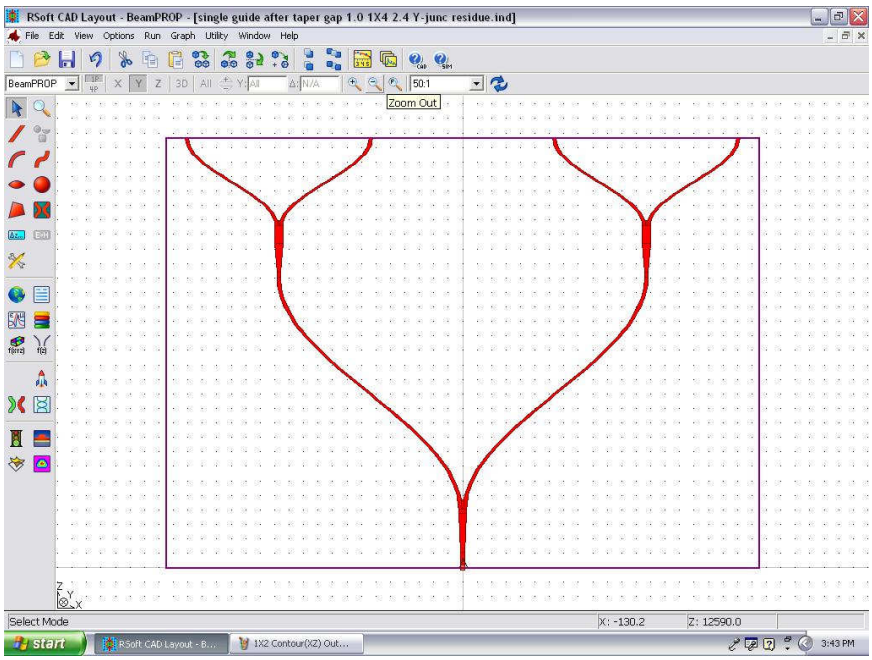

Fig. 5.3. Schematic of 1 × 4 power splitter

Here also, the 1 × 4 power splitter is realized by cascading two symmetrical Y-branching guides as shown in Fig. 5.3. Through a simulation program, the length of each segment used in the schematic is optimized with the main aim of achieving low propagation loss with symmetric distribution of power at all output ends. The overall device length achieved after optimizing segments is 1.43 cm as summarized in Table 1. The separation between the output ports of the first stage of device is 254 μm, and the second stage output port separation is 127 μm. The residue lengths as observed from the proposed design schematic lies in range of 160 μm–180 μm for the second stage of device, while for the first stage of the device, it lies in the range of 230 μm–250 μm, which is almost same the length of the residue in conventional case. Since the lengths of the area affected by the residual resist is of same order in both conventional and proposed designs, it becomes interesting to investigate and compare their

performance. The 1 × N power splitters can be realized by cascading (N - 1) symmetric Y-branch guides. The length of each segment of 1 × N device should be optimized to achieve low variance and low propagation loss at all output ends.

Table 5.1. Segment Lengths (in μm) of optimized 1 × 4 splitters

Device Segments	**Conventional**	**Proposed**
Input Waveguide	810	540
Tapered Waveguide	*NA*	1340
Straight Guide after Taper	*NA*	130
Cosine Bend	11369	5800
Input/Output Waveguide	180	130
Tapered Waveguide	*NA*	1770
Straight Guide after Taper	*NA*	610
Cosine Bend	4615	3040
Input/Output Waveguide	20	930
Overall Length (in μm)	16994	14290
Average Output (dB)	- 6.033	-6.599

5.2 BPM Simulation Results (1 × 4 Splitter)

One of the important input parameters for the BeamPROP^{TM} (Rsoft Design) is the refractive indices of core and cladding of waveguide. Accurate modeling of waveguides is possible if the refractive indices of SU-8 and NOA 61 are measured. The refractive indices of cross-linked thin films SU-8 and UV-cured NOA 61 were measured using a Metricon 2010 prism coupler. It may be recalled from chapter 4 that the refractive index for the SU-8 thin film was measured to be 1.57, while that for the UV-cured NOA 61 was 1.54 at 1550 nm, which agree well with publications by different researchers in previously reported literature. In the proposed design, the residue at the Y-junction was simulated as SU-8 itself, and a refractive index of 1.57 was used for this region in the simulations. It can be observed from Fig. 4.16 that the junction residue is visible as the dark shade in color between Y-branches, which suggests non-uniform surface after etching. The measurement of surface non-uniformity in

the affected area could be estimated by the average height of residue but measurements were not carried out due to lack of facilities. Thus, change in the height of the residue was ignored during simulations; i.e., the height of residue was kept the same as that of the waveguide, but the residue lengths differ at different stages of the cascaded structure of the device, and the estimated values were included accordingly in design before simulation. Although after optimum fabrication process steps, length and width of area affected by the residual resist decreases, the trench width after which the affected area was not considered in the simulation was 2 μm.

Table 5.2. Loss at outputs of the proposed 1 × 4 splitter (TE mode)

Proposed 1 × 4 power splitter		**No Residue**	**Residue present**
Loss in Output(s) in dB	**1**	6.66	7.70
	2	6.64	7.74
	3	6.61	7.88
	4	6.63	7.88
Average Output with Change (dB)		6.64±0.03	7.80±0.18

Fig. 5.4 (a) and 5.4 (b) compares a conventional and a proposed 1 × 4 splitter, having a gap of 1 μm at Y-junction of both stages of cascaded structure, without residue. As the segments are optimized in both the cases, the performance of the proposed design is slightly degraded as also listed in Table 5.2. But when conventional and proposed design with residue are compared as shown in Fig. 5.5 (a) and 5.5 (b), the outputs of both devices are comparable but proposed design distribute the power at outputs more uniformly. The fact is visible as monitor values are observed from Fig. 5.5 (a) and (b). The propagation loss (TE mode) evaluated for proposed design through BPM analysis using BeamPROP^{TM} is listed in Table 5.2. From Table 4.4 and 5.2, it can be concluded that the performance of the proposed device is comparable to that of a conventional design. Fig. 5.6 shows that the performance of

conventional and proposed device with residue is comparable independent of wavelength of the optical input.

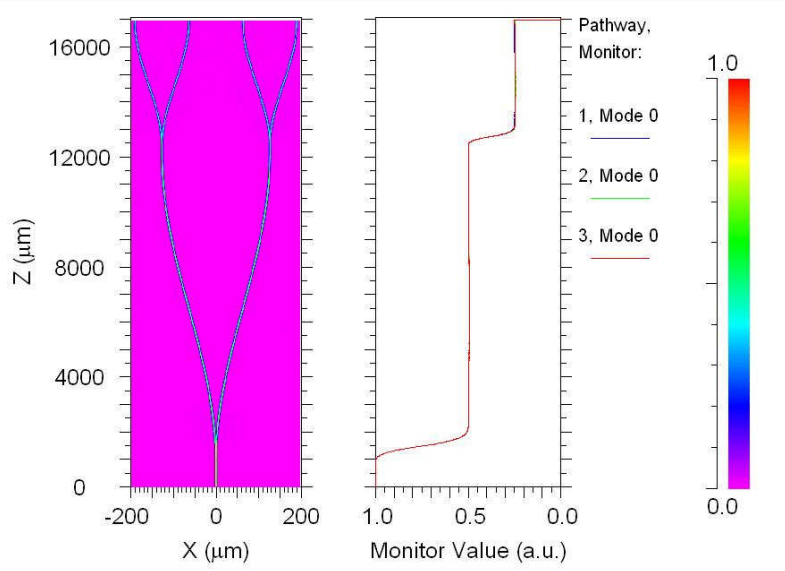

Figure 5.4. (a) Conventional 1 × 4 splitter without Y-junction residue.

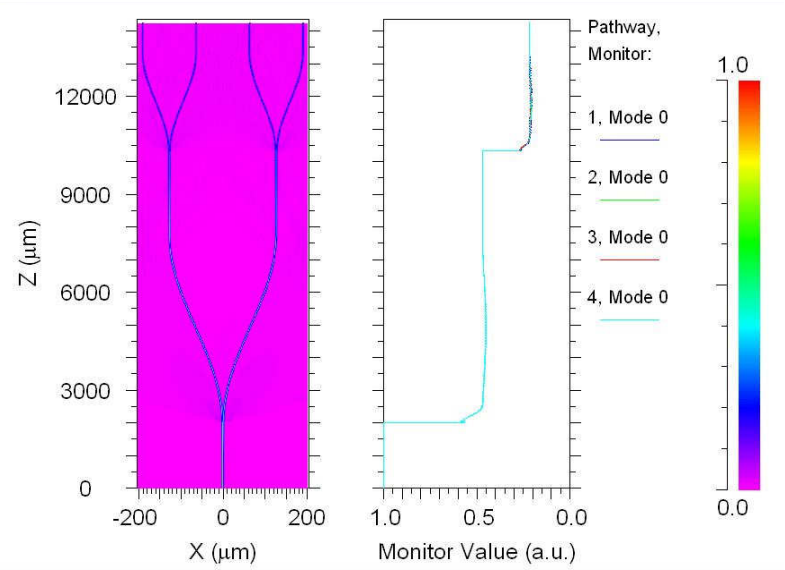

Figure 5.4. (b) Proposed 1 × 4 splitter without Y-junction residue.

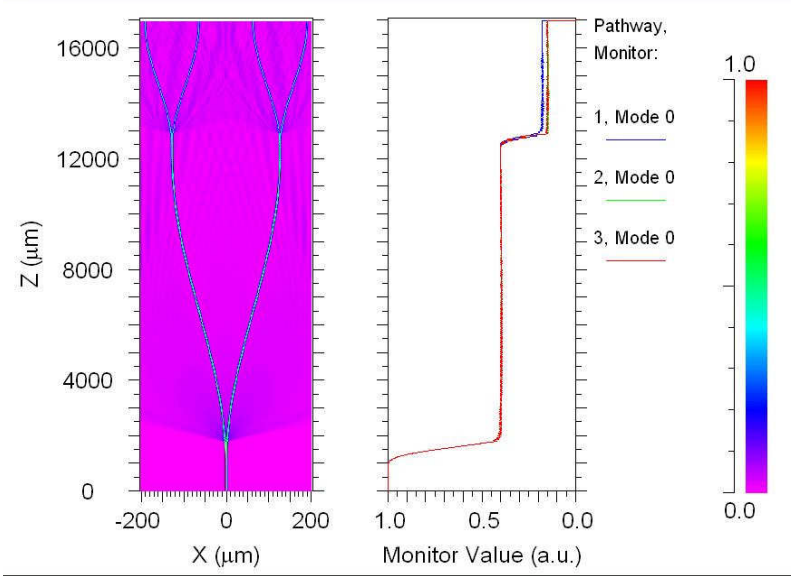

Figure 5.5. (a) Conventional 1 × 4 splitter with Y-junction residue.

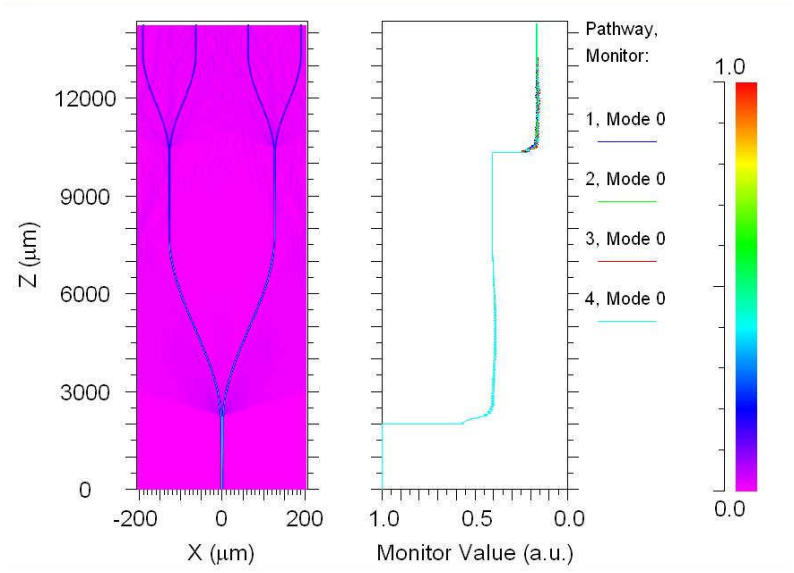

Figure 5.5. (b) Proposed 1 × 4 splitter with Y-junction residue.

The plot of Fig. 5.6 also suggests that the proposed design reduces the effect of Y-junction residue as the difference in loss is large in case of conventional than for proposed design after inclusion of junction residue. It can be seen from Fig. 5.6 that output of conventional design degrades by around 2 dB in presence of residual resist but the outputs of proposed design degrades by around 1 dB. In other words, it can be said that the proposed design is less affected by the presence of Y-junction residue than the conventional design. Fig. 5.7 shows

the variation in output ends of the conventional and proposed design before and after residue is included. The uniformity in power at the output ends of the proposed design is better than conventional device in presence of residue. With a compact device length of 1.43 cm, the proposed design provides an advantage in device insertion loss and symmetric power distribution among device outputs compared to the conventional design.

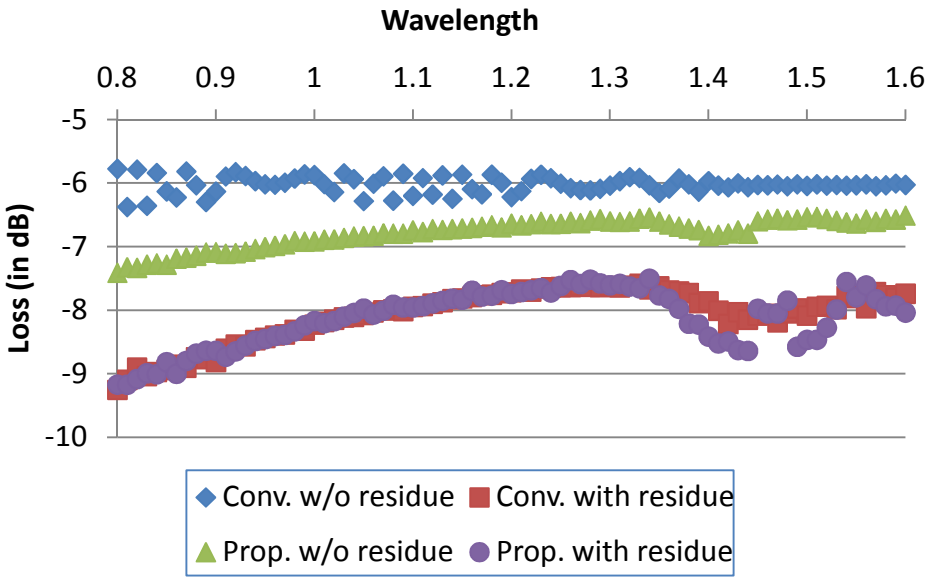

Figure 5.6. Average Splitter Loss (TE mode) versus Wavelength.

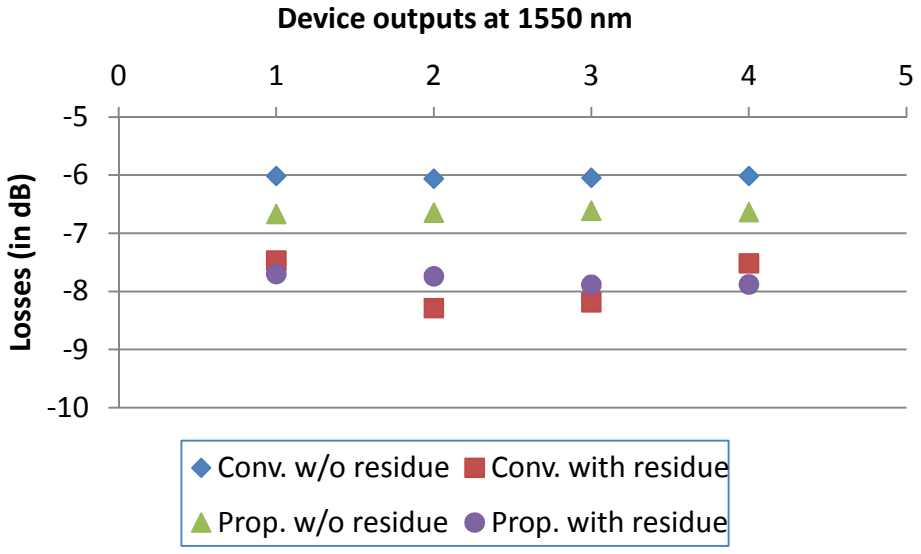

Figure 5.7. Variation in losses at device outputs at 1550 nm.

5.3 Fabrication and Characterization

The steps of the fabrication process presented in Chapter 3 and the characterization methods discussed in Chapter 4 were applied again to fabricate and characterize the devices based on the proposed design. The residue was visible in the Y-junction of proposed device as shown in Fig. 5.8 (b), but the area covered by the residue was reduced due to the gap of 1 μm introduced between the Y-arms as compared with Y-junction of conventional device shown in Fig. 5.8 (a). The proposed design reduces the length of residue, and thus, an improvement in performance of the device is expected.

Propagation losses reported previously have been 0.125 dB/mm (Tung 2005), 0.15 dB/mm (Yang 2009), and 0.18 dB/mm (Nordstrom 2007) at 1550 nm. The materials used to fabricate waveguides in (Tung 2005) are SU-8 2000 and NOA 61, and the measurements were done at 1550 nm for single mode propagation. The average propagation loss estimated here is 0.125 dB/mm when the loss for several over-cladded channel waveguides of different lengths are measured at 1550 nm. The insertion loss for the 1 × 4 splitter chip in this case includes intrinsic splitting losses estimated through the simulation in Fig. 5.6 along with losses in the waveguide that are independent of the splitter, e.g., Y-junction losses, radiation losses, and coupling losses. Coupling losses also include losses due to Fresnel reflection.

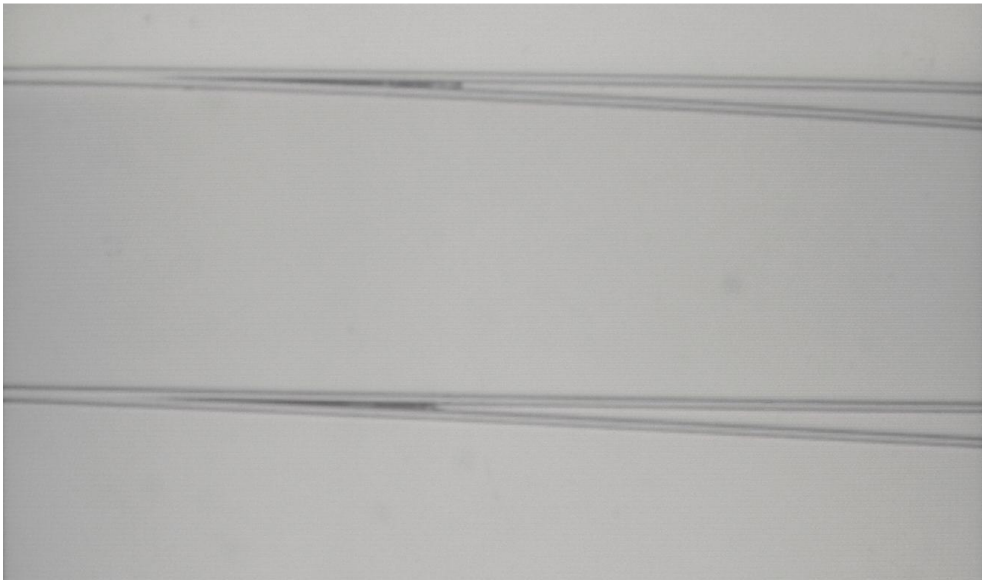

Figure 5.8. (a) Residue at Y-junction of Conventional device.

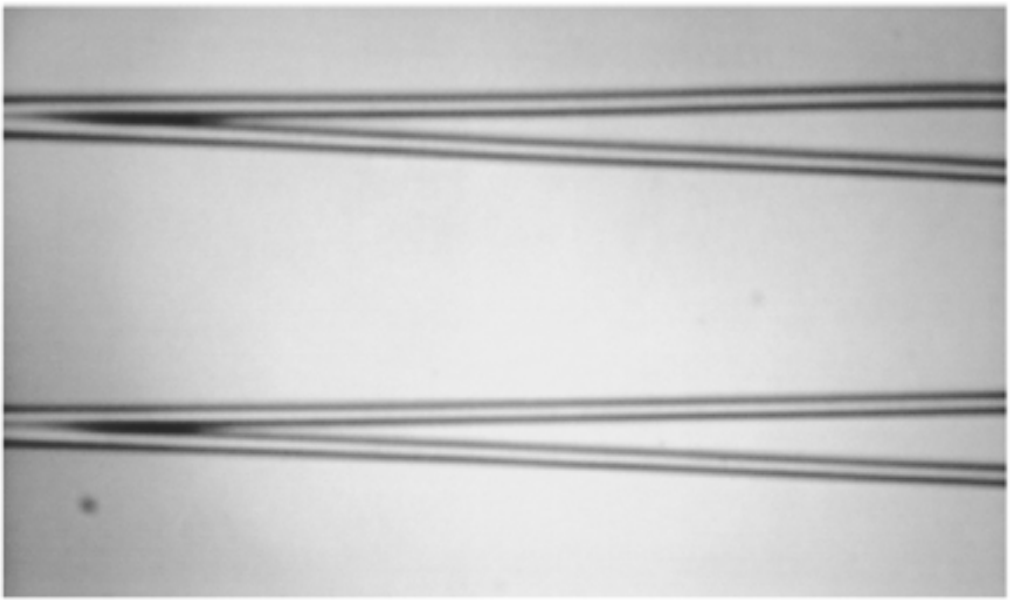

Figure 5.8. (b) Residue at Y-junction of Proposed device.

Since the waveguides were as narrow as 2 μm by 2 μm, it was very difficult to measure how much light got coupled into the waveguide, unless the input face of the waveguide is polished to a very high quality and the input/output ends are pigtailed. As earlier discussed in section 4.9 and 4.10 that edge polishing has not been taken up in this work, the input and output ends of the splitters were simply prepared by cleaving the Si wafer on which they were patterned. The optical power was fed to the end-face of the waveguide through end-fire coupling. The insertion losses obtained at the chip level are listed in Table 5.3 for 632.8 nm, 1310 nm and 1550 nm.

The length of the fabricated device is 1.43 cm, and the average propagation loss estimated at 1550 nm is 1.25 dB/cm (Tung 2005), which accounts for a loss of 1.8 dB for the device. An analysis was carried out when power was coupled to the input of the device through an optical fiber (Nufern PWG1-XP, Nufern, USA) under the condition that the axis of the input waveguide was perfectly aligned to that of the fiber. Power at each output port was measured with no interference from either of the adjacent ports. Even though theoretically the mode field diameters of fiber and waveguide match with each other, the fiber-to-waveguide coupling loss cannot be avoided, as the fiber and rectangular waveguides differ in their geometrical cross-sections. In addition, Fresnel reflection at the input and output results in an

estimated coupling loss of 3.7 dB/port. Similar coupling losses for SU-8 waveguides have been reported earlier (Tung 2005) (Dai 2009). Coupling losses for the conventional and proposed devices are the same as the geometric features of waveguides used in the design of both types of devices are the same. It must be reiterated that losses can only be estimated, as the light had been coupled from the optical fiber to the device with the ends of the device prepared only by cleaving.

The theoretical splitting loss of proposed device with residue at Y-junctions is around 8 dB at 1550 nm, as shown in Fig. 5.7. The theoretical splitting loss of 8 dB, when added to 1.8 dB of propagation loss and 7.4 dB of coupling loss between input and each of the output ports, results in 17.2 dB of insertion loss for the device. The difference between estimated and obtained results shown in Table 5.3 may account for radiation losses at Y-junctions and poor coupling of light due to cleaved end-facets of devices. Thus, the excess losses as defined in (Sohn 2005) can be estimated to be more than 10 dB.

Table 5.3. Insertion Loss of fabricated (Proposed)1 × 4 splitter chip

Wavelengths →		**632.8 nm**	**1310 nm**	**1550 nm**
Device No.	**Output Ports**	**Loss (in dB)**		
Dev.5 chip-1	**1**	-23.32	-18.29	-19.57
	2	-23.32	-14.36	-17.13
	3	-21.17	-14.73	-17.01
	4	-22.99	-13.82	-18.85

Table 5.3 suggests that the average insertion loss at 1550 nm is 18.14 dB with a maximum variation of 1.43 dB among the output arms of the proposed device compared to the insertion loss of 19.32 dB with a maximum variation of 5.8 dB as given in Table 4.3 for a conventional device. An advantage of ~1.2 dB in the device insertion loss due to compact

device length with the symmetric distribution of power at the output ends is observed in the proposed device at 1550 nm.

5.4 Conclusion

Polymer residues are generally left in the Y-junctions of the conventional splitters. Besides increased insertion loss, the Y-junction residue results in asymmetric splitting of optical power. A design incorporating a tapered waveguide beam expander is proposed, which offers better performance with Y-junction residue than the conventional 1 × N splitter in terms of insertion loss and symmetric power distribution at the output ends of the device at 1550 nm. SU-8 optical waveguides with a width of 2.5 μm, with an optical adhesive NOA 61 over- and under-cladding on silicon substrate, have been realized. The process to fabricate single-mode polymeric channel waveguide-based optical splitters using simple direct ultraviolet (UV) photolithography is optimized and presented. The characterization of the proposed 1 × 4 optical power splitter shows symmetric distribution of power at outputs of the splitter with a decrement of 1.2 dB in insertion loss compared to the conventional device at 1550 nm.

CHAPTER 6

CONCLUSIONS AND FUTURE WORK

6.1 Conclusion

Polymers have emerged as cost-effective materials suitable for development of affordable integrated components used for optical communications. Polymer waveguides are quick and simple to fabricate using an economic environmentally friendly fabrication processes. SU-8 polymer was introduced by IBM in 1989. It is an epoxy based chemically amplified, negative tone, near UV photo-resist. Cross-linked SU-8 films are highly resistant to a majority of acids, bases and solvents. Due to its physical, chemical, mechanical, and excellent optical transparency, it has been explored as an important material in diverse fields of manufacturing not only as a resist material but also as the core structural material. SU-8 has been preferred as a suitable material for the fabrication of optical waveguides, gratings, filters, photonic bandgap structures, on-chip light sources, pressure sensors, opto-fluidic sensors, etc.
Symmetric channel waveguides were designed with SU-8 2002 chosen as core material while NOA 61 was used as underclad as well as overclad. Refractive indices for both the materials were measured using prism coupling technique and were found to be 1.57 for SU-8 and 1.54 for NOA 61. To ensure single mode propagation through the channel waveguide, aspect ratio (w/d) of less than 1.125 was chosen so as to yield channel width below 3.1 μm for a guide thickness of 2.5 μm. Waveguide dimensions of 2.5 × 2.5 μm were chosen to design the single-mode channel waveguides. The refractive index profile and the mode profile of the fundamental mode were studied. The channel waveguides were designed and simulated for performance using BeamProp^{TM} (Rsoft Design Group, USA).

Y-branch waveguides were also designed as they are fundamental in designing most of the optical integrated circuits e.g. optical power dividers, modulators, switches, etc. and thus, can be considered as one of the essential structures used in integrated optics. Key design parameters for a Y-branch are branching angle, device length, type of bend, separation at output ports, etc. Conventional Y-branch structure was designed and simulated to realize an optimum branching structure with low loss and compact overall size. A conventional Y-

branch waveguide consists of a single linear input waveguide and two output bend waveguides. Cosine S-bends were used as arms of Y-branch structure to minimize radiation losses at Y-junction. Standard output ports separation was selected in design to match standard fiber ribbon pigtailing. Conventional 1 × N power splitters were designed using cascaded Y-branch waveguides. The device lengths of 1 × N splitters were optimized to accommodate the structures on a 3-inch wafer. The shortened device length (17 mm for 1 × 4) shows only a marginal increase in splitting loss, which was 6.03 dB.

The design results from simulations in previous section were converted to GDSII format in BeamPROP^{TM}. L-Edit (Tanner Tools) was used to design the mask layout. In actual fabrication, it is possible that the actual width of the channel may be different from what is present on the mask. With this in mind, 1 × 4 splitters of different channel widths were made in the mask layout. Various channel widths ranged from 1.8 μm to 2.6 μm. Single mode buried channel waveguides were fabricated using economical UV photolithographic techniques and wet-chemical etching processes. SU-8 optical waveguides buried in an optical adhesive NOA 61 on a silicon substrate were realized. A two-step pre-exposure soft bake and post-exposure baking was used to crosslink the polymer. Waveguides were obtained after SU-8 2002 polymer was exposed to UV through a photomask. The fabricated waveguides were smooth-walled and vertical. There were neither cracks nor defects in waveguide throughout the guide length. The experimental results have demonstrated light wave-guiding in the polymer material. The average insertion loss estimated for a 2-cm straight waveguide was 11 dB (TE_{00}) at 1550 nm.

In the conventional Y-branch based power splitters fabricated in this work , a small amount of residual resist remained in the region between the Y-junction guides. The residue left between the Y-junction arms is, in fact, SU-8, which was not removed after chemical wet etching due to limitations with the resolution of the mask aligner used for photoexposure. The mask aligner employed in this work had a resolution of 2 μm, whereas the waveguides separation near the junction region was less than the resolution of the mask aligner. The effect of remnant resist on the device performance was examined through simulation. Besides increased insertion loss, the Y-junction residue results in asymmetric distribution of power at device outputs. The fabrication process was optimized to reduce residual polymer at

branching point of Y-waveguide. Advantage of half a dB was observed for a 1 × 2 splitter due to optimized fabrication process. The advantage get bigger as the power splitting in cascaded Y-branch structures to obtain high-order power splitting is observed.

A Y-branch waveguide comprising a waveguide beam expander and cosine S-bend segment is also proposed in this work. The basic part of waveguide beam expander is a single-dimension linearly tapered waveguide. The tapered waveguide is followed by a straight guide with width equal to the broader end of the taper. At the end of each cosine S-bend segment, a straight waveguide is introduced for coupling power to the next stage efficiently, also acting as the input section for the next stage. The width of the waveguide kept was 2.5 μm for single-mode propagation. A gap between the branching waveguides is included at the splitting junction in order to overcome the fabrication limitations. This results in slight degradation in the simulated device output. During simulations, the separation between the two output waveguides of a Y-branch was varied and an optimum separation of 1 μm was obtained. The proposed Y-branch based splitters were fabricated using the same fabrication process optimized for conventional Y-branch to obtain reduced residue at branching junction. The proposed device has a shorter device length than the conventional device structure and thus, an improvement in performance of the device is observed. The performance of the proposed design reflects reduced insertion loss due to reduced residue and less propagation losses due to shorter device length. The uniformity in optical power at the output ports of the device based on the proposed design has also been observed to be better than the conventional device. The characterization of the proposed 1 × 4 optical power splitter shows improvements of ~1.2 dB in insertion loss and symmetric distribution of optical power at device outputs in comparison to the conventional one at 1550 nm.

6.2 Future Work

With establishment of economical waveguide fabrication procedures and parameters for UV lithography, several other areas of research can be further explored. These range from basic waveguide modeling to advanced waveguide applications involving some of the concepts, procedures and parameters adopted in this work. Further development may include the following:

a) Waveguide modeling of polymeric waveguides may be expanded to include a theoretical analysis of propagation losses estimated by characterization of polymers to be used in development of waveguides, scattering losses estimated from the surface roughness parameters, etc. The objective is to bring the theoretical values evaluated for polymeric waveguides closer to those obtained experimentally.

b) Polymers have a scope of tailoring their properties by blending and copolymerizing selected miscible monomers. Considerable effort may be put in development and application of organic non-linear optical material for active devices. Photoinitiators may also be added in case, doping of non-linear chromophores affect the cross-linking property of the polymer.

c) In practice, the results of fabrication processes were not perfect as expected. One of the limitations of UV photolithography technique is the resolution of mask aligner used in development of waveguides. The photolithography processes need to be critically optimized further or a mask aligner with lower resolution may be used in order to obtain better resolution.

d) Polymers and substrates such as silicon or glass have different hardness. While polymers are soft materials, the substrate on which they are deposited are hard materials. This creates a problem in preparation of end-facets which have to have a mirror finish in order to couple light in and out efficiently. In polishing polymer materials, conventional polishing techniques suitable for harder materials cannot be applied. Alternate methods such as chemical-mechanical polishing have been explored by many researchers, but such methods have not been used in this study owing to lack of facilities to carry out such work in the country. Once such facilities exist, improvements in dicing and end-facet polishing can be one interesting area to be explored further.

e) A critical part of the fabrication of integrated devices is the fiber pigtailing of the waveguide ends. Since cladding layer used here in this work was an optical adhesive, simple, precise and active fiber alignment method utilizing a UV curable adhesive to achieve a low coupling loss may be explored further.

f) An environmentally and mechanically stable packaging technique for pigtailed polymeric waveguide chip should be explored further for obtaining better efficiency and reliability.

New polymer based optical integrated devices e.g. Resonators, Gratings, Switches, Sensors, etc. may be designed and developed for applications in optical access networks, switching architectures, sensing applications, etc.

REFERENCES

(Adams 1981) Adams, M. J. (1981) *An Introduction to Optical Waveguides.* New York: John Wiley and Sons Ltd.

(Ahn 2005) Ahn et al (2005) Polymeric wavelength filter based on a Bragg grating using nanoimprint technique. *IEEE Photonics Technology Letters*, Vol 17, No 10, pp. 2122-2124.

(Anderson 1978) Anderson, I. (1978) Transmission performance of Y-junctions in planar dielectric waveguide. *IEE Journal on Microwaves, Optics and Acoustics*. Vol 2, No 1, pp. 7-12.

(Ashley 1991) Ashley et al (1991) Channel waveguides in electro□optic polymers using a photopolymer cladding technique. *Applied Physics Letters,* Vol 58, No 9, pp. 884-886.

(Asquini 2002) Asquini, R. and d'Alessandro, A. (2002) BPM Analysis of an Integrated Optical Switch using Polymeric Optical Waveguides and SSFLC at 1550 nm. *Journal of Molecular Crystals and Liquid Crystals*, Vol 375, pp. 243-251.

(Bach 1997) Bach, H. and Krause, D. (1997) *Thin Film on Glass*. Berlin Heidelberg: Springer-Verlag.

(Balslev 2005) Balslev et al (2005) Single-mode solid-state polymer dye laser fabricated with standard I-line UV lithography *in* Proceedings of Quantum Electronics and Laser Science Conference, Baltimore, MD, Vol 2, pp. 859-861.

(Becker 2008) Becker, H. and Gärtner, C. (2008) Polymer microfabrication technologies for microfluidic systems. *Analytical and Bioanalytical Chemistry,* Vol 390, No 1, pp 89-111.

(Beguin 1988) Beguin et al (1988) Fabrication and performance of low loss optical components made by ion exchange in glass. *Journal of Lightwave Technology*, Vol 16, No 10, pp. 1483-1487.

(Belanger 1983) Belanger et al (1983) Passive planar multibranch optical power divider: some design considerations**.** *Applied Optics,* Vol 22, No 15, pp. 2383-2389.

(Bettiol 2003) Bettiol et al (2003) Fabrication of microoptical components in polymer using proton beam micromachining and modification. *Nuclear Instruments and Methods in Physics Research B,* Vol 210, pp. 250-255.

(Blanco 2001) Blanco et al (2001) Electron-beam-induced densification of Ge-doped flame hydrolysis silica for waveguide fabrication. *Applied Physics Letters,* Vol 79, No 18, pp. 2889-2891.

(Borreman 2002) Borreman et al (2002). Fabrication of polymeric multimode waveguides and devices in SU-8 photoresist using selective polymerization *in* Proceedings Symposium IEEE/LEOS Benelux Chapter, Amsterdam, Netherlands, pp. 83-86.

(Burns 1975) Burns, W. K. and Milton, A. F. (1975) Mode conversion in planar-dielectric separating waveguides. *IEEE Journal of Quantum Electronics*, Vol 11, No 1, pp. 32-39.

(Burns 1990) Burns, W.K. and Milton, A.F. (1990) Chapter 3: Waveguides transitions and junctions *in* Tamir, T. (Eds.) *Guided-Wave Optoelectronics*. Springer-Verlag.

(Calvo 2007) Calvo, M. L. and Lakshminarayanan, V. (2007) *Optical Waveguides: From Theory to Applied Technologies*. Boca Raton, Florida: CRC Press, Taylor and Francis Group.

(Chan 1996) Chan et al (1996) Low loss wide angle symmetric Y-branch waveguide. *Electronics Letters*, Vol 32, No 7, pp. 652-654.

(Chang 2010) Chang, W. S. C. (2010) *Fundamentals of Guided-Wave Optoelectronic Devices.* New York: Cambridge University Press.

(Chang-Yen 2002) Chang-Yen, D. A. and Gale, B. K. (2002) A novel integrated optical dissolved oxygen sensor for cell culture and micro total analysis systems *in* Proceedings of the 15th IEEE International Conference on Micro Electro Mechanical Systems, Las Vegas, Nevada, pp. 574-577.

(Chang-Yen 2005) Chang-Yen, D. A. and Gale, B. K. (2005) Design and fabrication of a multianalyte-capable optical biosensor using a multiphysics approach *in* Proceedings of 3rd Annual International IEEE EMBS Special Topic Conference on Microtechnologies in Medicine and Biology, Kahaku, Oahu, Hawaii, pp. 326-328.

(Chaudhari 2001) Chaudhari et al (2001) A new technique for the reduction of the power loss in the Y-branch optical power splitter. *Optics Communications*, Vol 193, No 1-6, pp.121-125.

(Chen 2006) Chen, C-L. (2006) *Foundations for Guided-Wave Optics*, New Jersey, John Wiley and Sons.

(Chen 2007) Chen et al (2007) Fabrication and characterization of benzocyclobutene optical waveguides by UV pulsed-laser illumination. *Journal of Quantum Electronics*. Vol 43, pp. 303-310.

(Choi 2000) Choi et al (2000) All-active InGaAsP-InP optical tapered-amplifier 1 × N power splitters. *IEEE Photonics Technology Letters*, Vol 12, No 8, pp. 974-976.

(Choi 2003) Choi et al (2003) Fabrication of large-core 1 × 16 optical power splitters in polymers using hot-embossing process. *IEEE Photonics Technology Letters*, Vol 15, No 6, pp. 825-827.

(Chu 1991) Chu, F. S. and Liu, P.-L. (1991) Low-loss coherent-coupling Y branches. *Optics Letters*, Vol 16, No 5, pp. 309-311.

(Chuang 2005) Chuang et al (2005) A New Method to Fabricate Polymer Waveguides *in* Progress in Electromagnetics Research Symposium, Hangzhou, China, pp. 92-95.

(Chung 1990a) Chung, Y. and Dagli, N. (1990) An assessment of finite difference beam propagation method. *Journal of Quantum Electronics*, Vol 26, No 8, pp. 1335-1339.

(Chung 1990b) Chung et al (1990) Novel design of integrated optical beam splitters using symmetric Y-branch structures *in* Proceedings of IEE Optoelectronics Journal, Vol 137, No 5, pp. 340-344.

(Chung 2006) Chung et al (2006) A 1 × 4 polarization and wavelength independent optical power splitter based on a novel wide-angle low-loss Y-junction. *Optics Communications*, Vol 267, No 2, pp. 367-372.

(Dai 2009) Dai et al (2009) Compact microracetrack resonator devices based on small SU-8 polymer strip waveguides. *IEEE Photonics Technology Letters*, Vol 21, No 4, pp. 254-256.

(Das 2009) Das, S. and Pal, S. (2009) A simple silica-on-silicon technology-compatible design of 1×8 optical splitter based on field matching Y-branch with S-bend sine taper and arc waveguide. *Journal of Optics*, Vol 38, No 3, pp. 177-190.

(Deri 1988) Deri, R. J. and Hawkins, R. J. (1988) Polarization, scattering, and coherent effects in semiconductor rib waveguide bends. *Optics Letters*, Vol 13, No 10, pp. 922-924.

(Eldada 1996) Eldada et al (1996) Laser fabricated low-loss single-mode raised-rib waveguiding devices in polymers. *Journal of Lightwave Technology*, Vol 14, No. 7, pp. 1704-1713.

(Eldada 1998) Eldada, L. (1998) Integrated Multichannel OADM's Using Polymer Bragg Grating MZI's. *IEEE Photonics Technology Letters*, Vol 10, No 10, pp. 1416-1418.

(Eldada 2000) Eldada, L. and Shacklette, L. W. (2000) Advances in polymer integrated optics. *IEEE Journal of Selected Topics in Quantum Electronics*, Vol 6, No 1, pp. 54-68.

(Eldada 2002) Eldada L. (2002) Polymer integrated optics: promise versus practicality *in* Proceedings of SPIE Organic Photonic Materials and Devices IV 2002, Vol 4642 (2002), pp. 11-22.

(Eldada 2003) Eldada, L. (2003) Polymer microphotonics *in* Proceedings of SPIE, Nano- and Micro-Optics for Information Systems, Bellingham, Vol. 5225, pp. 49-60.

(Eldada 2005a) Eldada, L. (2005) Telcordia qualification and beyond: reliability of today's polymer photonic components *in* Organic Photonic Materials and Devices VII : Proceedings of SPIE, Bellingham, WA, Vol. 5724, pp. 96-106.

(Eldada 2005b) Eldada L. (2005) Advances in Polymer Optical Interconnects *in* Proceedings of the 18th Annual Meeting of the IEEE Laser and Electro-Optics Society, Sydney, Australia, 2005, New Jersey: IEEE, pp. 361-362.

(Ericson 2000) Ericson et al (2000) Precision passive alignment technologies for low cost array FTTH component *in* Proceedings of Conference on Optical MEMS, 2000 IEEE/LEOS International, pp. 115-116.

(Fan 2012) Fan et al (2012) Study of an Electro-Optic Polymer Modulator. *Journal of Lightwave Technology* , Vol 30, No 15, pp. 2482-2487.

(Feit 1978) Feit, M. D. and Fleck Jr., J. A. (1978) Light propagation in graded-index optical fibers. *Applied Optics*, Vol 17, No 24, pp. 3990-3998.

(Feit 1979) Feit, M. D. and Fleck Jr., J. A. (1979) Calculation of dispersion in graded-index multimode fibers by a propagating-beam method. *Applied Optics*, Vol 18, No 16, pp. 2843-2851.

(Feit 1980) Feit, M. D. and Fleck Jr., J. A. (1980) Computation of mode properties in optical fiber waveguides by a propagating beam method. *Applied Optics*, Vol 19, No 7, pp. 1154-1164.

(Feit 1983) Feit, M. D. and Fleck Jr., J. A. (1983) Comparison of calculated and measured performance of diffused channel-waveguide couplers. *Journal of the Optical Society of America*, Vol 73, No 10, pp. 1296-1304.

(Feit 1985) Feit, M. D. and Fleck Jr., J. A. (1985) Analysis of intersecting diffused channel waveguides. *IEEE Journal of Quantum Electronics*, Vol 21, No 11, pp. 1799-1805.

(Feit 1990) Feit, M. D. and Fleck Jr., J. A. (1990) Analysis of rib waveguides and couplers by the propagating beam method. *Journal of the Optical Society of America A (Optics and Image Science)*, Vol 7, No 1, pp. 73-79.

(Flory 1996) Flory et al (1996) Optical waveguide characterization of thin films. *Review of Laser Engineering-Laser Society of Japan*, Vol 24, No 1, pp. 94-102.

(Frandsen 2004) Frandsen et al (2004) Ultralow-loss 3-dB photonic crystal waveguide splitter. *Optics Letters*, Vol 29, No 14, pp. 1623-1625.

(Gamet 2004) Gamet, J. and Pandraud, G. (2004) Ultralow-loss 1 × 8 splitter based on field matching Y junction. *IEEE Photonics Technology Letters*, Vol 16, No 9, pp. 2060-2062.

(Gang 2004) Gang et al (2004) Fabrication of polymeric optical waveguides *in* Proceedings of RF and Microwave Conference, RFM 2004, pp. 265- 268.

(Gardelein 2006) Gardelein et al (2006) Characterization of electro-optic polymer applied to microwave sensing *in* International Topical Meeting on Microwave Photonics, 2006, pp. 1-4.

(Garner 1999) Garner et al (1999) Three-dimensional integrated optics using polymers. *IEEE Journal of Quantum Electronics*, Vol 35, No 8, pp. 1146-1155.

(Ghatak 1998) Ghatak, A. and Thyagarajan, K. (1998) *Introduction to Fiber Optics*. New York: Cambridge University Press.

(Green 2005) Green Jr., P. E. (2006) *Fiber To The Home: The New Empowerment.* New Jersey: John Wiley & Sons.

(Hammer 2012) Hammer, M. (2012) *Advanced Photonics Modeling* www.home.math.utwente.nl/~hammer/eims.html.

(Haux 1989) Haux et al (1989) Single mode optical components in integrated optics on glass *in* SPIE Proceedings for Glasses for Optoelectronics Paris, France, Vol 1128, pp. 165.

(Henry 1989) Henry, C. H. and Verbeek, B. H. (1989) Solution of the scalar wave equation for arbitrarily shaped dielectric waveguides by two-dimensional fourier analysis. *IEEE Journal of Lightwave Technology*, Vol 7, No 2, pp. 308-313.

(Hibino 1994) Hibino et al (1994) High reliability silica-based PLC 1 × 8 splitter on Si. *Electronics Letters*, Vol 30, No 8, pp. 640-642.

(Hibino 1995) Hibino et al (1995) High reliability optical splitters composed of silica-based planar lightwave circuits. *IEEE Journal of Lightwave Technology*, Vol 13, No 8, pp. 1728-1735.

(Hikita 1993) Hikita et al (1993) Optical intensity modulation in a vertically stacked coupler incorporating electro-optic polymer. *Applied Physics Letters*, Vol 63, No 9, pp. 1161-1163.

(Hikita 1998) Hikita et al (1998) Polymeric optical waveguides for optical interconnections. *Thin Solid Films*, Vol 331, No 1-2, pp. 303-308.

(Ho 2006) Ho (2006) Reliability Study of Optical Adhesive For Photonic Devices Under The High Temperature And High Humid Environment *in* International Conference on Electronic Materials and Packaging, EMAP 2006, pp. 1-4.

(Hoekstra 1997) Hoekstra, H. J. W. M. (1997) On beam propagation methods for modeling in integrated optics. *Optical and Quantum Electronics*, Vol 29, No 2, pp. 157-171.

(Hsu 1998) Hsu, J-M. and Lee, C-T. (1998) Systematic design of novel wide-angle low-loss symmetric Y-junction waveguides. *Quantum Electronics, IEEE Journal of* , Vol 34, No 4, pp. 673-679.

(Hu 1997) Hu et al (1997) A Low-loss and compact waveguide Y-branch using refractive-index tapering. *IEEE Photonics Technology Letters*, Vol 9, No 2, pp. 203-205.

(Huang 1997) Huang et al (1997) High-performance metal-coated multimode interference (mmi) devices for wdm applications. *Digest of the IEEE/LEOS Summer Topical Meetings*, Cat. No.97TH8276, pp.54-55.

(Huang 1998) Huang et al (1998) High-performance metal-clad multimode interference devices for low-index-contrast material systems. *IEEE Photonics Technology Letters*, Vol 10, No 4, pp. 561-563.

(Hung 1988) Hung et al (1988) Single-mode 1 × 3 integrated optical branching circuit-design using phase-front accelerators. *Electronics Letters*, Vol 24, No 22, pp. 1365-1366.

(Hunsperger 2009) Hunsperger, R. G. (2009) *Integrated Optics Theory and Technology*. 6th Ed. New York: Springer.

(Jamroz 2006) Jamroz, W. R., Kruzelecky, R., and Haddad, E. I. (2006) *Applied Microphotonics*. Boca Raton, Florida: CRC Press, Taylor and Francis Group.

(Jaouen 1999) Jaouen et al (1999) Eight-wavelength Er-Yb doped amplifier: combiner/splitter planar integrated module. *IEEE Photonics Technology Letters*, Vol 9, No 9, pp. 1105-1107.

(Johnson 1984) Johnson, L. M. and Yap, D. (1984) Theoretical analysis of coherently coupled optical waveguide bends. *Applied Optics*, Vol 23, No 17, pp. 2988-2990.

(Kan 2003) Kan et al (2003) Thin-film waveguide with lens effect terminal for optical sensing device *in* Proceedings of the 16th Annual International Conference on Micro Electro Mechanical Systems, Kyoto, Japan, 2003, New Jersey: IEEE, 2003, pp. 315-318.

(Kang 2001) Kang et al (2001) Low-loss fluorinated poly(arylene ether sulfide) waveguides with high thermal stability. *Journal of Lightwave Technology*, Vol 19, No 6, pp. 872-875.

(Kang 2003) Kang et al (2003) A hyperbranched aromatic fluoropolyester for photonic applications. *Macromolecules*, Vol 36, No 12, pp. 4355-4359.

(Kapany 1972) Kapany, N. S. and Burke, J. J. (1972) Optical Waveguides, New York: Academic Press.

(Keller 2008) Keller et al (2008) Processing of thin SU-8 films. *Journal of Micromechanics and Microengineering*, Vol 18, No 12, pp. 125020 (1-10).

(Kersten 1975) Kersten, R. T. (1975) The prism-film coupler as a precision instrument Part I Accuracy and capabilities of prism couplers as instruments. *Optica Acta: International Journal of Optics*, Vol 22, No 6, pp. 503-513.

(Khanarian 2001) Khanarian, G. (2001) Theory of design parameters for quasi-phase-matched waveguides and application to frequency doubling in polymer waveguides. *Journal of Selected Topics in Quantum Electronics*, Vol 7, No 5, pp. 793-805.

(Kieu 2006) Kieu, K. Q. and Mansuripur, M. (2006) Biconical Fiber Taper Sensors. *IEEE Photonics Technology Letters*, Vol 18, No 21, pp. 2239-2241.

(Kim 2007) Kim et al (2007) Synthesis and characterization of methacrylate-based UV-crosslinkable copolymers for polymeric optical waveguides. *Journal of Molecular crystals and Liquid Crystals*, Vol 463, pp. 101-106.

(Kim 2008) Kim, K-J. and Oh, M-C. (2008) Flexible Bragg Reflection Waveguide Devices Fabricated by Post-Lift-Off Process. *IEEE Photonics Technology Letters*, Vol 20, No 4, pp. 288-290.

(Kiyat 2005) Kiyat et al (2005) A compact silicon-on-insulator polarization splitter. *IEEE Photonics Technology Letters*, Vol 17, No 1, pp. 100-102.

(Knox, 1970) Knox, R. M. and Toulios, P. P. (1970) Integrated Circuits for the millimeter through optical frequency range *in* Symposium on sub-millimeter waves: proceedings of Symposium on sub-millimeter waves, 1970, Fox, J. (ed.), Polytechnic Institute of Brooklyn, pp. 497-516.

(Kogelnik 1974) Kogelnik, H. and Ramaswamy, V. (1974) Scaling rules for thin-film optical waveguides. *Applied Optics*, Vol. 13, No. 8, pp. 1857-1862.

(Ladouceur 1996) Ladouceur, F. and Love, J. D. (1996) *Silica-based Buried Channel Waveguides and Devices*. London: Chapman & Hall.

(Leinse 2005) Leinse et al (2005) A novel high-speed polymeric EO Modulator based on a combination of a microring resonator and an MZI. *Photonics Technology Letters, IEEE*, Vol 17, No 10, pp. 2074-2076.

(Lifante 2003) Lifante, G. (2003) *Integrated Photonics: Fundamentals*. New York: John Wiley & Sons.

(Lin 1994) Lin et al (1994) Single mode 1 × 3 integrated optical branching circuit design using microprism. *Electronics Letters*, Vol 30, No 5, pp. 408.

(Lin 1999a) Lin et al (1999) Novel optical single-mode asymmetric Y-branches for variable power splitting. *IEEE Journal on Quantum Electronics*, Vol 35, No 7, pp. 1092–1096.

(Lin 1999b) Lin, H. B. and Chang, W. C. (1999) A novel low-loss wide-angle Y-branch with a diamond-like microprism. *IEEE Photonics Technology Letters*, Vol 11, No 6, pp. 683-685.

(Liu 2000) Liu et al (2000) Epoxy adhesives for optical element attachment in planar passive optical components *in* Proceedings of 50th Electronic Components & Technology Conference, pp. 975-980.

(Liu 2005) Liu, J-M. (2005) *Photonic Devices*. New York: Cambridge University Press.

(Llobera 2006) Llobera et al (2006) Polymeric MOEMS Variable Optical Attenuator. *Photonics Technology Letters, IEEE*, Vol 18, No 22, pp. 2425-2427.

(Lukosz 1995) Lukosz, W. and Pliska, P. (1995) Determination of thickness, refractive indices, optical anisotropy of, and stresses in SiO2 films on silicon wafers. *Optics Communications*, Vol 117, No 1-2, pp. 1-7.

(Ma 2002) Ma et al (2002) Polymer-Based Optical Waveguides: Materials, Processing, and Devices. *Advanced Materials*, Vol 14, No 19, pp. 1339-1365.

(Madden 1990) Madden et al (1990) Optical channel waveguide fabrication based on electron beam irradiation of silica. *Applied Physics Letters*, Vol 57, No 27, pp.2902-2903.

(Madou 2002) Madou, M. (2002) *Fundamentals of Microfabrication - The Science of Miniaturization*. 2nd Ed. Boca Raton: CRC Press.

(Maeda 2001) Maeda et al (2001) FSAN OAN-WG and future issues for broad-band optical access networks. *IEEE Communications Magazine*, Vol 39, No 12, pp. 126-132.

(Manor 2003) Manor et al (2003) Microfabrication and characterization of liquid core waveguide glass channels coated with Teflon AF. *IEEE Sensors Journal*, Vol 3, No 6, pp. 687-692.

(Marcatili 1969) Marcatili, E. A. J. (1969) Dielectric rectangular waveguide and directional coupler for integrated optics. *Bell System Technical Journal,* Vol 8, No 7, pp. 2071-2102.

(Marcuse 1991) Marcuse, D. (1991) *Theory of Dielectric Optical Waveguides.* 2nd Ed. New York: Academic Press.

(Marz 1995) Marz, R. (1995) *Integrated Optics: Design and Modeling*. Norwood, MA: Artech House.

(Microchem 2000) MicroChem Company. (2000) *Product Literature: SU-8 2000 series 2002-2025*.

(Miller 1969) Miller, S. E. (1969) Integrated optics: An introduction. *The Bell System Technical Journal*, Vol 48, pp. 2059-2068.

(Min 1997) Min et al (1997) Wide-angle low-loss waveguide branching for integrated optics. *Fiber and Integrated Optics,* Vol 16, No 4, pp. 331-342.

(Mitachi 2006) Mitachi et al (2006) Reliability Test Results for Optical Devices Assembled with a Non-Smell & Highly Moisture Durable New Optical Adhesive *in* 19th Annual Meeting of the IEEE Lasers and Electro-Optics Society , pp. 170-171.

(Miya 1992) Miya (1992) Arrayed waveguide-type wavelength-insensitive coupler for FTTH network *in* Digest of Conference on Optical Fiber Communication, California, Vol 5, pp. 264.

(Miya 2000) Miya, T. (2000) Silica-based planar lightwave circuits: passive and thermally active devices. *IEEE Journal of Selected Topics in Quantum Electronics*, Vol 6, No 1, pp. 38-45.

(Mogul 1998) Mogul et al (1998) *Photonic Polymer Systems*. New York: Marcel Dekker.

(Mohammad 2004) Mohammad et al (2004) Fundamentals of Electron Beam Exposure and Development *in* Nanofabrication Techniques and Principles, M. Stepanova and S. Dew (Eds.), Springer-Verlag, pp. 11-41.

(Mohr 2004) Mohr et al (2004) Polymer technologies: a way to low-cost micro-optical components and systems in Micro-Optics, VCSELs, and Photonic Interconnects *in* Proceedings of SPIE Vol. 5453, pp. 1-12.

(Momotsu 1999) Momotsu et al (1999) Compact and economical high-density PLC-type splitters *in* APCC/OECC '99 Fifth Asia-Pacific Conference on Communications, 1999 and Fourth Optoelectronics and Communications Conference, (1999) Vol 2, pp.1636-1637.

(Munowitz 1992) Munowitz, M. and Vezzetti, D. J. (1992) Numerical modeling of coherent coupling and radiation fields in planar Y-branch interferometers. *Journal of Lightwave Technology*, Vol 10, No 11, pp. 1570-1573.

(Nakayama 1997) Nakayama et al (1997) Nonlinear optical waveguide fabrication by direct electron-beam irradiation and thermal development using a high Tg polymer. *Applied Physics Letters*, Vol 71, No 14, pp.1924-1926.

(Nguyen 2002) Nguyen, N.-T. and Wereley, S. (2002) *Fundamentals and Applications of Microfluidics.* Norwood, MA: Artech House.

(Nishihara 1985) Nishihara, H., Haruna, M. and Suhara, T. (1985) *Optical Integrated Circuits*. New York: McGraw-Hill Book Company.

(Nolte 2003) Nolte et al (2003) Femtosecond waveguide writing: a new avenue to three-dimensional integrated optics. *Applied Physics A Materials Science & Processing*, Vol 77, No 1, pp. 109-111.

(Nordstrom 2007) Nordström et al (2007) Single-mode waveguides with SU-8 polymer core and cladding for MOEMS applications. *IEEE Journal of Lightwave Technology*, Vol 25, No 5, pp.1284-1289.

(Norland Products) https://www.norlandprod.com/adhesives/NOA61.html

(Nourshargh 1989) Nourshargh et al (1989) Integrated optic 1 × 4 splitter in SiO2/GeO2. *Electronics Letters*, Vol 25, No 15, pp. 981-982.

(Okada 1997) Okada, K. (1997) NTT's scenario for optical access networks toward FTTH *in* Proceedings of Optical Fiber Communication Conference, Dallas, TX, pp. 26.

(Okamoto 2005) Okamoto, K. (2005) *Fundamentals of Optical Waveguides*, 2nd Ed. Burlington, MA: Academic Press.

(Pal 2005) Pal, B. P. (2005) *Guided Wave Optical Components and Devices: Basics, Technology, and Applications*. Burlington, MA: Academic Press.

(Pal 2009) Pal et al (2009) Fabrication and performance-analysis of a planar silica-based cascaded symmetric Y-branch 1× 8 optical power splitter. *Journal of Optics*, Vol 38, No 3, pp. 149-159.

(Pavesi 2006) Pavesi, L. and Guillot, G. (ed.) (2006) *Optical Interconnects The Silicon Approach*. New York: Springer.

(Pelletier 2004) Pelletier et al (2004) Integrated optical Mach-Zehnder on SU-8 polymer for designing thermal sensors Sensors *in* IEEE Sensors 2004: Proceedings of IEEE Sensors, 2004, Vienna: Austria, pp 868-871.

(Pelletier 2006) Pelletier et al (2006) Single-mode rib opticalwaveguides on SOG/SU-8 polymer and integrated Mach-Zehnder for designing thermal sensors. *IEEE Sensors Journal*, Vol 6, No 3, pp. 565-570.

(Pitois 2002) Pitois et al (2002) Fluorinated dendritic polymers and dendrimers for waveguide applications. *Optical Materials*, Vol 21, pp. 499-506.

(Pollock 1995) Pollock, C. R. (1995) *Fundamentals of Optoelectronics*. Chicago:R D Irwin, Inc.

(Pruessner 2005) Pruessner et al (2005) InP-based optical waveguide MEMS switches with evanescent coupling mechanism. *Journal of Microelectromechanical Systems*, Vol 14, No 5, pp. 1070-1081.

(Punke 2007) Punke et al (2007) Coupling of organic semiconductor amplified spontaneous emission into polymeric single-Mode waveguides patterned by deep-UV irradiation. *Photonics Technology Letters*, Vol 19, No 2, pp. 61-63.

(Queller 2004) Queller, A. (2004) Dynamic power distribution in PON/FTTP networks. http://www.lightwaveonline.com/articles/print/volume-21/issue-7/applications/dynamic-power-distribution-in-ponfttp-networks-53906787.html.

(Rahman 1984) Rahman B. M. A. and Davis J. B. (1984) Finite-element solution of integrated optical waveguides. *IEEE Journal of Lightwave Technology*, Vol 2, No 5, pp. 682-688.

(Ratovelomanana 1995) Ratovelomanana et al (1995) Active lossless monolithic one-by-four splitters/combiners using optical gates on InP. *IEEE Photonics Technology Letters*, Vol 7, No 5, pp. 511-513.

(Rsoft 1993) RSoft Design Group Inc. and Columbia University (2002) *BeamProp - The Complete BPM Package for Integrated and Fiber Optics*.

(Sanghadasa 2006) Sanghadasa et al (2006) A simplified technique for efficient fiber-polymer-waveguide power coupling using a customized cladding

with tunable index of refraction. *Jouranl of Lightwave Technology*, Vol 24, No 10, pp. 3816-3823.

(Satyanarayan 2006) Satyanarayan, M. N. (2006) Design of polymer waveguide based 1 × N optical power splitters *in* Proceedings of 8th International Conference on Fiber Optics and Photonics, Photonics-2006, Hyderabad, India.

(Scarmozzino 1991) Scarmozzino, R. and Osgood Jr., R. M. (1991) Comparison of finite-difference and Fourier-transform solutions of the parabolic wave equation with emphasis on integrated-optics applications. *Journal of Optical Society of America A*, Vol 8, No 5, pp.724-731.

(Scarmozzino 2001) Scarmozzino, R. (2001) BPM is a powerful tool for creating guided-wave optical devices. http://www.lightwaveonline.com /articles/wdm/print/volume-3/issue-8/bpm-is-a-powerful-tool-for-creating-guided-wave-optical-devices-54918382.html

(Schuller 2007) Schuller et al (2007) Highly efficient and compact photonic wire splitters on GaAs. *Applied Physics Letters*, Vol 91, No 22, pp. 221102 (0-3).

(Seino 1987) Seino et al (1987) Low-loss Mach–Zehnder waveguide *in* Proceedings of ECOC Conference, pp. 113–116.

(Shacklette 2004) Shacklette, L. (2004) Polymers in the Light Path *Optics and Photonics News*, Vol 15, No 11, pp. 22-27.

(Shaw 2003) Shaw et al (2003) Improving the process capability of SU-8. *Microsystem Technologies*, Vol 10, pp. 1-6.

(Shimizu 1983) Shimizu et al (1983) Fusion-splicing between optical circuits and optical fibers. *Electronics Letters*, Vol 19, No 3, pp. 96-97.

(Snakenborg 2006) Snakenborg et al (2006) Direct Milling and casting of polymer-based optical waveguides for improved transparency in the visible

range. *Journal of Micromechanics and Microengineering*, Vol 16, pp. 375-381.

(Snyder 2003) Snyder, A. W. and Love, J. (2003) *Optical Waveguide Theory*, London: Springer.

(Sohn 2005) Sohn et al (2005) Fabrication of optical splitter and passive alignment technique with a femtosecond laser. *IEEE Photonics Technology Letters*, Vol 17, No 11, pp. 2349-2351.

(Sum 2003a) Sum et al (2003) Proton beam writing of passive waveguides in PMMA. *Nuclear Instruments and Methods in Physics Research B*, Vol 210, pp. 266-271.

(Sum 2003b) Sum et al (2003) Proton beam writing of low-loss polymer optical waveguides. *Applied Physics Letters*, Vol 83, No 9, pp. 1707-1709.

(Sum 2004) Sum et al (2004) Proton beam writing of Passive Polymer Optical Waveguides *in* Proceedings of SPIE, Micromachining Technology for Micro-Optics and Nano-Optics II, Bellingham, Vol 5347, pp. 160-169.

(Suzuki 1996) Suzuki et al (1996) Integrated optic Y-branching waveguides with an asymmetric branching ratio. *Electronics Letters*, Vol 32, No 8, pp. 735736.

(Takahashi 1993) Takahashi et al (1993) Integrated-optic 1 × 128 power splitter with multifunnel waveguide. *IEEE Photonics Technology Letters*, Vol 5, No 1, pp. 58-60.

(Takahashi 2003) Takahashi, H. (2003) Planar lightwave circuit devices for optical communication: present and future *in* Proceedings of SPIE, Active and Passive Optical Components for WDM Communications III, Orlando: Florida, Vol 5246, pp. 520-531.

(Tamir 1975) Tamir, T. (1975) *Integrated Optic*. New York: Springer-Verlag.

(Tao 2008) Tao et al (2008) Cascade wide-angle Y-junction 1 × 16 optical power splitter based on silicon wire waveguides on silicon-on-insulator. *Optics Express*, Vol 16, No 26, pp. 21456-21461.

(Telcordia 2001) Telcordia Technologies (2001). *Generic Requirements for Passive Optical Components (GR-1209-CORE),* Issue 4, 2010.

(Tien 1971) Tien, P. K. (1971) Light waves in thin films and integrated optics. *Applied Optics*, Vol 10, No 11, pp. 2395-2413.

(Tien 1977) Tien, P. K., (1977) Integrated optics and new wave phenomena in optical waveguides. *Reviews of Modern Physics,* Vol 49, No 2, pp. 361-420.

(Tsai 2003) Tsai, D. P. (2003) *Topics in Applied Physics: Optical Nanotechnologies*, Vol. 88. Berlin:Springer-Verlag.

(Tsutsumi 1988) Tsutsumi et al (1988) Analysis of single-mode optical Y-junction by the bounded step and bend approximation. *Journal of Lightwave Technology*, Vol 6, No 4, pp. 590-600.

(Tumolillo 1991) Tumolillo Jr., T. A. and Ashley, P. R. (1991) Fabrication techniques of photopolymer-clad waveguides for nonlinear polymeric modulators *in* SPIE Proceedings of Photopolymer Device Physics, Chemistry, and Applications II, pp. 65.

(Tung 2005) Tung et al (2005) Polymeric optical waveguides using direct ultraviolet photolithography process. *Applied Physics A Material Sciences and Processing*, Vol 80, No 3, pp. 621-626.

(Ueda 2001) Ueda et al (2001) Deployment status and common technical specifications for a B-PON system. *IEEE Communications Magazine*, Vol 39, No 12, pp. 134-141.

(Unger 1977) Unger, H. G. (1977) *Planar Optical Waveguides and Fibers*. Oxford, UK : Clarendon Press.

(van Kan 2001) van Kan et al (2001) Proton beam micromachining: a new tool for precision three-dimensional microstructures. *Sensors and Actuators A*, Vol 92, pp. 370-374.

(Vassallo 1991) Vassallo, C. (1991) *Optical Waveguide Concepts*. New York: Elsevier.

(Verizon 2007) Jain, V. and Graff, L. C. (2007) *Verizon NEBSTM Compliance: Screening Requirements for Optical Components (VZ.TPR.9423)*, Issue 1, 2007.

(Vieu 2000) Vieu et al (2000) Electron beam lithography: resolution limits and applications. *Applied Surface Science*, Vol 164, No 1-4, pp. 111-117.

(Wale 1990) Wale, M. J. (1990) Self-aligned flip-chip assembly of photonics devices with electrical and optical connection in Proceedings of 40th Electronic Components and Technology Conference, Las Vegas, Vol 1, pp. 34-41.

(Wang 1994) Wang et al (1994) Travelling wave electro-optic phase modulator using cross-linked nonlinear optical polymer. *Applied Physics Letters*, Vol 65, No 8, pp. 929-931.

(Wang 2002) Wang et al (2002) A low-loss Y-branch with a multimode waveguide transition section. *IEEE Photonics Technology Letters* Vol 14, No 8, pp. 1124-1126.

(Wang 2003) Wang et al (2003) Wide-angle 1 x 3 optical power divider in LiNbO3 for variable power splitting. *IEEE Photonics Technology Letters*, Vol 15, No 10, pp. 1401.

(Wang 2004) Wang et al (2004) 1 × 8 cascaded multimode interference splitter in silicon-on-insulator. *Japanese Journal of Applied Physics*, Vol 43, No 8A, pp. 5085-5087.

(Wang 2008) Wang et al (2008) A non-destructive characterization and real time monitor technique for low-loss, polymeric waveguide circuits *in* Proceedings of Electronic Components and Technology Conference, Vol 58, pp. 2086-2090.

(Watanabe 1998) Watanabe et al (1998) Polymeric optical waveguide circuits formed using a silicone resin. *Journal of Lightwave Technology*, Vol 16, No 6, pp. 1049-1055.

(Watt 2000) Watt et al (2000) Three-dimesional microfabrication using maskless irradiation with Mev ion beams: *Proton beam micromachining. MRS Bulletin*, Vol 25, No 2, pp. 33.

(Weismann 1989) Weismann et al (1989) Mode-dependent radiation loss in Y-junction and directional couplers. *IEEE Journal of Quantum Electronics*, Vol 25, No 6, pp. 1200-1208.

(Wiesmann 1996) Wiesmann (1996)Monomode polymer waveguides with integrated mirrors *in* 22nd European Conference on Optical Communication, ECOC '96, Vol 2, pp. 265-268.

(Williams 2004) Williams, J. D. and Wang, W. (2004) Using megasonic development of SU-8 to yield ultra-high aspect ratio microstructures with UV lithography. *Microsystem Technologies*, Vol 10, pp. 694-698.

(Willner 2012) Willner, A. and Nuccio, S. (2012) Electro-Optic Polymer Modulators *in* OSA Technical Digest for Optical Fiber Communication Conference.

(Wong 2001) Wong et al (2001) Low-loss polymeric optical waveguides using electron-beam direct writing. *Applied Physics Letters*, Vol 78, No 15, pp. 2110-2112.

(Wong 2003) Wong et al (2003) Highly fluorinated trifluoro vinyl aryl ether monomers and perfluorocyclobutane aromatic ether polymers for optical waveguide applications. *Macromolecules*, Vol 36, pp. 8001-8007.

(Worboys 1990) Worboys et al (1990) Electro-optic polymer devices *in* IEE Colloquium on Optoelectronic Material, pp.7/1-7/4.

(Wosinski 2004) Wosinski, L. (2004) Silica-on-silicon technology for photonic integrated devices in Proceedings of the 6th International Conference on Transparent Optical Networks, New Jersey, pp.274-279.

(Wu 1991) Wu, J. (1991) Birefringent and electro-optic effects in poled polymer films: steady-state and transient properties. *Journal of Optical Society of America B*, Vol 8, pp. 142-152.

(Yabu 2001) Yabu et al (2001) New design method for low-loss Y-branch waveguides. *Journal of Lightwave Technology*, Vol 19, No 9, pp. 1376–1384.

(Yamada 1992) Yamada et al (1992) Low-loss and stable fiber-to-waveguide connection utilizing UV curable adhesive. *IEEE Photonics Technology Letters*, Vol 4, No 8, pp. 906-908.

(Yamada 2006) Yamada et al (2006) Si Photonic Wire Waveguide Devices. *IEEE Journal of Selected Topics in Quantum Electronics*, Vol 12, No 6, pp. 1371 - 1379.

(Yamauchi 2003) Yamauchi, J. (2003) *Propagating Beam Analysis of Optical Waveguides*. Institute of Physics Publishing Inc.

(Yang 2009) Yang et al (2009) Fabrication and characterization of small optical ridge waveguides based on SU-8 polymer. *IEEE Journal of Lightwave Technology*, Vol 27, No 18, pp. 4091-4096.

(Yeh 1979) Yeh et al (1979) Single-mode optical waveguides. *Applied Optics*, Vol 18, No 10, pp. 1490-1504.

(Yevick 1990) Yevick, D. and Hermansson, B. (1990) Efficient beam propagation techniques. *Journal of Quantum Electronics*, Vol 26, No 1, pp. 109-112.

(Yoon 2006) Yoon et al (2006) Multidirectional UV Lithography for complex 3-D MEMS structures. *Journal of Microelectromechanical Systems*, Vol 15, No 5, pp. 1121-1130.

(Yuan 2005) Yuan (2005) Electrooptic polymeric digital optical switches (DOSs) with adiabatic couplers. *IEEE Photonics Technology Letters*, Vol 17, No 12, pp. 2568-2570.

(Yulianti 2010) Yulianti et al (2010) Low Loss 1×2 Optical Coupler Based on Cosine S□bend with Segmented Waveguides *in* AIP Conference Proceedings of International Conference On Enabling Science And Nanotechnology, Escinano 2010 Kuala Lumpur, pp. 245-248.

(Zhang 2004) Zhang et al (2004) Effect of exposure dose on the replication fidelity and profile of very high aspect ratio microchannels in SU-8. *Lab Chip*, Vol 4, No 6, pp. 646-653.

(Zhong 2005) Zhong et al (2005) Chemical Mechanical Polishing of PC, PMMA and SU-8 polymers *in* Proceedings of the 5th International Conference on Polymers and Adhesives in Microelectronics and Photonics, Wroclaw, Poland, pp. 58-62.

APPENDIX A: NUFERN PWG1-XP SPECIFICATION SHEET

Nufern PWG1-XP

Planar Waveguide Single-Mode Fiber

Nufern's extra high-performance Planar Waveguide Fiber provides a solution to the splicing challenges for high NA wave-guiding structures. Industry developments indicate the call out for easy interfacing of new planar waveguide (PWG) technology with existing fiber infrastructures. Planar Waveguide Fiber is an excellent bridge fiber between high NA planar waveguides and low NA transmission fiber. This fiber allows outstanding optical coupling with planar waveguides. In addition, the composition of PWG1-HP is tailored to thermally expand the core during splicing and thus achieve low splice loss to transmission fibers.

OPTICAL SPECIFICATIONS

Operating Wavelength (nominal)	1550 nm
MFD @ 1550 nm	4.8 ± 0.5 μm
Second Mode Cut-Off	1330 ± 50 nm
Numerical Aperture (nominal)	0.26
Bend Loss @ 1550 nm (100 turns, 13 mm radius)	< 0.001 dB
Bend radius for 0.05 dB per 100 turns @ 1550 nm	Much less than LTBR

GEOMETRICAL AND MECHANICAL SPECS

Clad Diameter	125 ± 0.5 μm
Coating Diameter	245 ± 10 μm
Core-Clad Concentricity	< 0.3 μm
Coating/Clad Offset	≤ 5 μm
Proof Test Level	≥ 200 kpsi (1.4 GN/m²)
Coating Material	UV Curable, Dual Acrylate
Operating Temperature	- 55 to + 85° C
Short-Term Bend Radius	≥ 6 mm
Long-Term Bend Radius	≥ 13 mm

Fiber Construction

Applications:
- Fibertails for Planar Waveguides
- Bridge fiber

Features and Benefits:
- Superior fiber diameter tolerances
- Bend insensitive fiber for miniature packages
- Low splice loss to transmission fiber
- High coupling efficiency with Planar Waveguides

Standard specifications and design parameters are listed above. Other configurations such as alternative form factors, optimized cut-off and UV cured color coating may be available. Let us know how Nufern can assist with your requirements. Call 860-408-5000, toll free at 866-466-0214 or email us at info@nufern.com

NUFERN® Driven To Light.

Experience Determination

7 Airport Park Road • East Granby, CT 06026 • p: 860.408.5000
toll free: 866.466.0214 • f: 860.844.0210 • www.nufern.com

NU/0020-06/03

APPENDIX B: EIM 2D MODE-SOLVER RESULTS

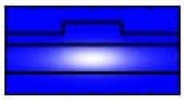

2-D multilayer waveguide mode solver
effective index approximation

Waveguide: 1 layer | Define | Solve | Inspect

Select a number of inner waveguide layers. *Define* opens a window that accepts the waveguide data. *Solve* invokes the mode solver. A frame reports on the mode properties. *Inspect* pops up a dialog for selecting components for mode profile plots. Choose *Plot* to view the figure. And be aware of the limitations of the effective index approximation. Should work properly for **reasonable** inputs ...

Waveguide definition

	Refractive index:	Thickness:
Cover:	1.54	
Layer 1:	1.57	2.5
Substrate:	1.54	

Wavelength:	Etching depth:	Rib width:
1.55	2.5	2.5

Default | Accept | Close

Modesolver status

```
------------------------------------------------------------ EIMS --
 l: 1.55   n: 1.54 1.57 1.54    t: 2.5    h: 2.5    w: 2.5
-----------------------------------------------------------------

Central slice,  1-D modes:
 TE 0:   beta: 6.320819   neff: 1.5592839
 TM 0:   beta: 6.319853   neff: 1.5590456
Lateral slices, 1-D modes:
 No guided modes, using substrate refractive index.

2-D effective index approximation:
 [****|TE 0|****] >>>
 TE 0 0:  beta: 6.2850766  neff: 1.5504665
 [****|TM 0|****] >>>
 TM 0 0:  beta: 6.284839  neff: 1.550408
```

APPENDIX C: TEST RESULTS FROM SAMEER, MUMBAI

TEST REPORT

Device Type : 1 × 4 ,1 × 8 splitter of SU8-NOA 61 on Si
Material : Silicon
Technical details : All devices are fabricated on Si wafer having NOA 61 as lower cladding and SU8 as core. Channel spacing is 127 µm
Number of samples checked : 8 samples:
Work completed : Chip-1 Device No5 is fiber pigtailed at input side
Tested by : Arun Kumar Mallik & Indrajit Boiragi

Packaged by : Anuj Bhatnagar

Devices tested and Packaged at : Optoelectronics Division, SAMEER, IIT Campus, Powai, Mumbai-400076.

Before pigtailing

	632.8 nm		1310 nm		1550 nm	
Device No.	**Input Power (µW)**	**Output power (µW)**	**Input Power (µW)**	**Output power (µW)**	**Input Power (µW)**	**Output power (µW)**
Dev.1-Chip1	537	1.92	398	7.7	553	1.7
		3.0		11.3		18.5
		1.56		6.1		9.1
		6.9		11.5		6.1
Dev.2-Chip1	537	3.5	398	18.1	553	10.6
		3.15		8.4		5.6
		6.8		18.2		9.0
		3.2		13.4		4.0
Dev.5 chip-1	537	2.5	398	5.9	553	6.1
		2.5		14.6		10.7
		4.1		13.4		11.0
		2.7		16.5		7.2

After pigtailing

	635 nm		1310 nm		1550 nm	
Device No.	**Input Power (mW)**	**Output power (µW)**	**Input Power (mW)**	**Output power (µW)**	**Input Power (mW)**	**Output power (µW)**
Dev.2 chip-1	3.7	5.7	2.5	5.3	1.57	4.4
		6.8		12.5		8.4
		7.9		29.3		2.8
		4.6		14.4		2.9

Report prepared by: Dr. Anuj Bharnagar
Signature:

Report verified by: Dr. K. Chalapathi
Signature:

Received by: M. N .Satyanarayan
Signature:
Date:

List of Publications and Presentations

1. Singhal, R., Satyanarayan, M. N. and Pal, S. (2012) Fabrication of single-mode Y-branch waveguides in photosensitive polymer with reduced Y-junction residue. *Optik - International Journal for Light and Electron Optics*, Vol 123, No 21, pp. 1911-1914.
2. Singhal, R., Satyanarayan, M. N. and Pal, S. (2011) Fabrication of monomode channel waveguides in photosensitive polymer on optical adhesive. *Optical Engineering*, Vol 50, No 9, pp. 094601(0-3).
3. Singhal, R., Satyanarayan, M. N. and Pal, S. (2010) Effect of residual resist on performance of single-mode 1 × 4 optical splitter in photosensitive polymer. *Fiber and Integrated Optics*, Vol 29, pp. 480–490.
4. Singhal, R., Satyanarayan, M. N. and Pal, S. (2009) Effect of Y-junction residue on performance of polymeric optical splitter *in* Proceedings of International Conference on Optics and Photonics - 2009, CSIR-CSIO, Chandigarh, India.
5. Singhal, R., Satyanarayan, M. N., Bhatia, R., Pradhan, N., Sharma, M. and Pal, S. (2008) Fabrication of polymeric optical power splitter *in* Proceedings of Photonics 2008, IIT-Delhi, New Delhi, India.
6. Singhal, R., Satyanarayan, M. N. and Pal, S. (2008) Design of polymeric optical splitter incorporating a taper *in* Proceedings of Photonics 2008, IIT-Delhi, New Delhi, India.

Biography of the Candidate

Rahul Singhal received his B. E. degree in Electronics Engineering from Nagpur University, Nagpur in 1999 and his M. Tech. degree in Digital Communication from Uttar Pradesh Technical University, Lucknow in 2007. He is currently pursuing the Ph.D. degree at Birla Institute of Technology and Science, Pilani, India.

Biography of the Supervisor

M. N. Satyanarayan holds a PhD in Physics from the Indian Institute of Science, Bangalore, India in the area of experimental condensed matter physics, and is presently with National Institute of Technology Karnataka, India. Prior to joining this institute, he was a faculty at Birla Institute of Technology & Science Pilani, India and also has worked for several years in industry. His research interests include nonlinear optical phenomena and materials, photonic devices, optical communication, etc. He has published many papers in peer reviewed journals as well as international conferences and also has a review article to his credit.